

## 3.8.6 Adsorbate properties of linear hydrocarbons

### 3.8.6.1 Introduction

#### 3.8.6.1.1 General considerations

The adsorption of organic molecules on surfaces plays a central role in our life on this planet. We live in a world full of organic molecules; all exposed surfaces are covered with them ranging from the car body and the top of the dining room table to the human skin. Thus, the properties of most surfaces we come in contact with are modified by the presence of this adsorbed organic layer that may contain small molecules such as acetylene or butadiene or large ones like proteins.

During the past 30-35 years a large number of techniques were developed that permit investigation of adsorbed organic layers on the molecular level. The studies that were performed indicated great complexity. Adsorption bond strength, the structure and reactivity of the adsorbed organic layer depends on: 1) the structure of the substrate on which adsorption occurs; 2) the coverage of the adsorbate. Usually the first layer (monolayer) adsorbs more strongly than subsequent layers. Even within the first monolayer, the heat of adsorption often declines rapidly with coverage; 3) the temperature of the adsorbate-substrate system. Elevated temperatures lead to bond breaking and sequential decomposition of the adsorbed organic molecules.

Another important feature has been the pressure range that was experimentally available for most of these molecular adsorption studies. Because of the predominance of electron scattering to determine surface structure by diffraction or vibrational spectroscopy most adsorption studies had to be performed at low enough pressures to satisfy the electron mean free path requirement of the signal detection. Only recently have photon in-photon out techniques gained popularity for these studies that can be performed at higher ambient pressures where there is equilibrium between the adsorbed organic molecules and the organic vapor over the surface.

In order to avoid experimental pitfalls and simplify studies of the adsorbed organic layer, most molecular adsorption studies were carried out using single crystal surfaces with well-defined, close packed surface structures. The use of powders and highly reactive surfaces with large concentrations of low coordination sites (steps and kinks) have been avoided. The studies were usually restricted to low coverages. The temperature range was limited to below 400 K to avoid excessive bond breaking and decomposition. Not surprisingly, most investigations were carried out at low pressures to take advantage of the available surface analytical techniques that can be employed only in this circumstance.

In this chapter, we summarize the investigations that reported studies of adsorbed short chain linear  $C_1$ - $C_{12}$  hydrocarbons; their structure and bonding on metal and semiconductor single crystal surfaces. It is our hope that these studies provide the foundation to investigate organic monolayers of greater complexity and higher molecular weights and organic molecules adsorbed on more reactive, more structurally complex surfaces. In future studies, a larger temperature and pressure range of adsorption must be explored to correlate adsorption behavior with reaction intermediates that are produced in high turnover catalytic reactions.

The adsorption studies of the small  $C_1$ - $C_{12}$  molecules on metal and semiconductor surfaces reveal several important findings. The adsorption bond is surface structure sensitive. Adsorbate-adsorbate repulsive interactions lead to weakening of the surface chemisorption bonds at higher coverages. The metal or semiconductor substrates restructure when adsorption occurs. This adsorbate induced restructuring may be local, occurring in the neighborhood of the adsorption site. It may also lead to complete restructuring of the substrate, especially for higher Miller-Index, more open surfaces. Increasing temperatures lead to sequential bond scission so that the molecular structure of the organic adsorbate markedly changes as the temperature is increased. Hydrogen coadsorption and coverage could have a large effect on the structure of the organic adsorbates. Unfortunately, hydrogen coadsorption has been investigated only in a few studies.

New techniques that may be used to investigate the adsorbed organic monolayers such as optical spectroscopies and the scanning probes will permit high pressure and high temperature in situ studies and also dynamical investigations to explore the roles of surface motions, diffusion and molecular rotation

and rearrangements in the adsorption process. The structure and bonding of adsorbed organic monolayers is an exciting field of surface science with impact on our understanding of the surface chemical bond, catalysis, friction and lubrication and in the case of adsorption of proteins at the polymer-water interface, biocompatibility. Indeed, adsorption of organic monolayers at the buried interfaces, solid-high pressure gas, solid-liquid, and solid-solid has yet to be explored.

### 3.8.6.1.2 Experimental aspects

Our knowledge of hydrocarbon adsorption is certainly still far from complete and this collection has inherent deficiencies. The majority of studies focused on small molecules ( $C_2H_4$ ,  $C_2H_2$ ) on close packed surfaces of Pt and Ni. This is illustrated in Fig. 1a and 1b showing which hydrocarbons and which substrates were studied most frequently. Furthermore, only a limited number of studies deal with quantitative parameters of hydrocarbon adsorption such as sticking and accommodation coefficients or adsorption energies as function of coverage. Many adsorption studies were motivated by heterogeneous catalysis since the initial step of every heterogeneous catalytic reaction is the same: the adsorption of the reacting gases on the surface of the catalyst (which may already strongly predetermine the catalytic properties). Consequently, geometrical (structural) information was mostly collected to determine adsorption sites and the molecular orientation of the hydrocarbon layers.

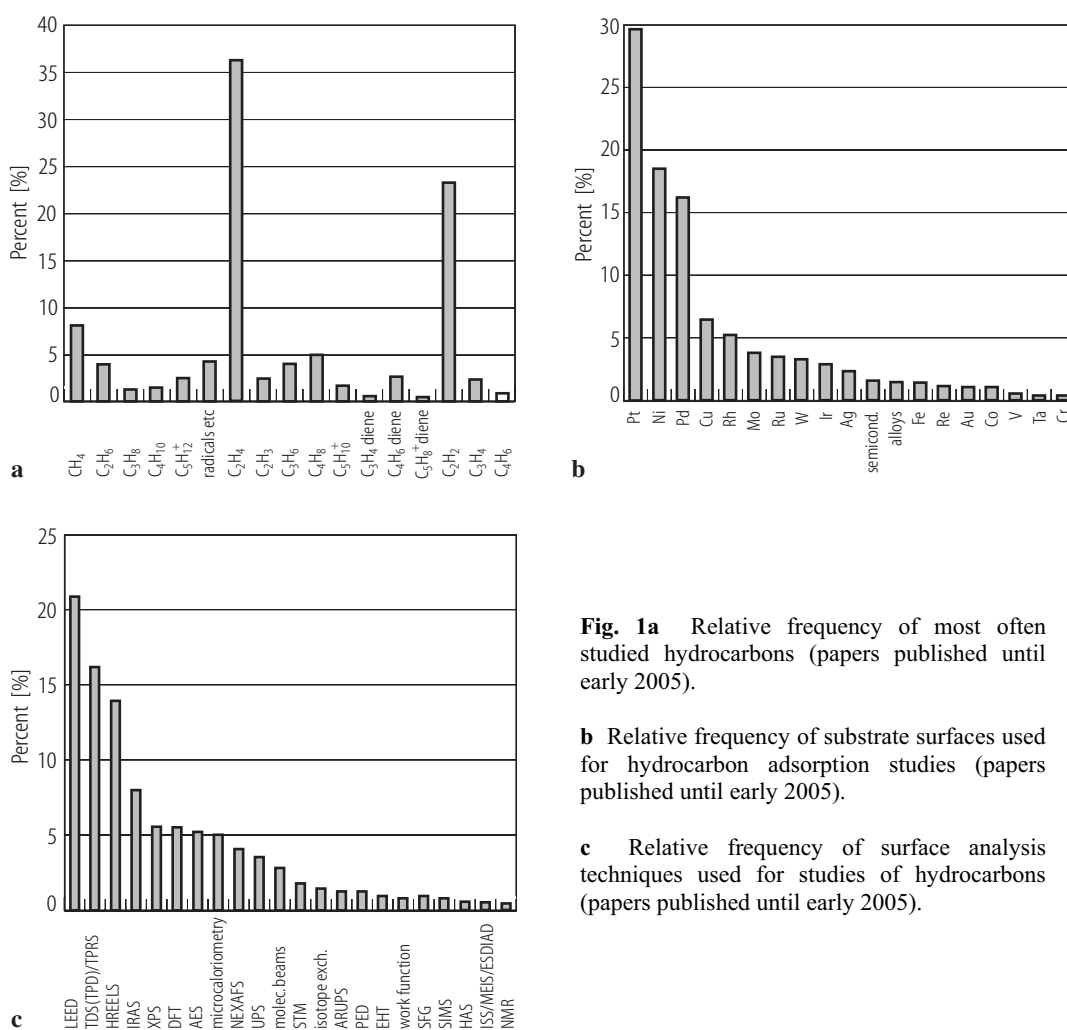


**Fig. 1a** Relative frequency of most often studied hydrocarbons (papers published until early 2005).

**b** Relative frequency of substrate surfaces used for hydrocarbon adsorption studies (papers published until early 2005).

**c** Relative frequency of surface analysis techniques used for studies of hydrocarbons (papers published until early 2005).

For experimental reasons, most studies report the adsorption of various hydrocarbons on one or two surfaces – experimentally, it is easier to change the adsorbate molecule than the substrate surface. Some authors report 3 or 4 hydrocarbons on one or two surfaces, sometimes including O-, N-, or C-precovered, i.e. there may be 8 or more adsorbate/substrate combinations appearing in a single article. Adsorption data of a specific hydrocarbon on various substrates are therefore typically “spread out” over many articles.

By contrast, this chapter is organized differently. To facilitate the comparison of the adsorption properties of a specific hydrocarbon on different substrates, the collected data are arranged by the adsorbate molecule first, and by the material (alphabetically) second (transition metals are discussed before alloys and semiconductors, though). For a given metal the order of surface geometries is (100), (110), (111), followed by higher-index or stepped surfaces. The most important findings are also summarized in the Tables 3.8.6.7.1 - 3.8.6.7.5. Adsorption studies on heterogeneous catalysts (supported metals) and modified single crystal surfaces (e.g. by oxide overlayers etc.) were not included due to the structural complexity of these systems. However, references to these studies can be typically found in the reviews and original articles summarized here. It is our hope that the collection in this chapter will assist to further evaluate hydrocarbon adsorption on different substrates.

### 3.8.6.1.3 List of symbols and abbreviations

The listings below collect symbols and abbreviations and the techniques most frequently used to study adsorbate properties of hydrocarbons on metal and semiconductor surfaces. A brief explanation of these methods and references to more detailed descriptions can be found e.g. in [93Nie, 94Som, 96She, 97Tho, 98Som]. Fig. 1c graphically displays how often the different methods were utilized, showing that for structure investigations LEED, HREELS and IRAS dominate, and that adsorption energies were mostly determined by thermal desorption spectroscopy/temperature programmed techniques, (micro)calorimetry and molecular beam methods (based on ca. 450 selected studies published until early 2005).

#### Symbols and abbreviations

bridge site	2-fold coordinated adsorption site
CVD	chemical vapor deposition
fcc site	3-fold coordinated hollow site with a substrate atom in the 3 <sup>rd</sup> layer underneath
$E_{proc}$	activation energy for various processes (“proc” may be desorption (des), dissociation (diss), diffusion (diff) or reaction (rcn))
$E_T$ or $E_i$	incident translational energy of gas particles
hcp site	3-fold coordinated hollow site with a substrate atom in the 2 <sup>nd</sup> layer underneath
L	Langmuir; one Langmuir is equivalent to a gas exposure of 10 <sup>-6</sup> Torr for 1 second
ML	“monolayer”, unit for absolute coverage (absolute coverage, i.e. ratio of adsorbed molecules to substrate surface atoms)
on-top	terminally adsorbed on a single atom
$S_0$	initial sticking coefficient (for zero coverage)
$T_{des}$	desorption temperature (usually peak maximum in TDS)
$\theta$	absolute coverage (adsorbed molecules per substrate surface atom)
UHV	ultrahigh vacuum

#### Most frequently applied surface analysis techniques (alphabetically)

AES	Auger Electron Spectroscopy
ARUPS	Angle Resolved Ultraviolet Photoelectron Spectroscopy
DFT	Density Functional Theory (ab initio)
EHT	Extended Hückel Theory Calculations (semi-empirical)
ESDIAD	Electron Stimulated Desorption Ion Angular Distribution
(HR)EELS	(High-Resolution) Electron Energy Loss Spectroscopy
HAS	Helium Atom Diffraction/Scattering

---

IETS	Inelastic Electron Tunneling Spectroscopy
ISS	Ion Scattering Spectroscopy
Isot. Exch.	Isotope Exchange
LEED	Low-Energy Electron Diffraction
MEIS	Medium Energy Ion Scattering
MB	Molecular Beam Techniques (sticking coefficient measurements)
NEXAFS	Near-Edge X-Ray Absorption Fine Structure
NMR	Nuclear Magnetic Resonance
PED	Photoelectron Diffraction
IRAS	Infrared Reflection-Absorption Spectroscopy (=RAIRS)
SFG	Sum Frequency Generation
SIMS	Secondary Ion Mass Spectrometry
STM	Scanning Tunneling Microscopy
TDS	Thermal Desorption Spectroscopy
TPD	Temperature-Programmed Desorption
TPRS	Temperature-Programmed Reaction Spectroscopy
UPS	Ultraviolet Photoelectron Spectroscopy
$\Delta\Phi$	Work Function Change
XAS	X-Ray Absorption Spectroscopy
XPS	X-Ray Photoelectron Spectroscopy

### 3.8.6.2 Reviews

The determination of quantitative adsorption parameters such as adsorption energies is not always part of adsorption studies. In many cases studies have rather focused on the adsorbate structure determined by electron diffraction, vibrational spectroscopy and other techniques. Adsorption energies were mainly determined by temperature programmed techniques, molecular beam methods or by calorimetry. Microcalorimetry is a useful tool for studies of heterogeneous catalysts, because it provides a direct measurement of the strength with which molecules interact with solid surfaces.

Hydrocarbon adsorption on low and high Miller-Index surfaces of Pt, Ir and Au as determined by low-energy electron diffraction surface crystallography was reviewed in [77Som,79Som].

Cerny [96Cer] and Spiewak and Dumesic [98Spi1, 98Spi2] have reviewed calorimetric methods for the determination of the heat of adsorption of gases on single crystals of metals but also for less defined surfaces such as filaments and vacuum-evaporated films. The development of the technique and advanced microcalorimetric techniques and their applications to the study of low surface area metal single crystals are discussed. The results on hydrocarbon adsorption were added to the Tables, for a complete list of the investigated systems and the measured heats of adsorption were refer to [96Cer] and Spiewak and Dumesic [98Spi1, 98Spi2].

Microcalorimetric measurements were also successfully applied by King and coworkers [95Stu, 99Bro1, 99Bro2] who measured the sticking probability and heat of adsorption of C<sub>2</sub>H<sub>4</sub> on various low-index and stepped Pt and Ni surfaces. Depending on coverage several different adsorbate species were identified. As an example, Fig. 2 presents C<sub>2</sub>H<sub>4</sub> adsorption on Pt(110)-(1×2) indicating that the heat of interaction (reaction) drops stepwise from 205 kJ/mol at low coverage to 125 kJ/mol with increasing coverage. Several stable surface species were identified (see section 3.8.6.4.1.10).

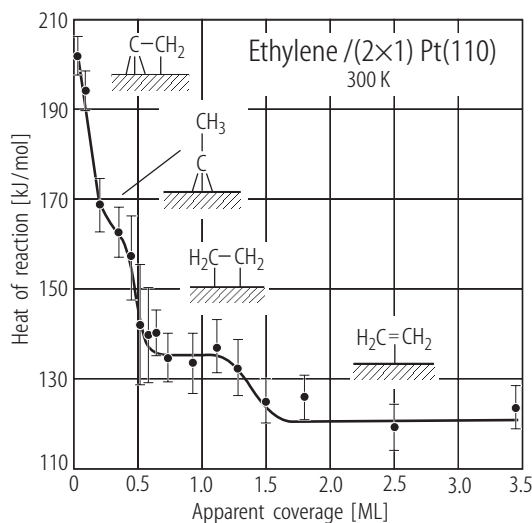


**Fig. 2:** Heat of interaction of ethylene on Pt(110)-(1x2) vs. coverage as determined by microcalorimetry; adapted from [95Stu].

Madix and coworkers [87Ham, 03Wea, 04Kao] performed extensive studies on the adsorption dynamics of methane, ethane, propane, n-butane, etc. on e.g. Ni(111), Ni(100), Pt(111) and Pd(111), utilizing molecular beam techniques and stochastic trajectory simulations. Typically, for each alkane the initial adsorption probability was measured as a function of incident energy and incident angle. In general, at a fixed incident energy and angle the trapping probability was highest on Pd(111), followed by Pt(111) and Ni(111). Three-dimensional stochastic trajectory simulations for alkane trapping on the three metals indicated that incoming molecules lose considerable energy to Pd lattice vibrations, resulting in a high trapping probability while the stiffer Ni lattice prevents the excitation of surface phonons.

Infrared reflection absorption spectroscopy has established itself as a powerful and versatile technique for monitoring molecular adsorption at well-defined single crystal metal surfaces. The technique itself and its application to hydrocarbon adsorption, both on single crystal surfaces and supported metals, was described in excellent and comprehensive reviews by Sheppard and De La Cruz [78She, 88She, 96She, 97She], including tables of vibrational frequencies, and by Hoffman [83Hof] and others [95Rav]. The technique provides a wide range of information, including the identification of hydrocarbon species and their structure, and of adsorbate-induced surface reconstructions. An important breakthrough was to recognize the analogy of surface-adsorbed hydrocarbons with organometallic complexes [78Kes, 79Kes, 99Ans, 04Ans]. The use of IR spectroscopy in determining the exact nature of chemisorbed species was, however, sometimes questioned [97Bra], in particular the validity of vibrational “fingerprints”. Implications of the surface infrared selection rule for structure determinations were discussed in [76Pea, 94Fan]. For an extensive description of vibrational spectra of hydrocarbon surface species we refer to [97She]. RAIRS spectra of C<sub>2</sub> to C<sub>6</sub> normal alkanes on Pt(111) were reported in [89Che].

Bradshaw [97Bra] described case studies determining structural parameters of molecular fragments created in simple heterogeneous reactions and of hydrocarbons adsorbed on single crystal metal surfaces using electron and X-ray diffraction techniques. Scanned energy mode photoelectron diffraction and diffuse low energy electron diffraction provide access also to adsorption layers that do not show long range order.

Dumas et al. [99Dum] reviewed recent developments in the major experimental vibrational spectroscopies (i.e. infrared absorption, Raman scattering, high resolution electron loss, helium atom scattering and sum frequency generation) and illustrated them with selected results. Particular emphasis was given to two important topics which have attracted much attention: complex surface reactions taking place on technologically relevant surfaces and interfaces, and vibrational dynamics with emphasis on energy dissipation at surfaces.

High resolution electron energy loss spectroscopy (HREELS) [85Koe, 94Iba], is another sensitive and versatile surface analysis technique that can be used to study surface vibrations at an unprecedented level. The most important application of this technique has been to characterize atoms and molecules adsorbed on single crystal metal surfaces.

Steinrück et al. [96Ste, 01Whe, 02Whe] examined the decomposition of unsaturated hydrocarbons on Ni(100) by temperature-programmed X-ray photoelectron spectroscopy using synchrotron radiation. The use of a third generation light source allowed to follow the thermal chemistry of acetylene, ethylene and propene by acquiring high resolution photoemission spectra within a few seconds, approaching “real-time” analysis. The evolution of the C1s core level spectra was monitored in situ between 90 and 530 K. Analysis of binding energies and intensity changes allowed to distinguish various surface intermediates formed during thermal decomposition. Steinrück [96Ste] also reviewed angle-resolved UPS studies employed to investigate the electronic structure and bonding of adsorbed hydrocarbons, the orientation and symmetry of the adsorbate on the surface, the influence of lateral interactions, and the formation of two-dimensional adsorbate band structures. Several examples were presented, including ethylene and acetylene, adsorbed on Ni(110), Ni(111), Ru(001) and the reconstructed Pt(110)1×2 surface.

Solymosi [98Sol] summarized X-ray and ultraviolet photoelectron spectroscopy, high resolution electron energy loss spectroscopy and temperature programmed desorption studies of reactions of hydrocarbon fragments (methylene, methyl, ethyl, propyl and butyl) (with adsorbed oxygen) on various single crystal metal surfaces. The hydrocarbon species were generated by the thermal and photo-induced dissociation of the corresponding iodo-compounds or by azomethane pyrolysis. C<sub>x</sub>H<sub>y</sub> fragments readily combine with adsorbed oxygen atoms above 150 K but the exact oxidation pathways sensitively depend on the nature of the metals.

A comprehensive review of the coordination, structure and reactivity of hydrocarbon ligands on metal cluster compounds, including structural conclusions for adsorbates on single-crystal metal surfaces, was given by Zaera [95Zae]. This topic was also discussed by Bradshaw [95Bra]. Ceyer summarized surface studies of hydrogenation reactions of ethylene, acetylene and hydrocarbon fragments on Ni surfaces, focusing in particular on the reactivity of bulk (dissolved) hydrogen vs. those of surface hydrogen [01Cey].

STM is a very versatile tool that even allows to probe *individual* adsorbed atoms and molecules to reveal properties which otherwise would be hidden in the study of an ensemble of atoms and molecules. Imaging, atom manipulation and chemical modification, as well as spectroscopic characterization by inelastic electron tunneling spectroscopy are fascinating new approaches to study e.g. electronic and vibrational properties of *single* adsorbed hydrocarbon molecules, as discussed by Ho [02Ho].

### 3.8.6.3 Alkanes

Alkanes are chemically saturated molecules which tempers their bond breaking activity even on transition metal surfaces. In the absence of C-H or C-C bond breaking these molecules prefer to adsorb with their carbon chain parallel to the surface since their heat of adsorption increases by ~9 kJ/mol per -CH<sub>2</sub>- group. Thus at low temperatures and on relatively chemically inactive low Miller-index metal surfaces the molecules adsorb intact and in a flat-lying configuration.

As the temperature is increased and/or the metal substrate becomes more corrugated sequential C-H bond breaking occurs to produce organic fragments that become increasingly dehydrogenated as the temperature is raised. The presence of hydrogen would slow down the extent of dehydrogenation. However, few of these alkane adsorption studies have been carried out in the presence of hydrogen.

Adsorption, surface structure and dehydrogenation studies were mostly carried out at low pressures ( $\leq 10^{-7}$  Torr). Studies of these parameters at high reactant pressures (Torr range or higher) are very much needed.

#### 3.8.6.3.1 Methane CH<sub>4</sub>

##### 3.8.6.3.1.1 Co

Burghgraef et al. [95Bur] studied the adsorption of CH<sub>3</sub>, CH<sub>2</sub>, CH, C and H on a one-layer 7-atom cluster and a spherical 13-atom cluster model of cobalt. Starting from gas phase CH<sub>4</sub>, the formation of adsorbed

CH<sub>3</sub> and adsorbed H was endothermic on all clusters, but the endothermicity was strongly reduced on the 13-atom cluster (135 kJ/mol on Co-7, 8 kJ/mol on Co-13). The formation of adsorbed CH<sub>2</sub> and H from CH<sub>3</sub> was endothermic by 25-40 kJ/mol on Co-13, but exothermic on Co-7 (3 kJ/mol), mainly because of the much stronger adsorption of CH<sub>2</sub> on this cluster. The formation of adsorbed CH and H from CH<sub>2</sub> was exothermic on all clusters, but the exothermicity differs by a factor of two between the 7- and 13-atom clusters (60 kJ/mol on Co-7, 32 kJ/mol on Co-13). Finally, the formation of adsorbed C and H from CH was strongly endothermic on the 7 atom clusters, but the endothermicity was again strongly reduced on the 13-atom clusters (77 kJ/mol on Co-7, 14 kJ/mol on Co-13).

#### 3.8.6.3.1.2 Cu

Adsorption of methane on Cu(100) at 24 K was studied by Camplin et al. [95Cam] using RAIRS. Physisorbed mono- and multi-layers were observed. The photochemistry of CH<sub>4</sub> physisorbed on Cu(111) at 35 K was investigated by Watanabe and Matsumoto using TPD [00Wat1]. Methane was photodissociated into hydrogen, methylene, and methyl by 6.4 eV photon irradiation. Post-irradiation TPD showed desorption peaks of ethylene at 115, 380 and 430 K. The peaks were attributed to molecular desorption of ethylene photochemically formed from methane at 35 K, associative thermal recombination of two methylene groups, and thermal disproportional reactions of four methyl groups, respectively. The photoreaction cross-section of methane depletion was estimated to be  $2.0 \times 10^{-20} \text{ cm}^2$ .

#### 3.8.6.3.1.3 Ir

Verhoef et al. [95Ver] measured the initial probability of dissociative chemisorption of CD<sub>4</sub> on the reconstructed Ir(110) surface as a function of polar angle of incidence using vibrationally hot supersonic molecular beams (beam temperature 290 -745 K). The probability of chemisorption scaled approximately with the component of translational energy normal to the surface ( $E_i \cos^2 \theta_i$ ).

#### 3.8.6.3.1.4 Mo

CH<sub>4</sub> adsorption and subsequent decomposition on Mo(100) produced c(4×4)-C, c(2×2)-C, c(6√2 × 2√2)R45°-C and (1×1)-C structures [76Gui].

#### 3.8.6.3.1.5 Ni

Using LEED to study CH<sub>4</sub> adsorption on Ni(100), Maire et al. [70Mai] observed c(2×2) and (2×2) structures. On Ni(110) (2×2), (4×3), (4×5)-C and (2×3)-C were detected, the latter in the temperature range 473-579 K [70Mai, 77Sch, 78Sch]. Above 600 K carbon diffuses into the Ni bulk and forms (4×5)-C superstructures. On Ni(111) (2×2), (2×2)-C, (2×√3), (16√3 × 16√3)R30°-C, (4×5)-C and graphite overlayers were reported at 298 - 660 K [70Mai, 79Sch, 84Ben].

Yoshinobu and Kawai [96Yos1] studied CH<sub>4</sub> adsorption on Ni(100) at 20 K using IRAS and TPD. For the first CH<sub>4</sub> layer bands at 3000, 2884 and 1298 cm<sup>-1</sup> were observed, while only two bands at 3017 and 1304 cm<sup>-1</sup> were observed for the second CH<sub>4</sub> layer. The bands between 3000 and 3017 cm<sup>-1</sup> were assigned to the degenerate CH stretching mode, the bands between 1294 and 1304 cm<sup>-1</sup> to the degenerate deformation mode, and the 2884 cm<sup>-1</sup> band to the symmetric CH stretching mode, respectively. Desorption temperatures of the first and second CH<sub>4</sub> layer were 51 and 34 K, respectively. Interlayer mixing between the first and second methane layers during adsorption was observed.

For dissociative chemisorption of CH<sub>4</sub> on Ni(100) Nielsen et al. [95Nie] measured the initial sticking coefficient between 0.010-7.0 mbar and 375-500 K. A strong pressure dependence was observed,

consistent with a direct dissociation mechanism under these thermal conditions. This was confirmed by experiments where the gas at a low pressure was heated by a thermal finger facing the crystal surface. With the thermal finger at the same temperature as the surface, it was possible to ensure that the methane was fully equilibrated to the crystal and an activation energy of  $59 \pm 1.5$  kJ/mol was determined under isothermal conditions.

McCabe et al. [00McC] described eigenstate-resolved measurements of the dissociative chemisorption of CH<sub>4</sub> on Ni(100) using a supersonic molecular beam-surface scattering apparatus. Infrared light from a narrow-bandwidth tunable laser intersecting a supersonic molecular beam was employed to prepare an ensemble of molecules in a single rotational and vibrational quantum state. Schmid et al. [02Sch] reported state resolved sticking coefficients for highly vibrationally excited CH<sub>4</sub> on Ni(100) at well-defined kinetic energies in the range of 12-72 kJ/mol. Incident CH<sub>4</sub> molecules were prepared by pulsed laser radiation in single rovibrational levels of the first overtone of the antisymmetric stretch  $2\nu_3$  at  $6004.69\text{ cm}^{-1}$  and collided at normal incidence with clean Ni(100). The vibrational excitation enhanced the reaction probability by a factor 100 at an incident translational energy of 72 kJ/mol, but this enhancement increased to more than 4 orders of magnitude at low kinetic energy (from  $\sim 2 \times 10^{-8}$  to  $5 \times 10^{-4}$  (12 kJ/mol)). Despite this large increase in the sticking coefficient, vibrational energy in  $2\nu_3$  appeared to be about 80% as effective as an equivalent amount of translational energy in promoting the chemisorption reaction.

Denecke et al. [05Den, 05Fuh2] reported high resolution XPS spectra of activated CH<sub>4</sub> adsorption on Ni(111) at 120 K, followed by thermal decomposition between 120 and 450 K (Fig. 3). C-H bond breaking occurred already upon adsorption producing adsorbed CH<sub>3</sub>. Species observed during thermal treatment encompass CH, C<sub>2</sub>H<sub>2</sub> and carbon. Fig. 3a shows a series of C 1s spectra taken during annealing of a methyl layer, produced by CH<sub>4</sub> molecules from a molecular beam impinging on Ni(111) with a kinetic energy of 0.54 eV. The spectra, acquired every 10 K (linear heating ramp of 0.4 K/s), showed distinct binding energy changes, characteristic of the occurrence of the different hydrocarbon species. In particular, a vibrational fine structure was observed for the methyl species at low temperature, caused by excitation of the C-H stretching mode in the photoemission process [05Fuh2, 05Den]. The fine structure was then utilized to identify different hydrocarbons and a quantitative analysis was performed employing a fitting routine (Fig. 3b). Interestingly, the CH species could only be observed in a very narrow temperature range.

Kratzer et al. [96Kra] carried out a DFT study of the first step of CH<sub>4</sub> adsorption on Ni(111), i.e. dissociation into adsorbed CH<sub>3</sub> and H. The rupture of the C-H bond occurs preferentially on top of a Ni atom, with a dissociation barrier of  $\sim 100$  kJ/mol (Fig. 4). The transition state involves considerable internal excitation of the molecule. The active C-H bond was both stretched to 1.6 Å and tilted relative to the methyl group. Alloying the surface with gold also affects the reactivity of the Ni atoms on adjacent surface sites. The dissociation barrier was increased by 16 and 38 kJ/mol for a Ni atom with one or two gold neighbors, respectively. These changes were attributed to a shift in the local density of d states at the nickel atoms in the neighborhood of gold.



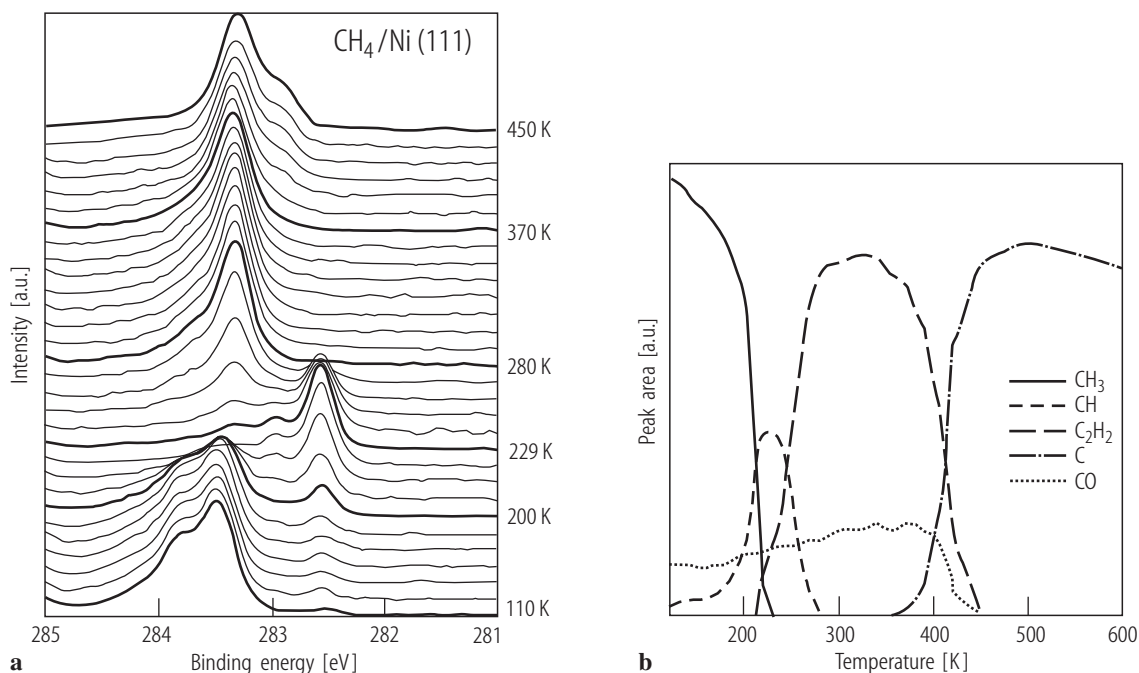


**Fig. 3** (a) Thermal annealing of a CH<sub>3</sub> layer on Ni(111), produced at a surface temperature of 120 K by a molecular beam of CH<sub>4</sub> molecules with a kinetic energy of 0.54 eV. XPS C1s spectra were taken approximately every 10 K (heating ramp 0.4 K/s). Important spectra are highlighted by thick lines and labeled with the respective temperatures. (b) Quantitative analysis of the spectra in (a), shown are total intensities of the marked species (small amounts of CO result from background adsorption); adapted from [05Den].

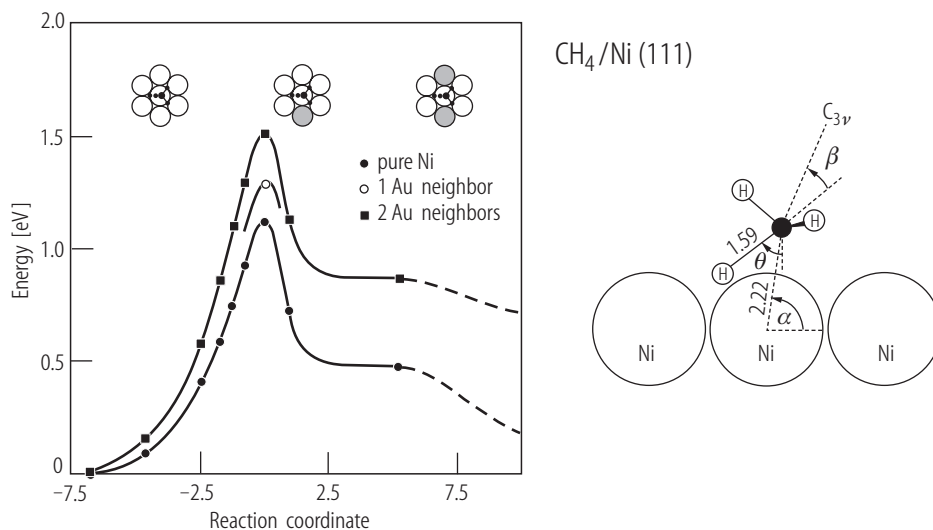


**Fig. 4.** The energy along the reaction path for CH<sub>4</sub> dissociation over a Ni atom in the Ni(111) surface, as calculated by DFT. The rightmost data points (dashed curves) refer to infinite separation of the dissociated H and CH<sub>3</sub> group on the surface. The geometry of the transition state is shown on the right. The angles  $\alpha \sim 80^\circ$  and  $\theta = 55^\circ$  denote the orientation of the C-Ni and C-H bond. The C<sub>3v</sub> symmetry axis of the CH<sub>3</sub> group (note that one H atom is hidden) forms an angle  $\beta \sim 30^\circ$  with the active C-H bond; adapted from [96Kra].

Burghgraef et al. [95Bur] studied the adsorption of CH<sub>3</sub>, CH<sub>2</sub>, CH, C and H on a one-layer 7-atom nickel cluster and a spherical 13-atom cluster. Starting from gas phase CH<sub>4</sub>, the formation of adsorbed

CH<sub>3</sub> and adsorbed H was endothermic on all clusters, but the endothermicity was strongly reduced on the 13-atom clusters (142 kJ/mol on Ni-7, 30 kJ/mol on Ni-13). The formation of adsorbed CH<sub>2</sub> and H from CH<sub>3</sub> was endothermic by 25-40 kJ/mol on all clusters. The formation of adsorbed CH and H from CH<sub>2</sub> was exothermic on all clusters, but the exothermicity differs a factor two between the 7- and 13-atom clusters (61 kJ/mol on Ni-7, 27 kJ/mol on Ni-13). Finally, the formation of adsorbed C and H from CH was strongly endothermic on the 7 atom clusters, but the endothermicity was strongly reduced on the 13-atom clusters (92 kJ/mol on Ni-7, 27 kJ/mol on Ni-13).

#### 3.8.6.3.1.6 Pd

Activated adsorption of CH<sub>4</sub> on clean and oxygen modified Pd(110) was studied by Valden et al. [97Val] using molecular beam methods. The absolute dissociation probability of CH<sub>4</sub> was measured as a function of the incident normal energy and the surface temperature and a direct dissociation mechanism was suggested. The dissociation probability decreased linearly with increasing oxygen coverage.

Klier et al. [97Kli] studied C-H bond dissociation of CH<sub>4</sub> at 400-600 K on Pd(111) and Pd(311) surfaces, and compared it to Pd(679). C-H bond dissociation was found to be structure sensitive, in the order Pd(111)<Pd(311)<Pd(679), while the effective activation energies range from 32-34 kJ/mol for Pd(111) and Pd(311) to 44 kJ/mol for Pd(679). However, the Pd(679) surface provides a driving force of 26 kJ/mol due to the defects compared to smooth planar Pd(111) and 22 kJ/mol compared to the Pd(311) surface.

Liu and Hu [03Liu] reported a DFT study of CH<sub>4</sub> dissociation to CH<sub>3</sub> and H and the reverse reaction on flat, stepped and kinked Pd surfaces. For the CH<sub>4</sub> to CH<sub>3</sub> + H reaction, the dissociation barrier was reduced by ~0.3 eV on steps and kinks as compared to that on flat surfaces. On the other hand, there was essentially no difference in the barrier for the association reaction of CH<sub>3</sub> + H on the flat surfaces and the defects. The DFT calculations show that surface defects such as steps and kinks can largely facilitate bond breaking, while whether surface defects could promote bond formation rather depends on the individual reaction as well as the particular metal. On late transition metals reactions are more likely to proceed on defects than on early transition metals.

#### 3.8.6.3.1.7 Pt

The dynamics of CH<sub>4</sub> trapping on clean Pt(111) was investigated by Carlsson, Madix [00Car, 01Car] and others [89Aru] using molecular beam techniques at 50 K, well below the desorption temperature of 67 K. The initial trapping probability for CH<sub>4</sub> scales with normal incident energy ( $E_T \cos^2 \theta$ ), indicating a smooth gas-surface potential. The trapping probability decreased from 0.7 to zero as the incident normal energy was increased from 3 to 20 kJ mol<sup>-1</sup> (Fig. 5). Trapping on the methane-saturated surface was greatly enhanced compared to the clean surface at all incident energies and angles, and exhibited near total energy scaling ( $E_T \cos^{0.3} \theta$ ), indicating a corrugated gas-surface potential. The trapping probability increased with coverage, indicating that trapping into an extrinsic precursor state is more efficient than trapping onto the bare Pt(111) surface. Molecular beam experiments on Pt(111) were also reported by Yagyu et al. [99Yag].

Fuhrmann et al. [04Fuh, 05Fuh1] studied the activated adsorption of methane on Pt(111) by combining a supersonic molecular beam and in situ high-resolution X-ray photoelectron spectroscopy. Exposing the surface at 120 K to a CH<sub>4</sub> beam with kinetic energies between 0.30 and 0.83 eV produced CH<sub>3</sub>. The spectra show a unique fine structure, caused by vibrational excitations of C-H stretching modes in the photoemission process. Upon heating to ~260 K adsorbed methyl partly dehydrogenated to CH and partly recombined to methane, which desorbed. Adsorption at 300 K yielded CH as surface species.

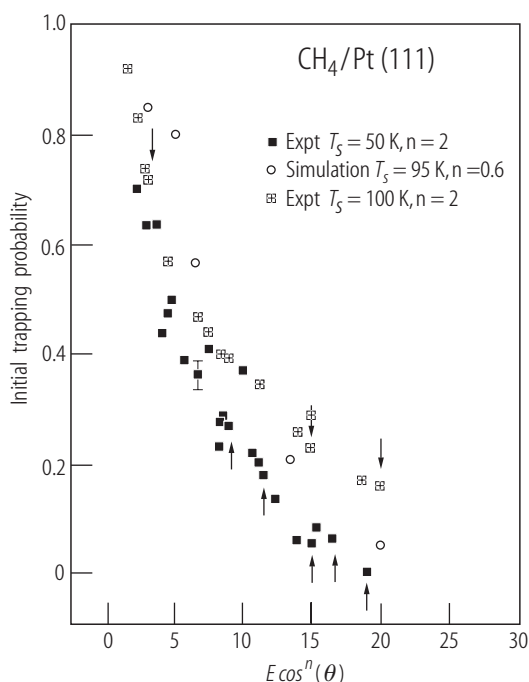


**Fig. 5** The adsorption probability of CH<sub>4</sub> on Pt(111) versus the scaling function  $E_T \cos^n \theta$  for molecular beam measurements at 50 K and 100 K, compared with molecular dynamics simulations. Adsorption probabilities are plotted with the optimum scaling parameter. Points at normal incidence are indicated; adapted from [00Car].

Yoshinobu et al. [96Yos2] studied CH<sub>4</sub> adsorption on Pt(111) and processes photoinduced by ArF laser irradiation (193 nm) using IRAS. The symmetry of the first layer methane was degraded from T<sub>d</sub> to C<sub>3v</sub> (or lower symmetry), but the symmetry of subsequent methane layers maintained T<sub>d</sub>. The CH<sub>4</sub> multilayer and first layer molecules desorbed from Pt(111) at ~40 and ~70 K, respectively. The first layer C<sub>3v</sub> CH<sub>4</sub> photodissociated into CH<sub>3</sub> and H species. These reaction products modified the surface such that the remaining first-layer CH<sub>4</sub> molecules became photochemically inactive, and thus the reaction became self-limiting. The photoreaction kinetics was studied with time-resolved IRAS, and the total cross-sections were estimated to be  $\sigma = 2.6 \times 10^{-19} \text{ cm}^2$  for CH<sub>4</sub> and  $\sigma = 1.7 \times 10^{-19} \text{ cm}^2$  for CD<sub>4</sub>.

Activated adsorption of CH<sub>4</sub> on clean and oxygen modified Pt(111) was studied by Valden et al. [97Val] with molecular beams. The results from clean Pt(111) were consistent with a direct dissociation mechanism and the dissociation probability decreased linearly with increasing oxygen coverage.

#### 3.8.6.3.1.8 Rh

Liu and Hu [03Liu] reported a DFT study of CH<sub>4</sub> dissociation to CH<sub>3</sub> and H and the reverse reaction on flat, stepped and kinked Rh surfaces. For the CH<sub>4</sub> to CH<sub>3</sub> + H reaction, the dissociation barrier was reduced by ~0.3 eV on steps and kinks as compared to that on flat surfaces. On the other hand, there was essentially no difference in the barrier for the association reaction of CH<sub>3</sub> + H on the flat surfaces and the defects. The DFT calculations show that surface defects such as steps and kinks can largely facilitate bond breaking. However, whether surface defects promote bond formation or not rather depends on the individual reaction as well as on the particular metal.

#### 3.8.6.3.1.9 Ru

Goodman and coworkers [94Wu, 02Cho] studied the surface species formed during CH<sub>4</sub> decomposition on Ru(0001) and Ru(1120) by HREELS and TPD. Methane dissociated on Ru(0001) to methylidyne (CH) and vinylidene (CCH<sub>2</sub>), while on Ru(1120) CH, CCH<sub>2</sub> and ethylidyne (CCH<sub>3</sub>) were found. Above 700 K graphitic phases formed.

### 3.8.6.3.1.10 Si

Adsorption of hot filament activated  $\text{CH}_4$  on Si(100) was reported in [93Jac, 94Chu1]. Thermal dehydrogenation to carbon competes with thermal desorption and polymerization to volatile species.

### 3.8.6.3.1.11 W

Nahm and Gomer [97Nah] investigated the adsorption of  $\text{CH}_4$  and  $\text{CD}_4$  on W(110). A monolayer of methane, probably containing  $7 \times 10^{14}$  molecules  $\text{cm}^{-2}$  was adsorbed at 25 K and desorbed near 50 K. A desorption activation energy of ca. 8  $\text{kJ mol}^{-1}$  was determined.  $(5 \times 1)$ -C carbon overlayers were detected upon  $\text{CH}_4$  adsorption on W(100) and  $(6 \times 6)$ -C on W(111) [69Bou].

### 3.8.6.3.1.12 Various

Au et al. [98Au] presented a comprehensive theoretical treatment of the partial oxidation of  $\text{CH}_4$  to syngas on Ni, Pd, Pt and Cu catalysts. Using cluster models of 7-13 atoms, the adsorption energies for a number of intermediates in the dissociation of methane on the metals were calculated and reaction energies for methane dissociation were determined. Larsen and Chorkendorff [98Lar] investigated the reactivity of Co films deposited on Cu(111) towards  $\text{CH}_4$  dissociation using a molecular beam source. A few layers of Co on Cu were found to be more active than pure Co itself.

### 3.8.6.3.2 Ethane $\text{C}_2\text{H}_6$

#### 3.8.6.3.2.1 Ir

The initial probability of dissociative chemisorption of  $\text{C}_2\text{H}_6$  and  $\text{C}_2\text{D}_6$  on the reconstructed Ir(110) surface was measured as a function of polar angle of incidence using vibrationally hot supersonic molecular beams [95Ver, 95Sou]. The chemisorption probability scaled approximately with the component of translational energy normal to the surface ( $E_i \cos^2 \theta_i$ ), for  $\text{C}_2\text{D}_6$  (Fig. 6) [95Ver]. Steinrück et al. [86Ste] reported that  $S_0$  is constant at  $\sim 0.03$  at kinetic energies  $< 62$   $\text{kJ/mol}$  and increased nearly linear to a value of 0.40 at an energy near 165  $\text{kJ/mol}$ .

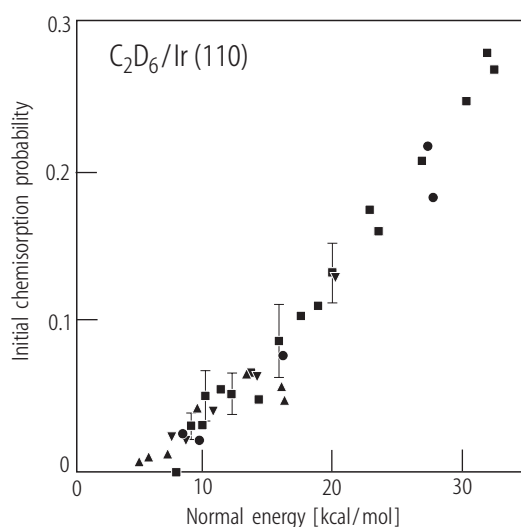


**Fig. 6** The initial probability of dissociative chemisorption as a function of normal ( $E_i \cos^2 \theta_i$ ) translational energy of  $\text{C}_2\text{D}_6$  on Ir(110) for a beam temperature of 745 K (molecular beam measurements). Data are for polar angles of incidence  $\theta_i$  with respect to the surface normal of  $0^\circ$  (■),  $22.5^\circ$  (●),  $30^\circ$  (▼) and  $45^\circ$  (▲); adapted from [95Ver].

### 3.8.6.3.2.2 Ni

LEED studies of  $C_2H_6$  adsorption detected  $c(2\times 2)$  and  $(2\times 2)$  structures on Ni(100) [70Mai],  $(2\times 2)$  on Ni(110) [70Mai], and  $(2\times 2)$ ,  $(2\times\sqrt{3})$ ,  $(\sqrt{7}\times\sqrt{7})R19^\circ$ -C,  $(2\times 2)$ -C and disordered graphite on Ni(111) [69Ber, 70Mai, 84Ben].

### 3.8.6.3.2.3 Pd

Kao et al. [02Kao] investigated the  $C_2H_6$  trapping on Pd(111) by molecular beam techniques and stochastic trajectory simulations. The initial trapping probability was measured over the range of incident energy,  $E_T$ , from 10 to 34 kJ/mol and incident angles,  $\theta$ , from  $0$ – $45^\circ$  at 95 K. The trapping probability scales with  $E_T \cos^{0.9} \theta$ , indicating a corrugated gas-surface potential. Simulations predicted the experimental values of the initial trapping probability within 30%. Calculations of energy transfer for  $C_2H_6$  after the first bounce on Pd(111) clearly indicated that vibrational excitation of the lattice phonons account primarily for the increase in trapping probabilities of  $C_2H_6$  on Pd(111) compared with Pt(111).

### 3.8.6.3.2.4 Pt

The molecular adsorption probability of  $C_2H_6$  on clean Pt(110)- $(1\times 2)$  at 95 K was measured by Stinnett et al. [96Sti] using molecular beams. At normal incidence the adsorption probability decreased with incident translational energy from near unity ( $E_T$  10 kJ/mol) to 0.5 (40 kJ/mol). For molecules incident with the tangential velocity component directed along the  $[1\bar{1}0]$  (smooth) direction, the initial adsorption probability increased with increasing  $\theta_i$ , scaling with  $E_T \cos^{0.6} \theta_i$ ; however, the adsorption probability decreased with  $\theta_i$  for molecular beams directed along the  $[100]$  (rough) direction. Stochastic trajectory simulations illustrated that collisions on the ridges of Pt(110)- $(1\times 2)$  mitigate against trapping of ethane while collisions within the troughs facilitate trapping.

Madix and coworkers [90Aru, 92McM, 93McM1, 94Sou, 97Sti, 98Sti1, 00Kao] studied  $C_2H_6$  trapping on Pt(111) and Pt(111)- $p(2\times 2)$ -O by supersonic molecular beams. The initial trapping probability at 100 K was measured in the range of incident energy from 10 to 45 kJ/mol and incident angles from  $0^\circ$  to  $60^\circ$ , yielding e.g. 0.85 for  $E \cos \theta = 10$  and 0.06 for  $E \cos \theta = 35$ . A broad angular distribution of scattered ethane and total energy scaling with  $E_T \cos^{0.2} \theta$  for ethane trapping indicated a corrugated gas-surface potential. Calculations of energy transfer for ethane after the first bounce on Pt(111) and Pt(111)- $p(2\times 2)$ -O clearly indicate that interconversion of parallel and perpendicular momentum and energy transfer to lattice vibrations account primarily for the differences in trapping probabilities between ethane on the two surfaces. At glancing incidence trapping is not significantly reduced on the oxygen-covered Pt(111) because the parallel momentum appears to be transferred partially to phonons.

Newell et al. [98New] reported the IRAS spectrum of adsorbed ethyl ( $C_2H_5$ ) on Pt(111) produced by the dissociative adsorption of  $C_2H_6$  from a supersonic molecular beam at 150 K. The thermal chemistry of the  $C_2H_5$  fragment was followed by IRAS and TPD, indicating the presence of ethylidene ( $=CHCH_3$ ) and ethylidyne ( $\equiv CCH_3$ ) at 250 and 350 K, respectively. This implies the stepwise loss of one and two hydrogen atoms from the ethyl moiety during the heating process. TPD measurements showed that hydrogen desorption was not accompanied by desorption of either saturated or unsaturated C-2 hydrocarbons or methane. RAIRS spectra of  $C_2H_6$  on Pt(111) were also reported by Chesters et al. [89Che]. The spectra indicated that the orientation of the plane containing the carbon chains was almost exclusively parallel to the metal surface in the case of monolayers. Multilayers were consistent with liquid-like films.

### 3.8.6.3.2.5 Ru

Disordered C<sub>2</sub>H<sub>6</sub> layers were reported for Ru(0001) at 80 K [78Mad].

### 3.8.6.3.2.6 W

(1×1) C<sub>2</sub>H<sub>6</sub> layers were reported for W(111) [78Win].

### 3.8.6.3.3 Propane C<sub>3</sub>H<sub>8</sub>

#### 3.8.6.3.3.1 Ir

Precursor-mediated dissociative adsorption of C<sub>3</sub>H<sub>8</sub> on Ir(110)-(1×2) dominates over direct dissociation at low incident kinetic energies for surface temperatures at least up to 1000 K [95Sou].

#### 3.8.6.3.3.2 Mo

Microcalorimetric studies of C<sub>3</sub>H<sub>8</sub> adsorption on polycrystalline Mo film reported a heat of adsorption of 558 kJ mol<sup>-1</sup> at 295 K ( $\theta \rightarrow 0$ ) [77Smu].

#### 3.8.6.3.3.3 Ni

Hamza and Madix [87Ham] used supersonic molecular beam techniques to examine the dissociative chemisorption of C<sub>3</sub>H<sub>8</sub> (and other saturated C<sub>1</sub> to C<sub>4</sub> hydrocarbons) on Ni(100) using molecular beams. For incident translational energies less than 10 kJ/mol no measurable adsorption was observed at 500 K. The initial sticking probability for propane at 120 kJ/mol incident beam energy was independent of surface temperature from 300 to 700 K (~0.25), suggesting a direct mechanism for dissociation.

#### 3.8.6.3.3.4 Pt

McMaster et al. [93McM2] measured the molecular adsorption probability of C<sub>3</sub>H<sub>8</sub> on clean and propane-covered Pt(110)-(1×2) at 95 K using molecular beams. Adsorbed propane facilitated trapping; S<sub>0</sub> increased linearly with propane coverage up to 0.55 ML saturation coverage.

IRAS spectra of C<sub>3</sub>H<sub>8</sub> on Pt(111) were reported by Chesters et al. [89Che], both for monolayers and multilayers. The spectra indicated that the orientation of the plane containing the carbon chains was almost exclusively parallel to the metal surface in the case of monolayers. Propane multilayers were consistent with liquid-like films. Microcalorimetric studies of C<sub>3</sub>H<sub>8</sub> adsorption on polycrystalline Pt film report a heat of adsorption of 248 kJ mol<sup>-1</sup> at 295 K ( $\theta \rightarrow 0$ ) [84Pal].

Wang [03Wan] studied the effect of surface steps on Pt(655) on the molecular adsorption of C<sub>3</sub>H<sub>8</sub> by molecular-dynamics simulations. Incidences along the step edge and perpendicular to the step edge with upstairs and downstairs momentum were considered. In general, the surface step enhanced the initial trapping probability of C<sub>3</sub>H<sub>8</sub> except for the downstairs incidences. The most efficient adsorption zone was near the bottom of the surface step on the lower terrace. The least efficient zone was the top of the surface step on the upper terrace. The surface steps also created a steric effect, i.e. more incident molecules along the upstairs azimuth impact the step-bottom zone but significantly less molecules along the downstairs azimuth. This “shadowing effect” reduces the high trapping efficiency of the step-bottom zone and causes the downstairs incidences to have the lowest trapping probabilities. However, the influence of surface

steps diminished at low incident energies and large incident angles because longer contact times and less normal momenta result in a high trapping probability across the entire stepped surface.

#### 3.8.6.3.4 Butane $C_4H_{10}$

##### 3.8.6.3.4.1 Ag

Pawela-Crew and Madix [95Paw1, 95Paw2] applied TPD, XPS and NEXAFS to study the desorption kinetics of butanes on Ag(110) which shows evidence of weak attractive intermolecular interactions. Activation energies of desorption at zero coverage were  $44 \pm 1.2$  and  $41 \pm 1.2$  kJ/mol for n-butane and isobutane, respectively.

##### 3.8.6.3.4.2 Mo

Kelly et al. [86Kel] investigated the chemisorption and reactions of n-butane on clean Mo(100), and with sulfur or carbon overlayers, using TDS. At low additive coverage (0-0.2 monolayers of S or C), and at low ambient pressure ( $10^{-10}$  Torr) a large fraction (95%) of butane desorbed molecularly at all additive coverages. As additive (S or C) coverage increased the amount of decomposition decreased, enabling hydrogenation, partial dehydrogenation, and isomerization to become more probable. Molecular binding on the additive overlayers was also found to be very different. On S overlayers the binding of the hydrocarbon was weak (physisorption), usually on the order of the heat of sublimation (38-42 kJ/mol). However, molecular binding on C overlayers was stronger: the heat of desorption was 46 kJ/mol.

##### 3.8.6.3.4.3 Pt

Using LEED Firment and Somorjai reported various superstructures and order-disorder transitions of butane on Pt(111) at 100-220 K (Fig. 7) [77Fir]. The chain axis is aligned parallel to the Pt surface and to  $Pt[1\bar{1}0]$ .

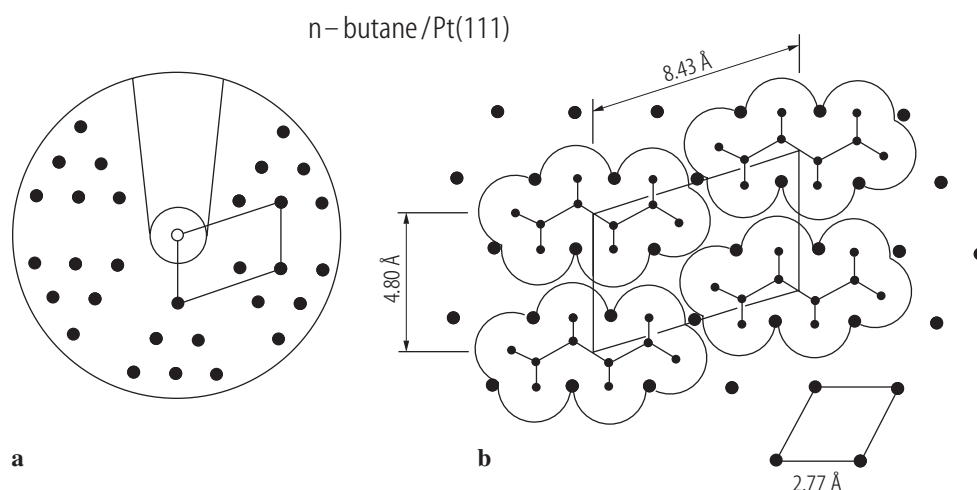


**Fig. 7** (a) Schematic LEED pattern at 19.5 eV of an n-butane monolayer on Pt(111) (below 105 K). (b) Real space unit mesh of the structure with the proposed arrangements of molecules; adapted from [77Fir].

Raut et al. [97Rau] used molecular-dynamics simulations to study the structure and mobility of n-butane adlayers on Pt(111), for submonolayers and the multilayer regime. At submonolayer coverages n-butane molecules adsorb with their molecular plane parallel to the surface. Upon increasing coverage close to a monolayer, some of the molecules form a tilted structure with their long axes oriented away from the surface. At monolayer saturation, the molecules exhibit temperature-dependent ordering similar to previous LEED studies [77Fir]. At moderate submonolayer coverages, the diffusion activation energy is coverage-independent. In the multilayer regime, molecules in the top layer were an order of magnitude more mobile than those in the layer adjacent to the surface. Vibrational characteristics of the adsorbed butane molecules were also discussed.

IRAS spectra of  $C_4H_{10}$  on Pt(111) were reported by Chesters et al. [89Che], both for monolayers and multilayers. The spectra indicated a parallel orientation of the plane containing the carbon chains with respect to the metal surface for monolayers. The multilayers appeared to be crystalline again with molecules aligned so that the plane containing the carbon atoms was parallel to the substrate.

Weaver et al. [01Wea] studied n-butane adsorption on Pt(111) using molecular beam techniques, TPD and LEED. Below 0.14 ML coverage a disordered monolayer formed, from 0.14 to 0.20 ML ordered regions developed, with the  $C_4H_{10}$  molecules preferentially oriented parallel to the surface. After the low-coverage ordered phase saturates at 0.20 ML, a more densely-packed ordered phase formed at 98 K, with the n-butane molecules probably tilted away from the surface. After the high coverage ordered phase saturated at 0.35 ML, a disordered second layer was observed.

#### 3.8.6.3.4.4 V

Chen [95Che] investigated the adsorption and decomposition of n-butane on clean and carbide-modified V(110) by HREELS and TDS. The formation of carbide significantly modified the reactivity of vanadium. n-butane interacted very weakly and reversibly with the clean surface but the reactivity was enhanced on carbide-modified surfaces.

#### 3.8.6.3.5 Pentanes $C_5H_{12}$ and higher alkanes

##### 3.8.6.3.5.1 Au

Chesters and Somorjai observed no n-heptane  $C_7H_{16}$  adsorption on Au(111) and Au(S)-[6(111)  $\times$  (100)] under low pressure ( $\sim 10^{-6}$  Torr) at 300 K [75Che]. Scoles and coworkers [98Wet, 00Lib] used helium atom reflectivity to study the adsorption of n-alkanes on Au(111). For the long-chain n-alkanes studied ( $C_6H_{14}$  -  $C_{12}H_{26}$ ), the physisorption energy increased linearly with the chain length by  $6.2 \pm 0.2$  kJ/mol per additional methylene unit. Collision-induced desorption (CID) of n-alkanes of various chainlengths ( $C_nH_{2n+2}$ ,  $n = 5, 7, 10, 12$ ) physisorbed on Au(111) was reported in [00Lib]. The adsorbed layers were exposed to a beam of hyperthermal Xe generated in a supersonic expansion (translational energies of 1.6-5.8 eV), with adsorbate coverages detected by He atom reflectivity. The n-alkanes show a strong chain-length-dependent reduction of the CID cross sections.

##### 3.8.6.3.5.2 Cu

Fuhrmann and Wöll [97Fuh] studied monolayers of saturated long-chain hydrocarbons (n-octane, perdeuterated n-octane, n-nonane and n-decane) adsorbed on a Cu(111) surface by high-resolution elastic and inelastic He atom scattering. At low temperatures ( $< 160$  K) the alkane chains form an ordered, well-defined two-dimensional lattice with the molecular C-C-C planes being oriented parallel to the surface. At higher temperatures a phase transition to a disordered, liquid-like state with the transition temperature dependent on the length of the hydrocarbon chain was observed.



### 3.8.6.3.5.3 Pt

Adsorption of n-hexane  $C_6H_{14}$  on Pt(111) at 100-220K was reported in [77Fir]. n-heptane  $C_7H_{16}$  adsorption on Pt(111) produced (2×2) overlayers [74Bar, 77Fir]. On the stepped Pt(S)-[4(111) × (100)] surface, (4×2) and (4×2)-C structures were observed while on Pt(S)-[6(111) × (100)] (2×2) and (9×9)-C appeared [74Bar]. On Pt(S)-[7(111) × (310)]  $C_7H_{16}$  adsorbed disordered, on Pt(S)-[9(111) × (100)] (2×2), (5×5)-C, (2×2)-C and 2 (one-dimensional order)-C was detected [74Bar]. n-octane adsorption was reported in [77Fir].

Using supersonic molecular-beam techniques Weaver et al. [97Wea, 98Wea] measured adsorption probabilities for neopentane on Pt(111) for coverages from zero to monolayer saturation (for incident translational energies up to 110 kJ mol<sup>-1</sup> and incident angles between 0° and 60° at 105 K). The adsorption probability increased with coverage up to near monolayer saturation and an enhanced trapping into the second layer was suggested. Dissociative chemisorption occurs by both direct collisionally activated and trapping-mediated mechanisms. Direct dissociation dominates at translational energies > ~110 kJ mol<sup>-1</sup> while the trapping-mediated pathway occurred at translational energies <110 kJ mol<sup>-1</sup>. Trapping-mediated dissociation seemed facilitated by surface defects.

IRAS spectra of pentane and hexane on Pt(111) were reported by Chesters et al. [89Che], both for monolayers and multilayers. The spectra indicated that the orientation of the plane containing the carbon chains was parallel to the metal surface in the case of monolayers. The multilayers appeared to be crystalline with molecules aligned so that the plane containing the carbon atoms was parallel to the substrate in the case of hexane but with this plane at an angle to the surface in the case of pentane.

### 3.8.6.3.6 Various (Hydrocarbon fragments, Radicals, etc)

For an extensive description of vibrational spectra of hydrocarbon surface species, obtained from the dissociative adsorption of halogen- or nitrogen-substituted alkanes and olefins see [97She].

### 3.8.6.3.6.1 Cu

Chuang et al. [99Chu] investigated the interactions of methyl and methylene radicals on Cu(111) with XPS, AES and HREELS. The  $CH_2$  and  $CH_3$  radicals were generated through a hot nozzle source with ketene and azomethane gases. It was shown that at 300 K the impinging  $CH_3$  radicals were trapped mainly as  $CH_3$ , while a part decomposed to  $CH_2$  and H. The hydrocarbon adspecies desorbed at ~420 K. Exposing the clean Cu surface to methylene radicals resulted not only in the trapping of  $CH_2$ , but also in the formation of complex aromatic species. The adlayer was sensitive to annealing and desorption and partial conversion to methylidyne took place at ~420 K. The CH species survived up to 700 K and then decomposed to form residual carbon above 800 K. In both radical-Cu(111) systems, surface coverage appeared to saturate near one monolayer.

### 3.8.6.3.6.2 Mo

Wu et al. [99Wu] measured IRAS spectra (700-2300 cm<sup>-1</sup>) of  $CH_3I$ ,  $CD_3I$ ,  $CH_2I_2$  and  $CD_2I_2$  adsorbed on Mo(100) at 80 K. Initially, the strongest infrared absorption was the  $\delta_s(CH_3)$  mode of  $CH_3I$  at 1236 cm<sup>-1</sup>, which shifts on heating to 135 K, yielding a new peak at 1106 cm<sup>-1</sup> indicating the formation of a surface- $CH_3$  species.  $CH_3$  species dominated the spectrum after annealing to 160 K and disappeared at 235 K, where TPD showed methane desorption. When  $CH_2I_2$  was adsorbed on Mo(100), the  $\omega(CH_2)$  mode at 1107 cm<sup>-1</sup> was the strongest feature, and upon heating to 135 K, a new peak appeared at 1061 cm<sup>-1</sup>, which was ascribed to a surface- $CH_2I$  species. This peak disappeared on heating to about 200 K, where UPS data showed the formation of a surface C-1 species. No IRAS data were detected for adsorbed-

methylene species, because of either a low-adsorption cross section or the lack of appropriate symmetry of these modes.

Parker et al. [97Par] used HREELS and LEED to examine the adsorption of methyl radicals on two different oxygen-modified Mo(100) surfaces at 300 K. CH<sub>3</sub> radicals produced CH<sub>4</sub>, H<sub>2</sub> and CO as reaction products. No surface methoxy but rather a metal alkyl analog was observed.

#### 3.8.6.3.6.3 Ni

Dickens and Stair [98Dic] studied the adsorption of CH<sub>3</sub> radicals on clean Ni(100), on Ni(100) with a chemisorbed oxygen overlayer, and on Ni(100) with a NiO(111) oxide overlayer by XPS and TPD. Methyl radical dosing at surface temperatures of 120-170 K produced carbon coverages in excess of 5 monolayers with a C1s peak indicative of an adsorbed hydrocarbon species. The carbon coverage never saturated on any surface. TPD indicated C<sub>2</sub>-C<sub>4</sub> formation following very large methyl radical exposures. The results were indicative of the formation of surface hydrocarbon chains. The methyl radical gas temperature had no effect on the surface chemistry. However, hydrocarbon chains formed with higher selectivity on the oxygen-modified surfaces compared to the clean surface suggesting that a direct reaction between incoming methyl radicals and adsorbed hydrocarbon groups is not involved. The chains are likely produced by polymerization of surface methylene species (-CH<sub>2</sub>-) produced by dehydrogenation of chemisorbed methyl groups via a mechanism similar to the Fischer-Tropsch synthesis reaction. On NiO, TPD indicated that surface alkoxy groups were formed based on the low-temperature desorption of CO.

The chemistry of various alkyl fragments on Ni(100), produced from iodo-precursors, was described by Tjandra and Zaera [95Tja]. 1-iodopropane, 1-iodobutane, 2-iodobutane, 1-iodo-2-methylpropane, 2-iodo-2-methylpropane, 1-iodopentane and 1-iodohexane on Ni(100) surfaces were studied by TPD and XPS. Below 100 K, all compounds adsorbed molecularly through the iodine atom. The hydrocarbon chain oriented parallel to the surface at first, but flipped as the coverage increased, and became perpendicular to the surface at saturation. The C-I bond dissociated between 120 and 180 K to yield the corresponding alkyl fragment on the surface. At higher temperatures the alkyl groups decomposed further, directly to carbon and hydrogen at low coverages (below half-saturation), but mainly to a mixture of alkanes and alkenes at saturation.

Yang et al. [95Yan] reported HREELS spectra of CH<sub>3</sub>, CH<sub>2</sub>D and CD<sub>3</sub> on Ni(111) (and of products of their reactions). Adsorbed methyl radicals originated from CH<sub>4</sub>, CH<sub>3</sub>D, or CD<sub>4</sub>. The CH<sub>3</sub> radical was adsorbed with C<sub>3v</sub> symmetry on a threefold hollow site and dissociated to form adsorbed CH above 150 K. The CH species adsorbed on a threefold hollow site with the geometry of Ni<sub>3</sub>-C-H being pyramidal. Above 250 K, carbon-carbon bond formation between CH species produced C<sub>2</sub>H<sub>2</sub>. Low coverages of C<sub>2</sub>H<sub>2</sub> dehydrogenated at 400 K while high coverages of C<sub>2</sub>H<sub>2</sub> trimerized to adsorbed benzene (no C<sub>2</sub>H<sub>2</sub> dissociation to adsorbed CH). The relative stabilities of the hydrocarbon species on Ni(111) were suggested to be CH<sub>3</sub> < CH + 2H < 1/2 C<sub>2</sub>H<sub>2</sub> + 2H < 1/6 C<sub>6</sub>H<sub>6</sub> + H<sub>2(g)</sub>.

Adsorbed CH<sub>3</sub> on Ni(111) was examined by Kratzer et al. [96Kra] using DFT (see section 3.8.6.3.1.5). The adsorption of CH<sub>x</sub> (x = 1-3) species on Ni(111) was examined by Watwe and coworkers [00Wat2] using periodic infinite plane wave slab calculations in conjunction with DFT and ultrasoft pseudopotentials. The reaction of surface carbon with dihydrogen to methane (or, equivalently, the conversion of methane to surface carbon) was described by a potential energy diagram, including all adsorbed intermediates and transition states. All CH<sub>x</sub> intermediates prefer threefold sites. The transition states involve the formation of C-H bonds on top of a Ni atom, with the reaction coordinate being primarily a C-H stretch. The calculated activation energies to form the C-H bond are near 70-85 kJ/mol for different CH<sub>x</sub> species. The calculated results were applied to estimate kinetic parameters involved in the CO methanation over nickel. Adsorbed CO and CH are the most abundant species on the surface, and the energies of the transition states to form methyl species from methylene species and to form methane from methyl species seemed to control the rate of the methanation reaction.

Azizian and Gobal [00Azi] studied the decomposition of methyl iodide on Ni(111) by bond order conservation-Morse potential (BOC-MP) analysis. The decomposition of methyl iodide on clean Ni(111) (or in the presence of hydrogen) gives rise to the desorption of methane which appears as two peaks at

two different temperatures (150 and 250 K) in course of TPD. Methyl groups adsorbed on 3-fold sites react with adsorbed hydrogen atoms with an activation energy of 58 kJ/mol to form gaseous methane desorbing at 250 K. The methane peak at 150 K in TPD was attributed to mobile methyl groups (at high coverage) reacting with hydrogen with zero activation energy. These CH<sub>3</sub> groups traverse over on-top sites and have higher energy than the methyl groups adsorbed on 3-fold sites. The cleavage of C-I bond with an activation energy of 12 kJ/mol constituted the rate determining step.

#### 3.8.6.3.6.4 Pt

Minot et al. [83Min] performed a molecular orbital study of the location of CH<sub>n</sub> and C-CH<sub>n</sub> (n=1-3) species on Pt(111) by using both a cluster model and a band structure calculation within the framework of the Extended Hückel Theory (EHT). The reported dependence of the adsorption site on the number of hydrogens in the CH<sub>n</sub> fragments suggested that any C-H bond breaking in CH<sub>n</sub> species must involve a change of the adsorbate bonding site. The carbon was found to be located on the surface in such a way as to complete its tetra-valency. Thus, CH occupies a three-fold coordinated hollow site, CH<sub>2</sub> a two-fold coordinated bridge site and CH<sub>3</sub> a one-fold coordinated top site, C-CH<sub>3</sub> (ethynylidyne) was found to be perpendicular to the surface in a three-fold hollow site in agreement with experimental observations. It was also found that a displacement of -C-CH<sub>2</sub>-R to a top site makes a β C-R cleavage easier.

Henderson et al. [87Hen, 91Hen] used HREELS, TPD, SIMS and AES to study methyl iodide on Pt(111). CH<sub>3</sub>I decomposes to CH<sub>3</sub> and I at ~250 K. CH<sub>4</sub> is formed at 290 K by hydrogenation of CH<sub>3</sub> groups with H being supplied from the decomposition of other CH<sub>3</sub> groups.

Newell et al. [98New] reported the IRAS spectrum of adsorbed ethyl (C<sub>2</sub>H<sub>5</sub>) on Pt(111) produced by the dissociative adsorption of C<sub>2</sub>H<sub>6</sub> from a molecular beam at 150 K. IRAS indicated the presence of ethylidene ([77Fir] =CHCH<sub>3</sub>) and ethynylidyne (≡CCH<sub>3</sub>) at 250 and 350 K, respectively. This implies the stepwise loss of one and two hydrogen atoms from the ethyl moiety during the heating process. TPD measurements showed that hydrogen desorption was not accompanied by desorption of either saturated or unsaturated C-2 hydrocarbons or methane.

Zaera [99Zae, 02Zae1, 02Zae2] reviewed the surface chemistry of hydrocarbons on transition metal surfaces, focusing on the clean production of alkyl surface moieties on well characterized metals and the thermal chemistry of those moieties. Alpha, beta and gamma hydride eliminations, reductive elimination with hydrogen or other alkyl groups, methylene insertions, and C-C bond breaking reactions were all treated.

#### 3.8.6.3.6.5 Rh

Klivenyi and Solymosi [95Kli] examined the thermal and photochemistry of methylene iodide (CH<sub>2</sub>I<sub>2</sub>) on Rh(111) by HREELS, XPS, AES and TPD. CH<sub>2</sub>I<sub>2</sub> adsorbs dissociatively at submonolayer coverage at 90 K and molecularly at higher coverages. The dissociation of a monolayer starts above 170 K and is complete below 250 K. The primary products of thermal dissociation were adsorbed CH<sub>2</sub> and I. The CH<sub>2</sub> species was stable up to 300 K. A larger fraction undergoes self-hydrogenation to CH<sub>4</sub> at 200-300 K, and a much smaller fraction dimerizes into C<sub>2</sub>H<sub>4</sub>. Co-adsorbed O atoms inhibited the C-I bond breaking and, in addition, reacted with adsorbed CH<sub>2</sub> to give formaldehyde at 170-340 K, and CO<sub>2</sub> and H<sub>2</sub>O at 340-460 K. No coupling between CH<sub>2</sub> and CH<sub>3</sub>, and CH<sub>2</sub> and C<sub>2</sub>H<sub>5</sub> was observed.

#### 3.8.6.3.6.6 Ru

Kis and coworkers [00Kis] investigated the adsorption and dissociation of CH<sub>2</sub>I<sub>2</sub> on Ru(001) at 110 K using XPS, UPS, TPD, AES and work function measurements, with the aim of generating CH<sub>2</sub> species. Adsorption of CH<sub>2</sub>I<sub>2</sub> was characterized by a work function decrease (0.96 eV at 1 ML), indicating that adsorbed CH<sub>2</sub>I<sub>2</sub> has a positive outward dipole moment. Three adsorption states were distinguished: a

multilayer (200 K), a weakly bonded state (220 K) and an irreversibly adsorbed state. A new observation was the formation of  $\text{CH}_3\text{I}$ , which desorbs at 160 K. The adsorption of  $\text{CH}_2\text{I}_2$  at 110 K was dissociative at submonolayer, but molecular at higher coverages. Dissociation of the monolayer to  $\text{CH}_2$  and I proceeded at 198–230 K, as indicated by a shift in the  $3d_{5/2}$  binding energy from 620.6 eV to 619.9 eV. A fraction of adsorbed  $\text{CH}_2$  was self-hydrogenated into  $\text{CH}_4$  (220 K), and another one was coupled to di- $\sigma$ -bonded ethylene, which – instead of desorption – was converted to ethylidyne at 220–300 K.

Zhou et al. [89Zho] investigated methyl iodide on Ru(001) by TPD, AES and HREELS.  $\text{CH}_3\text{I}$  adsorbs dissociatively at 110 K. During TPD methane and C–C bonds were formed with  $\text{CH}_2$ ,  $\text{CH}_3$ ,  $\text{CCH}_3$  and CH being identified by HREELS.

Goodman and coworkers [94Wu, 02Cho] used HREELS and TPD to examine surface species formed from  $\text{CH}_4$  decomposition on Ru(0001) and Ru( $11\bar{2}0$ ). Methane dissociated on Ru(0001) to methylidyne ( $\equiv\text{CH}$ ) and vinylidene ( $=\text{CCH}_2$ ), while for Ru( $11\bar{2}0$ ) CH,  $\text{CCH}_2$  and ethylidyne ( $\equiv\text{CCH}_3$ ) were reported.

### 3.8.6.3.6.7 Various

Au et al. [98Au] presented a theoretical treatment of  $\text{CH}_x$  fragments on Ni, Pd, Pt and Cu catalysts (see 3.8.6.3.1.12).

### 3.8.6.4 Alkenes

Because of the availability of  $\pi$ -electrons that can readily be donated to the metal, the bonding of alkenes to the metal surface is much stronger than the bonding of alkanes. There are two consequences: 1) the reactant alkene undergoes molecular rearrangements depending on the substrate surface structure and the temperature; 2) the metal substrate may restructure during alkene adsorption to optimise bonding to the adsorbed species.

The various adsorbate geometries of ethylene represented a controversial topic for some time (see below). However, based on many studies using a variety of methods the different adsorbed species could be eventually unambiguously identified. At low enough temperatures di- $\sigma$  bonding of alkenes is often preferred. An example of this is shown in Fig. 8 for ethylene adsorption on Pt(111). The center of the molecule occupies a three-fold site and the molecular axis is at  $23^\circ$  with respect to the surface plane. As the temperature is increased, a hydrogen shift occurs from one carbon atom to the other to form ethylidene ( $=\text{CHCH}_3$ ) (Fig. 9). As the temperature rises, another hydrogen atom splits off from the carbon nearest to the metal and the molecule assumes an up-right position to become ethylidyne,  $\text{C}_2\text{H}_3$ , at the same three-fold metal site [95Cre1, 96Cre2, 97Döl].

The metal surface restructures around the adsorption site with movements of the metal atoms in the proximity of the site. These rearrangements are shown for the Pt(111) and Rh(111) crystal faces in Fig. 10. It should also be noted that it is too simplistic to consider that only the nearest-neighbor metal atoms of the substrate participate in the bonding. There is evidence that the atoms at next-nearest-neighbor sites change their location when chemisorption occurs, moving either closer or further away from the chemisorption bonds.

The nature of the chemical bonds of alkenes is similar to that in organo-metallic clusters, and this analogy holds for a large number of alkene-transition metal surface adsorption systems [88Van]. Not surprisingly the vibrational spectra of the adsorption and the cluster systems are very similar. As the temperature is increased the adsorbed alkenes undergo sequential decomposition just as the adsorbed alkanes do, as evident from sequential hydrogen evolution during temperature programmed desorption (Fig. 11).

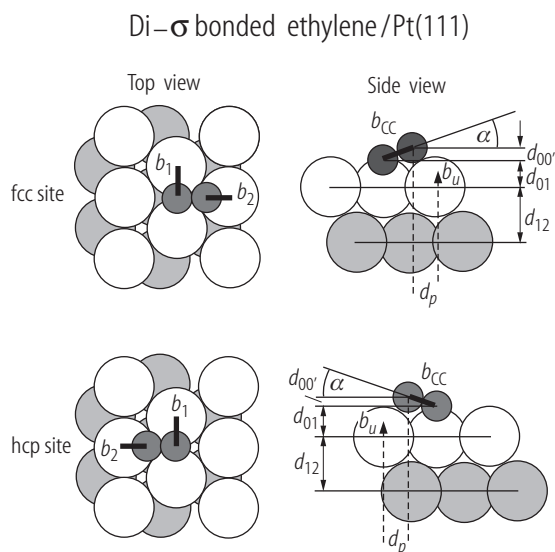


**Fig. 8** The structure of di- $\sigma$  bonded ethylene on Pt(111) as determined by LEED; adapted from [97Som].

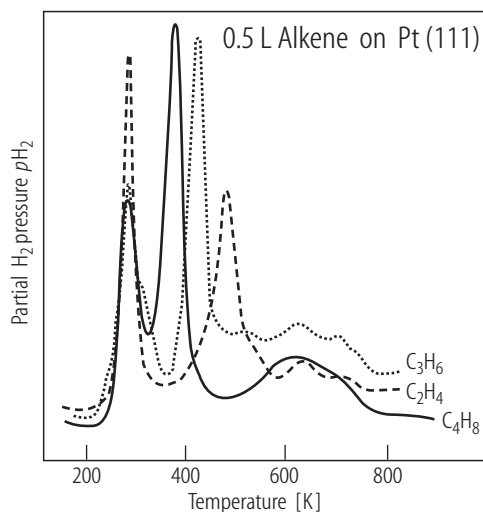


**Fig. 11** Temperature programmed desorption (TPD) of  $C_2$ - $C_4$  alkenes on Pt(111) (exposure 0.5 Langmuir at 150 K). Hydrogen evolution indicates the sequential decomposition/dehydrogenation of the alkenes and carbon deposition; adapted from [77Fir].

	$a$ [° degr]	$b_1$ [Å]	$b_2$ [Å]	$b_{CC}$ [Å]	$b_u$ [Å]	$d_p$ [Å]	$d_{00'}$ [Å]	$d_{01}$ [Å]	$d_{12}$ [Å]
fcc site	23	1.92	2.07	1.56	0.03	0.83	0.61	1.32	2.27
	+21/-11	±0.15	±0.30	±0.50	±0.07	±0.25	±0.07	±0.12	±0.05
hcp site	22	1.96	2.05	1.53	0.02	0.74	0.57	1.35	2.27
	+21/-11	±0.15	±0.30	±0.40	±0.07	±0.25	±0.07	±0.12	±0.05

#### Ethylene decomposition on Pt(111)

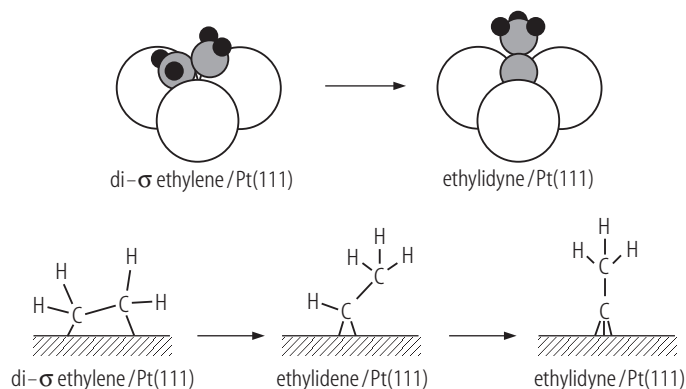


**Fig. 9** Schematic of ethylene decomposition on Pt(111); adapted from [95Cre1, 97Som]

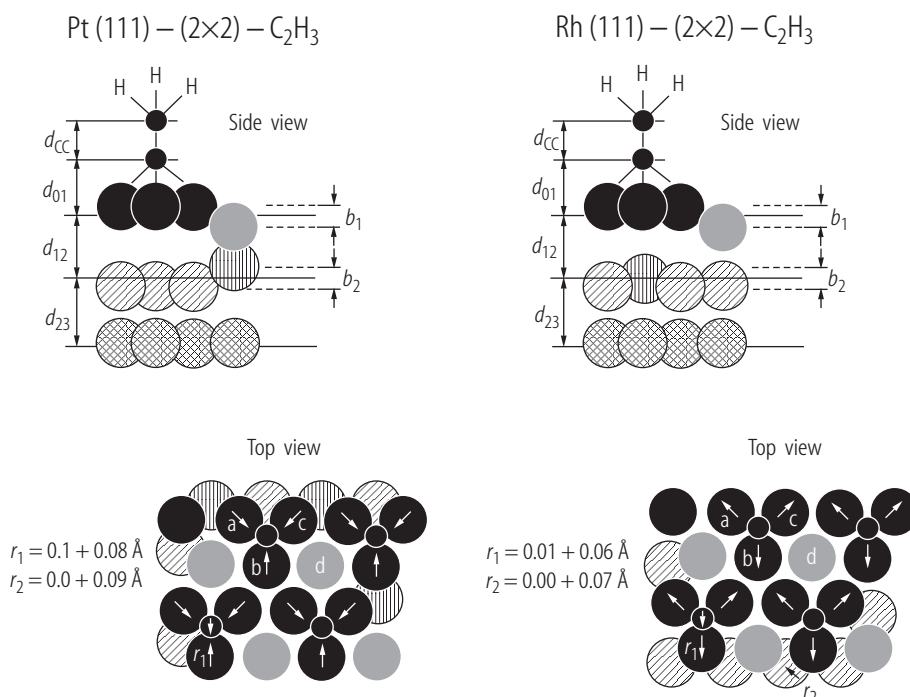


**Fig. 10** The structure of ethynylidyne adsorbed on Pt(111) and Rh(111) as determined by LEED. On Pt(111), ethylene forms an ethynylidyne molecule which binds to an fcc threefold hollow site. That is, there is no metal atom directly underneath the carbon in the second metal layer. In this circumstance, the surface metal atoms move inward to presumably provide a bond to the carbon as strong as possible and metal-metal distances are altered on the surface as well. The second metal atom next to the chemisorption bond moves downward to produce a corrugated surface.

On Rh(111), ethynylidyne is bonded to the hcp 3-fold hollow site. This site has a metal atom right underneath the carbon bonding site in the second layer. The metal atoms move away from the carbon atom bound to the hollow site to allow the carbon to bind to the Rh atom directly underneath the carbon in the second layer. The adsorption-induced distortion in the top metal layers pulls the nearest neighbor metal atoms up out of the surface plane; adapted from [97Som].

#### 3.8.6.4.1 Ethylene C<sub>2</sub>H<sub>4</sub> and Ethynylidyne C<sub>2</sub>H<sub>3</sub>

##### 3.8.6.4.1.1 Ag

Slater et al. [94Slal] used IRAS, LEED and electron spectroscopies to examine low-temperature adsorption of C<sub>2</sub>H<sub>4</sub> on Ag(100) (as well as the effect of preadsorbed chlorine). On Ag(100) ethene was found weakly  $\pi$ -bonded at all coverages with dynamic pressures being required to saturate the monolayer at 100 K. At low coverages, the molecule lies parallel to the surface plane, but further adsorption induced a reorientation involving rotation about the C-C axis. The influence of preadsorbed Cl depended critically on the Cl coverage. At low coverage adsorption was enhanced producing ordered ethene-chlorine structures. High Cl coverage progressively passivated the surface. Rovida et al. observed no (ordered) C<sub>2</sub>H<sub>4</sub> adsorption on Ag(110) at 293–423 K [80Ron]. IRAS spectra of C<sub>2</sub>H<sub>4</sub> adsorbed on oxygen-activated Ag(111) at 300 K at a pressure of 1 Torr were reported by Stacchiola et al. [01Sta2].

#### 3.8.6.4.1.2 Au

Chesters and Somorjai observed no C<sub>2</sub>H<sub>4</sub> adsorption on Au(111) and Au(S)-[6(111) × (100)] at 300 K [75Che].

#### 3.8.6.4.1.3 Cr

Upon adsorption of C<sub>2</sub>H<sub>4</sub> Gewinner et al. observed c(2×2)-C and ( $\sqrt{2} \times 3\sqrt{2}$ )R±45°-C structures on Cr(100) [82Gew].

#### 3.8.6.4.1.4 Cu

C<sub>2</sub>H<sub>4</sub> adsorption on Cu(100) at 80 K was investigated by Nyberg and coworkers [82Nyb] using EELS and LEED. Ethylene was found adsorbed in a configuration parallel to the Cu(100) surface with the molecule-metal interaction of  $\pi$ -character.

Ertl observed a (2×2) C<sub>2</sub>H<sub>4</sub> structure on Cu(100), one-dimensional order on Cu(110), while no ordered structure was reported on Cu(111) [77Ert]. On Cu(111) a weakly physisorbed adsorbate state without noticeable structural changes with respect to the gas phase molecule is typically observed experimentally. Witko and Hermann [98Wit] have examined C<sub>2</sub>H<sub>4</sub> on Cu(111) by ab-initio DFT cluster studies, yielding potential energy curves  $E(z)$  which exhibited two minima. One minimum referred to an undistorted (physisorbed) adsorbate while the other minimum pointed to a strongly distorted adsorbate (suggesting a competitive binding state). The  $E(z)$  curves also explained experiments on C<sub>2</sub>H<sub>4</sub>-Cu(111) which have observed only one of the two adsorbate states so far.

Schaff et al. [95Sch] examined the adsorption geometry of C<sub>2</sub>H<sub>4</sub> on Cu(110) by PED in the scanned energy mode as well as by angle-resolved valence level photoemission. The molecule adsorbed either in an atop site on the close-packed Cu rows at a perpendicular height of 2.08±0.02 Å with a C-C bond length of 1.32±0.09 Å, or in a short bridge site on the Cu rows at a perpendicular height of 2.09±0.02 Å with a C-C bond length of 1.53±0.13 Å. In each case the molecular plane was parallel to the surface, but the C-C axis can be twisted azimuthally out of the [110] direction by as much as 24°.

STM at 4 K was used by Buisset et al. [96Bui] to directly determine the binding site of C<sub>2</sub>H<sub>4</sub> on Cu(110) by simultaneously imaging the adsorbate and the underlying lattice. The molecule was found to bond in the short bridge site on the close-packed rows with its C-C axis oriented in the [110] direction.

Ethylene may show strong geometrical distortions when adsorbed on transition metals with the bonding normally described in terms of a  $\pi$ -donation- $\pi^*$ -backdonation process. Triguero et al. [98Tri] demonstrated the importance of considering the available excited states of the free molecule in analyzing the bonding scheme of the adsorbate on cluster models of Cu(100), (110), and (111). By comparison to the structures of the triplet excited states in the gas phase it was shown that these must be considered as the states actually involved in the bonding.

Yu and Leung [98Yu] investigated the effect of irradiating Cu(100) (and also O-precovered and N-precovered Cu(100) surfaces) with low-energy (<200 eV) ethylene ions at room temperature using HREELS and TPD. Ion irradiation of a clean Cu(100) surface at 200 eV impact energy was found to produce hydrocarbon fragments that adsorbed readily on the surface at 300 K and decomposed completely after annealing to >600 K. For an O-precovered Cu(100) surface at 300 K, the hydrocarbon species produced appeared to react with the pre-deposited O atoms to form CO. In addition to a red-shifted CO stretch observed at a low ethylene ion dose, a blue-shifted CO stretch was also found at a higher ethylene ion dosage. The observed red and blue shifts were attributed to adsorption of CO stabilized by a proposed direct interaction mechanism involving neighbouring surface O atoms and C-containing species. In the case of low-energy ion irradiation of a N-precovered Cu(100) surface in ethylene, EELS features attributable to C=N and N-H stretching vibrations were observed, giving support to the formation of CN and NH radicals as a result of surface reactions between the hydrocarbon species and the pre-deposited N atoms.

#### 3.8.6.4.1.5 Fe

Hung and Bernasek [95Hun] studied the adsorption of  $C_2H_4$  on Fe(100), and on the C- and O-covered surface using HREELS, TPD, AES and LEED. On the clean surface,  $C_2H_4$  adsorbed molecularly as di- $\sigma$ -bonded  $C_2H_4$  which desorbed at 240 K or decomposed to form methylidyne ( $\equiv CH$ ) and ethynyl ( $-C\equiv CH$ ) below 260 K. Hydrogen was the only desorption product of  $C_2H_4$  decomposition. Heating the adsorbate to 523 K produced a  $c(2\times 2)$ -C surface. Preadsorbed carbon and oxygen blocked the chemisorption of di- $\sigma$ -bonded  $C_2H_4$  and induced physisorption of  $C_2H_4$  at 100 K. Preadsorbed O appeared to inhibit the dehydrogenation of di- $\sigma$ -bonded  $C_2H_4$  and induced the adsorption of  $\pi$ -bonded  $C_2H_4$ . A  $c(2\times 2)$ -C structure on Fe(100) was also reported in [77Bru, 85Vin]. Using LEED on Fe(111),  $(1\times 1)$ ,  $(5\times 5)$  and  $(3\times 3)$  structures were observed [78Yos].

#### 3.8.6.4.1.6 Ir

$C_2H_4$  adsorption on Ir(100) produced disordered and  $c(2\times 2)$ -C structures [76Bro] while on Ir(110) disordered and  $(1\times 1)$ -C [78Nie] and on Ir(111)  $(\sqrt{3}\times\sqrt{3})R30^\circ$  and  $(9\times 9)$ -C were observed [76Nie]. On the stepped surface Ir(S)-[6(111)  $\times$  (100)] a  $(2\times 2)$  appeared [76Nie]. HREELS, SIMS and XPS studies of ethylidyne on Ir(111) were reported in [87Mar2, 87Mar1, 88Mar].

#### 3.8.6.4.1.7 Mo

$C_2H_4$  adsorption on Mo(100) produced  $c(2\times 2)$ -carbide,  $(1\times 1)$  and “streaked”  $(1\times 1)$  [76Gui, 80Ko, 81Ko, 81Oya, 82Ove]. Wang and Tysoe [90Wan] applied ARUPS, AES and TDS to monitor  $C_2H_4$  on Mo(100). At 80 K ethylene adsorbed in the four-fold hollow site on Mo(100) and was substantially rehybridized to  $\sim sp^3$  ( $\theta C_2H_4 = 0.8\pm 0.1$ ). At 220 K chemisorbed  $C_2H_4$  dehydrogenated to distorted  $C_2H_2$ . Further heating to 300 K led to carbon-carbon bond scission producing  $CH_x$  with, according to TDS, an average surface stoichiometry of  $C_1H_1$ .

$C_2H_4$  interaction with Mo(100) and oxygen-covered Mo(100) was described in [97Wu]. Ethylene either thermally decomposed to hydrogen and adsorbed carbon, desorbed molecularly, self-hydrogenated to produce ethane or dissociated to form adsorbed  $C_1$  species which may hydrogenate to form methane. Thermal decomposition was proposed to take place on the four-fold sites of Mo(100) since the hydrogen yield decreased linearly with the oxygen coverage. The ethylene desorption activation energy increased with increasing oxygen coverage suggesting that ethylene bonds to Mo(100) predominantly by donation of  $\pi$ -electrons to the surface. Accordingly, the  $C_2H_4$  hydrogenation activation energy also increased as a function of oxygen coverage. The  $CH_4$  yield also varied with oxygen coverage so that no methane desorption was detected for clean Mo(100) but the yield increased with oxygen coverage reaching a maximum at  $\sim 0.6$  ML and decreasing at higher coverages. XPS spectroscopy suggested that adsorbed oxygen increased the dissociation probability of ethylene. Experiments in which carbenes were grafted onto the surface by decomposing methylene iodide showed that carbenes were stabilized by oxygen on the surface.

#### 3.8.6.4.1.8 Ni

Steinrück and coworkers [02Whe, 03Neu] used temperature-programmed XPS to monitor  $C_2H_4$  on Ni(100) between 90 and 530 K. The use of a third generation synchrotron light source allowed measurements of high-resolution C1s XPS spectra in “real-time” (within a few seconds), enabling to follow the thermal dehydrogenation in a quantitative and quasi-continuous manner. For  $C_2H_4$  dehydrogenation, a vinyl species ( $-CH=CH_2$ ) was observed, with acetylene ( $C_2H_2$ ) being the subsequent dehydrogenation product. Upon further heating, acetylide ( $-C\equiv CH$ ) and methylidyne ( $\equiv CH$ ) were successively formed. Carbide carbon was the final dehydrogenation product.



Zarea et al. [86Hall, 87Zae1, 87Zae2] studied  $C_2H_4$  adsorption and decomposition on Ni(100) by TPD and HREELS. Molecular adsorption of  $C_2H_4$  at 90 K was observed, with little rehybridisation. Vinyl was observed at higher temperature.

Using LEED to study  $C_2H_4$  adsorption on Ni(110), (2×1)-C, (4×5)-C, c(2×4)- $C_2H_4$ , c(2×2)-CCH and graphite overlayers were reported [75McC, 77Abb, 77McC, 84Str]. HREELS, LEED and TDS were used to study the adsorption and decomposition of ethylene on Ni(110) at 80-500 K [79Leh, 84Str, 86Ban]. Ethylene adsorbed molecularly at 80 K, but showed rehybridization to  $\sim sp^3$ . Its site group symmetry at 80 K is lower than  $C_{2v}$ . A complex ordered LEED pattern was formed on adsorption at low temperatures. Above 200 K decomposition produced CCH intermediates, yielding CH upon further heating. At 500 K atomic carbon forms a (4×5) ordered overlayer.

Weinelt et al. [92Wei1] studied the electronic structure of a dilute  $C_2H_4$  layer ( $\theta=0.5 \theta_{sat}$ ) on Ni(110) by ARUPS, TPD, LEED and model cluster calculations. Ethylene adsorbed with the molecular plane coplanar to the surface and the C-C axis was preferentially aligned along the  $[1\bar{1}0]$  ( $C_1$  symmetry). Similar bonding was predicted for  $\pi$ - and di- $\sigma$  coordination, for both cases the  $\pi$ -donation to the substrate being stronger than the  $\pi^*$  backdonation. The optimized geometry parameters for the  $\pi$ -bonded species were: C-C: 1.42 Å; Ni-C: 2.01 Å; tilting of  $CH_2$  relative to the (110) crystal plane: 23°. The same authors also investigated the saturated  $C_2H_4$  layer on Ni(110) [92Wei2]. The layer exhibited a c(2×4) LEED pattern corresponding to a structure containing two adsorbates per primitive unit cell. The  $C_2H_4$  molecules were again adsorbed with the molecular plane parallel to the surface and the C-C axis preferentially aligned along  $[1\bar{1}0]$ .

Brown et al. [99Bro1] measured the heats of adsorption and sticking probabilities for  $C_2H_4$  on Ni(110) at 300 K. The initial sticking probability and heat of adsorption are 0.78 and 120 kJ mol<sup>-1</sup>. CCH species were formed on the surface initially with a Ni-C bond strength of 191 kJ mol<sup>-1</sup>. This is in excellent agreement with the average calculated value of 204 kJ mol<sup>-1</sup> for hydrocarbon adsorption on Ni(100).

Giessel et al. [99Gie] used scanned-energy mode PED to determine the adsorption geometry of the c(2×4) phase of  $C_2H_4$  on Ni(110) at 0.5 ML (saturation coverage), and at 0.2 ML when no long-range order was observed. For the c(2×4) phase the two molecules per primitive unit mesh occupied slightly different low-symmetry sites approximately midway between short-bridge and atop. The C-C axis was tilted with respect to the surface plane by  $\sim 10^\circ$ . The C-C axes of the molecules were preferentially aligned along the close-packed Ni rows, but were offset in  $[100]$  directions away from the ridges by about 0.2 Å. At low coverage the local adsorption site was also one of low symmetry sites between atop and bridge.

Steinrück and coworkers [96Ste, 01Whe, 02Whe] examined the adsorption on  $C_2H_4$  on Ni(110) by angle-resolved UPS. For a "dilute" 0.25 ML layer (0.8 L exposure below 120 K) and for a saturated c(2×4) layer (0.5 ML) the C-C axis was parallel to surface, oriented along  $[1\bar{1}0]$ .

Gutdeutsch et al. [96Gut] investigated the adsorption of  $C_2H_4$  on Ni(110) by angle resolved inverse photoemission (ARIPE) and DFT model cluster and slab model band structure calculations. Cluster calculations gave a slight preference for the di- $\sigma$  over the  $\pi$ -coordinated geometry on top of the ridges, but only a very weak binding over the troughs. The half-bridge position on top of the ridges, intermediate between the short bridge (di- $\sigma$ ) and the top site ( $\pi$ ), was identified as the adsorption site in the densely packed c(2×4)  $C_2H_4$ /Ni(110) adsorption system.

Cooper and Raval [95Coo] studied  $C_2H_4$  on Ni(111) at 110 K using IRAS. Adsorption at low temperatures produced the di- $\sigma$  complex, with the spectra showing good agreement with the analogous vibrational data for the model organometallic compound  $[Os_2(CO)_8(u_2-\eta_2-(C_2H_4))]$ . IR data obtained at coverages  $\theta < 0.25$  were interpreted in terms of a local  $C_{2v}$  site symmetry. No evidence for significant non-planarity of the  $C_2M_2$  skeleton was found.

Using EELS Lehwald and Ibach [79Leh] studied  $C_2H_4$  adsorption at 150 K and  $C_2H_4$  decomposition upon annealing to higher temperature. On Ni(111) ethylene rehybridized upon adsorption and dehydrogenated to acetylene above 230 K. Ethylene partially dehydrogenated on the stepped Ni  $[5(111) \times (110)]$  surface. Further annealing produced coadsorbed H and CH. Hammer et al. [86Ham] performed combined LEED/EELS measurements of  $C_2H_4$  on Ni(111). Long-range order phases were c(4×2) and (2×2) with bridge positions being suggested as adsorption sites for the carbon atoms. Dalmái-

Imelik and Bertolini [74Dal] reported a change in work function upon adsorption of  $C_2H_4$  on Ni(111) of  $-0.3$  eV for adsorbed ethylene at  $3 \times 10^{-9}$  and  $10^{-8}$  Torr.

Bao et al. [95Bao] performed a quantitative evaluation of the local geometry of  $C_2H_4$  on Ni(111) using C1s scanned-energy PED. At 120 K  $C_2H_4$  had its C-C axis parallel to the surface, adsorbed on an “aligned” bridge site such that the C atoms were approximately atop Ni atoms. Heating led to dehydrogenation to acetylene and, while the C-C axis remained parallel to the surface, the C-C bond length and C-Ni layer spacing were reduced.  $C_2H_2$  occupied a “cross-bridge site” with the C atoms above inequivalent hollow sites on the surface. Both adsorbed species had C-C bond lengths larger than those of the associated gas-phase molecules indicating a significant reduction of C-C bond order.

Khan and Chen [03Kha] examined the reactivity of monolayer Ni films on Pt(111), W(110), and Ru(0001) single crystal surfaces. The bonding and decomposition of  $C_2H_4$  was studied by TPD. The 1 ML Ni/Pt(111) surface was relatively inactive toward  $C_2H_4$  decomposition, while the 1 ML Ni/Ru(0001) surface remained active toward  $C_2H_4$  dissociation.

#### 3.8.6.4.1.9 Pd

Among the platinum metals, Pd is considered the most selective for hydrocarbon hydrogenation. The characterization of hydrocarbon intermediates is therefore of great interest. Stuve and Madix [85Stu1] studied  $C_2H_4$  adsorption and reaction on Pd(100) by TPRS and HREELS, detecting both di- $\sigma$  and  $\pi$ -bonded  $C_2H_4$  at 80 K. IRAS spectra were reported in [97Cam].

Madix and coworkers [85Stu2, 95Guo1] investigated  $C_2H_4$  adsorption and reaction on an atomic oxygen-covered Pd(100)-p(2 $\times$ 2)-O surface using TPRS. Compared to the dehydrogenation reaction on clean Pd(100), O inhibits both  $C_2H_4$  adsorption and reaction. Combustion products were  $H_2O$ , CO and  $CO_2$  but no partial oxidation products were observed. Isotope experiments showed that initial reactions occur predominantly with the vinylic C-H bonds. The same group [95Guo2] also investigated the adsorption and reactions of  $C_2H_4$  (and of propene and 1-butene) on the Pd(100)-p(1 $\times$ 1)-H and Pd(100)-p(1 $\times$ 1)-D surfaces by TPRS. Efficient H-D exchange reactions below 300 K occurred for all C-H bonds for ethylene, propene and 1-butene, whereas no hydrogenation products (alkanes) were observed. The exchange reaction was proposed to occur via reversible hydrogenation to a half-hydrogenated intermediate. The absence of alkene hydrogenation may be due to stronger metal-hydrogen bonds on Pd(100) than on other metals such as Pt and Rh (or may be influenced by hydrogen dissolution [04Rup]).

The adsorption structure of  $C_2H_4$  on Pd(110) was analyzed by NEXAFS and STM by Ogasawara et al. [01Oga] pointing to the C-C bond aligned along  $[1\bar{1}0]$ . Interaction of  $C_2H_4$  with Pd(110)-(2 $\times$ 1)-H, studied by TDS and HREELS, was reported in [92Sek]. On the same surface, Ichihara et al. [98Ich, 00Ich] observed one-dimensional (3 $\times$ 1) and c(2 $\times$ 2) domains by STM and HREELS.  $\pi$ -bonded ethylene adsorbed at on-top Pd sites.

On Pd(111), Gates and Kesmodel [81Kes, 83Gat] concluded from angle resolved EELS that the dominant species for 300 K adsorption is ethylidyne with the C-C axis perpendicular to the surface while low temperature spectra showed essentially undistorted  $\pi$ -ethylene. ARUPS results by Lloyd and Netzer supported this [83Llo]. The exact structure of ethylidyne had been already resolved for the Pt(111) system (see 3.8.6.4.1.10) by LEED, EELS and by comparisons to analogous organometallic complexes.

Using a combination of TPD and IRAS, Tysoe and coworkers [97Kal, 01Sta1, 02Sta1] reported that  $C_2H_4$  adsorbed on clean Pd(111) in a di- $\sigma$  configuration but converted to  $\pi$ -bonded species when the surface was presaturated by hydrogen. Subsurface hydrogen was made responsible for the formation of  $\pi$ -bonded ethylene on hydrogen-covered Pd(111) [03Sta1]. Ethane was formed with an activation energy of  $12.5 \pm 1.2$  kJ/mol only when Pd(111) was pre-covered with hydrogen and not when ethylene and hydrogen were co-dosed, indicating that ethylene blocks hydrogen adsorption [01Sta1]. Upon  $C_2H_4$  adsorption on Pd(111) at 300 K an ethylidyne species was observed by IRAS (methyl mode at  $1329\text{ cm}^{-1}$  [97Kal]). Upon increasing the pressure up to 1 mbar a loss in the order was reported probably caused by coadsorption of  $C_2H_4$  [97Kal]. Ethylidyne spectra could still be observed at elevated gas pressure because the methyl bending mode falls into a window of the gas phase  $C_2H_4$  features. Coadsorption studies with CO indicated that ethylidyne adsorbed in fcc threefold hollow sites of Pd(111) [00Sta, 01Sta1]. Ethylene

adsorption on ethynylidyne-saturated Pd(111) at 80 K indicated the presence of di- $\sigma$ -bonded ethylene [02Stac2]. TPD revealed that the saturation ethylene coverage on ethynylidyne-covered Pd(111) was 0.25 ML compared to 0.33 ML for ethylene on clean Pd(111). TPD indicated a desorption activation energy of 28 kJ/mol for  $\pi$ -bonded ethylene on Pd(111) [84Tys, 01Sta1].

Sock et al. [03Soc] investigated  $C_2H_4$  adsorption and its thermal evolution on clean and oxygen precovered Pd(111) by HREELS, high-resolution XPS, TDS and by ab initio DFT. On clean Pd(111) at 100 K  $C_2H_4$  was found in a di- $\sigma$  bonding state, whereas on Pd(111)- $2\times 2$ -O the  $\pi$ -bonded configuration was more stable. Upon adsorption at 300 K ethynylidyne was formed on both surfaces, but neither di- $\sigma$  nor  $\pi$ -bonded ethylene were observed to transform into ethynylidyne on heating from low temperature up to 450 K. Complete molecular desorption was observed in both cases, with no signs of dehydrogenation. Ethynylidyne  $C_2H_3$  on Pd(111) was also characterized by high-resolution C1s core level photoemission spectra by Sandell et al. [98San].

$C_2H_4$  adsorption and hydrogenation on Pd(111) was studied by SFG spectroscopy, both under UHV and atmospheric pressure [02Rup, 03Fre, 05Mor]. Fig. 12 shows SFG spectra after adsorption at different temperatures. Under UHV and at 100-200 K, ethylene adsorbed in a di- $\sigma$ -configuration with a characteristic peak at  $2910\text{ cm}^{-1}$  ( $\nu_s(CH_2)$ ; Fig. 12a(1)). The second weak peak around  $2960\text{ cm}^{-1}$  was attributed to the  $\nu_s(CH_2)$  of  $\pi$ -bonded ethylene. Its low intensity may be due to a small surface concentration and/or the orientation of  $\pi$ -bonded  $C_2H_4$ . On single crystal surfaces the  $\nu_s(CH_2)$  signal for  $\pi$ -bonded  $C_2H_4$  (with the C-H bonds nearly parallel to the metal surface [02Ge]) is supposed to be weak due to the surface-dipole selection rule for metal surfaces (dynamic dipoles parallel to the surface plane are cancelled by image dipoles inside the metal [83Hof]). A surface covered by  $\pi$ -bonded  $C_2H_4$  was produced by adsorbing hydrogen first (which blocks threefold hollow sites), followed by  $C_2H_4$  adsorption at 100 K (Fig. 12a(2)), in agreement with corresponding IRAS measurements [01Sta1, 02Stac1]. When the  $C_2H_4$  layer was heated to 300 K nearly all of the ethylene desorbed and only a small amount was dehydrogenated to ethynylidyne [03Soc]. Compared to Pt(111) (see below), on Pd ethylene has a smaller tendency to produce ethynylidyne. Only after adsorbing ethylene at 300 K [97Kal], a signal of ethynylidyne ( $M\equiv C-CH_3$ ) could be observed at  $\sim 2875\text{ cm}^{-1}$  ( $\nu_s(CH_3)$ ; Fig. 12a(3)) due to ethylene decomposition. Under mbar pressure of ethylene/hydrogen mixtures no distinct signals were observed providing indirect evidence that both di- $\sigma$ -bonded ethylene and ethynylidyne are not reacting and that rather  $\pi$ -bonded ethylene is the active species in  $C_2H_4$  hydrogenation (similar as for Pt(111)).

As mentioned above,  $C_2H_4$  adsorption on Pd(111) and its coadsorption with H was examined by a number of groups using TPD [01Sta3, 03Doy, 04Doy, 04Rup] (Fig. 12b). TDS spectra of  $C_2H_4$  adsorption (Fig. 12b(2)) show a broad desorption peak around 260 K and a small desorption feature at 195 K. While the first can be attributed to di- $\sigma$ -bonded ethylene, the origin of the low temperature desorption is unclear. It may be due to  $\pi$ -bonded ethylene but may also originate from rearrangements in a di- $\sigma$  bonded ethylene layer [03Mor, 05Mor]. When 1 L hydrogen was adsorbed before 1 L  $C_2H_4$  was dosed at 95 K (Fig. 12b(4)),  $C_2H_4$  was (mainly) bonded in a  $\pi$ -configuration which desorbed at lower temperature. Preadsorbed H occupied threefold hollow sites but  $\pi$ -bonded  $C_2H_4$  could still adsorb at on-top sites (while di- $\sigma$ -bonded ethylene was (partly) blocked). An influence of subsurface hydrogen on the  $C_2H_4$  binding state was also suggested [03Stac1]. A small amount of ethylene decomposed into ethynylidyne  $C_2H_3$  around 300 K and its further decomposition led to the small  $H_2$  peak at  $\sim 425\text{ K}$  (Fig. 12b(3)).

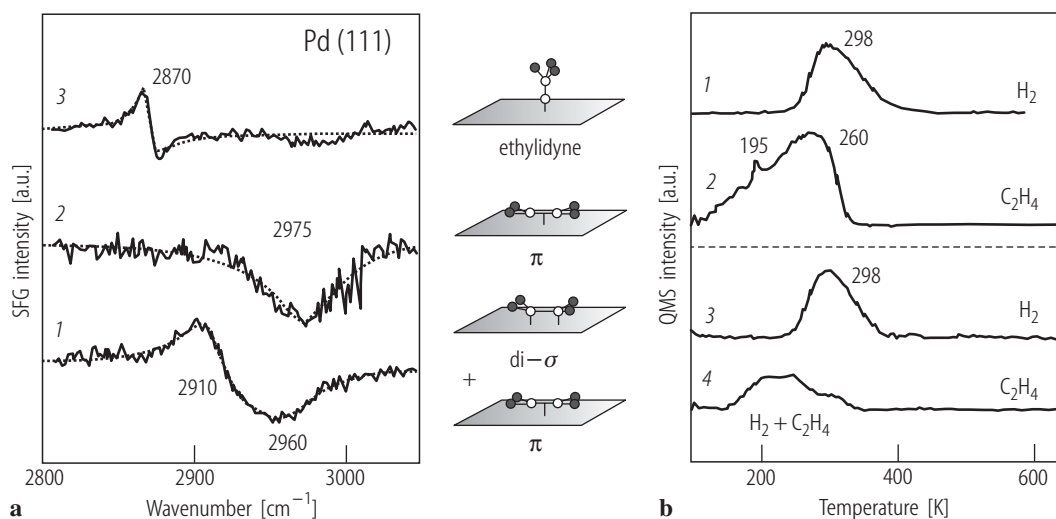


**Fig. 12** (a) SFG spectra of  $\text{C}_2\text{H}_4$  species on Pd(111). Exposures were 2.5 L  $\text{C}_2\text{H}_4$  at 100 K (1), 1 L  $\text{H}_2$  followed by 2.5 L  $\text{C}_2\text{H}_4$  at 100 K (2). Trace (3) was acquired at 300 K after annealing in  $5 \times 10^{-7}$  mbar  $\text{C}_2\text{H}_4$  from 100 to 300 K; adapted from [05Mor]. (b) Thermal desorption spectra of hydrogen (mass 2) and  $\text{C}_2\text{H}_4$  (mass 27) on Pd(111). TDS spectra of the individual components are shown in (1, 2), those of coadsorption in (3, 4). Exposures were: (1) 1 L  $\text{H}_2$  at 95 K; (2) 1 L  $\text{C}_2\text{H}_4$  at 95 K; (3) and (4) display the desorption traces after exposing Pd(111) to 1 L  $\text{H}_2$  and subsequently to 1 L  $\text{C}_2\text{H}_4$  at 95 K; adapted from [04Rup].

Although vibrational and photoelectron spectroscopy of  $\text{C}_2\text{H}_4$  adsorption at  $\sim 100$  K indicated di- $\sigma$  bonded  $\text{C}_2\text{H}_4$  as stable species (e.g. [01Sta1, 03Fre, 03Soc, 05Mor]), theoretical studies rather suggest a combination of di- $\sigma$  bonded  $\text{C}_2\text{H}_4$  at bridge sites and  $\pi$ -bonded  $\text{C}_2\text{H}_4$  at on-top sites [00Neu1, 02Ge]. Neurock et al. [00Neu2, 02Ge] used first principles DFT calculations to study  $\text{C}_2\text{H}_4$  chemisorption on the (111), (100) and (110) surfaces of Pd. On all the three low-index surfaces the most stable site and geometry for  $\text{C}_2\text{H}_4$  was that where the C-C bond axis is parallel to the surface along the bridge site. The calculated binding energies  $E_{\text{ads}}$  followed the trend  $111 < 100 < 110$ . Ethylene dehydrogenation paths over Pd(111) [02Pal] and  $\text{C}_2\text{H}_4$  hydrogenation on Pd(100) [00Han, 00Neu1] were also examined. The DFT-calculated binding energies for ethylene ( $\pi$ ), ethylene (di- $\sigma$ ), ethyl, vinyl, ethynidyne, atomic oxygen, and atomic carbon on a Pd-19 cluster (and a Pd(111) slab) were found to be  $-30$  ( $-27$ ),  $-60$  ( $-62$ ),  $-130$  ( $-140$ ),  $-237$  ( $-254$ ),  $-620$  ( $-636$ ),  $-375$  ( $-400$ ) and  $-610$  ( $-635$ ) kJ/mol. Mittendorfer et al. [03Mit] also carried out a comparative DFT study of the adsorption of ethylene, 1-butene, acetylene, and 1,3-butadiene on Pd(111) and Pt(111), analyzing structural, electronic, energetic, and spectroscopic properties.

Chemisorption of  $\text{C}_2\text{H}_4$  on ultrathin (mono-, bi-, and trilayer) Pd films on Mo(100) was studied by Heitzinger et al. [93Hei] using AES, TPD and HREELS.  $\text{C}_2\text{H}_4$  was weakly chemisorbed on the Pd monolayer, and the adsorbed species was much less rehybridized from  $\text{sp}^2$  in the gas phase toward  $\text{sp}^3$  as compared to  $\text{C}_2\text{H}_4$  chemisorbed on Pd(100). Reversible  $\text{C}_2\text{H}_4$  adsorption was increased on the Pd monolayer, i.e. a smaller fraction dehydrogenated during TPD.

#### 3.8.6.4.1.10 Pt

Ethylene adsorption, particularly on Pt, has received much attention due to its importance for  $\text{C}_2\text{H}_4$  hydrogenation. The reaction takes place already at  $\sim 300$  K presumably by stepwise hydrogenation of ethylene, as proposed already by Horiuti and Polanyi [34Hor]. LEED studies of  $\text{C}_2\text{H}_4$  adsorption on Pt(100) revealed a  $c(2 \times 2)$  structure [68Mor, 69Mor, 75Lan1, 75Lan2, 77Fis1, 78Fis].

$\text{C}_2\text{H}_4$  adsorption and dehydrogenation on the hexagonally reconstructed Pt(100)-hex-R0.7° surface was examined by Ronning et al. [01Ron] using STM and LEED. The reconstruction was lifted upon ethylene adsorption and heterogeneous nucleation of highly anisotropic ( $1 \times 1$ ) domains was observed.

C<sub>2</sub>H<sub>4</sub> adsorption and C<sub>2</sub>H<sub>4</sub>-H coadsorption on Pt(110) at 93 K was examined by Yagasaki and Masel using EELS and TPD [89Yag, 90Yag2]. Adsorbed H substantially modified the adsorption of ethylene. While C<sub>2</sub>H<sub>4</sub> adsorption on clean (2×1) Pt(110) resulted in di-σ and π-bound ethylene, little di-σ ethylene was observed if the sample was preexposed to 100 L H<sub>2</sub>. Hydrogen acts as a site blocker and prevents di-σ ethylene formation, and also inhibits C<sub>2</sub>H<sub>4</sub> decomposition.

King and coworkers [95Stu] reported the calorimetric heat of interaction for ethylene on Pt(110)-(1×2) (Fig. 2). Being ~205 kJ/mol at low coverages, it drops in several steps to 120 kJ/mol with increasing coverage. Three stable species were identified on the surface, and the average bond dissociation energy of a Pt-C single bond was extracted for each. The mean value was ~223 kJ/mol, systematically decreasing from 235 to 214 kJ/mol as the number of single Pt-C bonds per adsorbate molecule increased from 2 to 4.

On Pt(111) it was shown by UPS and EELS that below 50 K C<sub>2</sub>H<sub>4</sub> molecules interact weakly with the surface via π-coordination [91Cas]. LEED surface crystallography was able to reveal the detailed atomic structure of the different adsorbed ethylene species [94Sta,97Döl]. Below 50 K ethylene is physisorbed with its C-C bond parallel to the surface, and the interatomic distance between the two carbon atoms is almost unchanged with respect to the gas-phase molecule [91Cas,94Sta,97Döl]. The molecule's π orbital bonds directly with the platinum surface with π-bonded C<sub>2</sub>H<sub>4</sub> bound to on-top sites. Stöhr et al. [84Stö] studied C<sub>2</sub>H<sub>4</sub> on Pt(111) with NEXAFS and also found it parallel to the surface, with a C-C bond length of 1.49±0.03 Å. Albert et al. [82Alb] used ARUPS and reported the carbon-carbon bond axis to be parallel to the surface at low temperature. Kubota et al. reported a desorption activation energy of 40±10 kJ/mol for π-bonded ethylene [94Kub].

At temperatures between 60 K and 240 K, the ("gas phase like") carbon-carbon double bond of the adsorbed molecule is broken and the carbon atoms attain nearly sp<sup>3</sup> hybridization (Fig. 8). Two σ-bonds are formed with the underlying platinum surface atoms and this species is usually referred to as di-σ bonded ethylene [82Iba1]. Di-σ-ethylene occupies three-fold, face centered cubic (fcc) adsorption sites (Fig. 8). This species was characterized in detail by EELS (Fig. 13) [77Iba2, 78Iba]. When the temperature was further increased di-σ-ethylene was dehydrogenated to form ethylidyne ≡C-CH<sub>3</sub> (by transferring a hydrogen atom to the other carbon and by losing one hydrogen) [95Cre1] (Figs. 9-11). As shown by LEED, both ethylidyne and di-σ-ethylene are located in fcc threefold hollow sites with the molecular axis of di-σ-ethylene tilted 23° away from the surface plane [93Sta, 97Döl]. Ethylidyne is stable up to 450 K and is further dehydrogenated at higher temperature (≡C-H species).

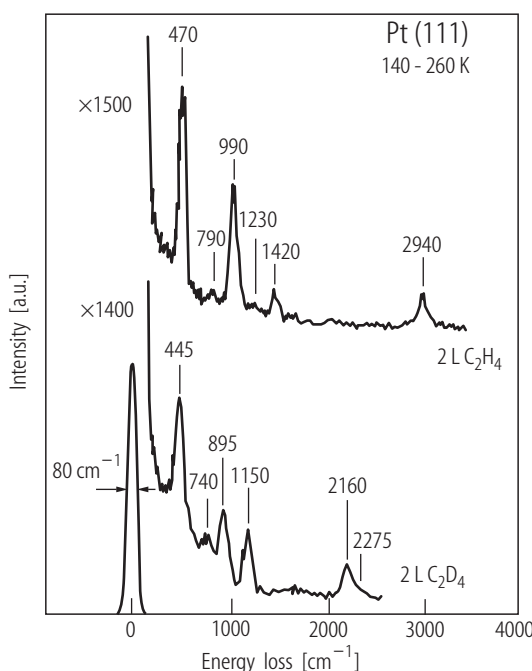


**Fig. 13** Electron energy loss spectra of  $\text{C}_2\text{H}_4$  adsorption on Pt(111) at high coverage. The observed vibrations indicated  $\text{sp}^3$  hybridization and are consistent with di- $\sigma$  bonding to the surface. A spectrum of  $\text{C}_2\text{D}_4$  is shown for comparison; adapted from [78Iba].

A detailed description of the initial studies that led to the discovery of ethylidyne  $\text{C}_2\text{H}_3$  can be found e.g. in [85Bee]. The earliest structural studies were carried out by Kesmodel et al. on  $\text{C}_2\text{H}_2$  on Pt(111) using LEED [77Kes] concluding that a stable di- $\sigma$   $\text{C}_2\text{H}_2$  species was formed. EELS studies of  $\text{C}_2\text{H}_4$  adsorption by Ibach [77Iba2, 77Iba1] proposed an ethylidene ( $=\text{CHCH}_3$ ) species. After a LEED analysis and reinterpretation of vibrational spectra by Kesmodel et al. [78Kes, 79Kes] ethylidyne was proposed as stable species with the C-C bond normal to the surface and a bond length of 1.5 Å (slightly less than the single carbon-carbon bond length of 1.54 Å). It was suggested that three equivalent Pt-C bonds form in a threefold hollow site on Pt(111) (Fig. 10). Based on vibrational data from transition metal clusters with ethylidyne ligands it was shown that Ibach's EELS data were consistent with the ethylidyne structure. A crucial proposal from Kesmodel et al. [78Kes, 79Kes] was the analogy to the organometallic clusters  $\text{CH}_3\text{CCo}_3(\text{CO})_9$  and  $\text{CH}_3\text{CRu}_3(\text{CO})_9$  which was used as model compound to interpret EELS data (an analogy that is also valid for other hydrocarbons [99Ans, 04Ans]). Albert et al. confirmed the upright orientation using ARUPS [82Alb]. Horsley et al. [85Hor] studied ethylidyne on Pt(111) using NEXAFS and found it disordered but with a C-C bond of  $1.47 \pm 0.03$  Å perpendicular to the surface. Wang et al. [85Wan] used NMR to study ethylidyne on Pt(111) and found it disordered but perpendicular to the surface, with a C-C bond of  $1.49 \pm 0.02$  Å. Using TPD methods, a carbon to hydrogen ratio of 2:3 was determined, further confirming the ethylidyne  $\text{C}_2\text{H}_3$  picture [79Dem1, 82Ste]. Convincing evidence came also from a normal mode analysis for the ethylidyne nanocarbonyl tricobalt complex  $\text{CH}_3\text{CCo}_3(\text{CO})_9$  by Skinner et al. [81Ski] showing an excellent agreement with EELS spectra. It is now generally agreed that ethylidyne is the stable product of  $\text{C}_2\text{H}_4$  decomposition on Pt(111) (and Pd and Rh(111)).

The different  $\text{C}_2\text{H}_4$  adsorbate species could also be identified by vibrational spectroscopy. Mainly infrared spectroscopy [88Moh, 92Rek] was applied but sum frequency generation (SFG) data were also obtained recently, including mbar pressure ranges [95Cre2, 95Cre1, 96Cre2, 96Cre3, 96Cre4, 99Som, 03Fre]. Three prominent features at  $2880\text{ cm}^{-1}$ ,  $2910\text{ cm}^{-1}$  and  $3000\text{ cm}^{-1}$  were observed. The peak  $2880\text{ cm}^{-1}$  was the  $\nu_s(\text{CH}_3)$  of ethylidyne ( $\text{M}\equiv\text{CCH}_3$ ), the feature at  $2910\text{ cm}^{-1}$  resulted from the  $\nu_s(\text{CH}_2)$  of chemisorbed di- $\sigma$  bonded ethylene, and the peak just below  $3000\text{ cm}^{-1}$  was the  $\nu_s(\text{CH}_2)$  of (weakly bonded) physisorbed  $\pi$ -bonded ethylene. On single crystal surfaces the  $\nu_s(\text{CH}_2)$  signal for  $\pi$ -bonded molecules was weak due to the surface-dipole selection rule for metal surfaces (dynamic dipoles parallel to the surface plane are canceled by image dipoles inside the metal) [83Hof]. Ethylidyne and the di- $\sigma$  ethylene compete for the same (hollow) adsorption sites. The transition from di- $\sigma$  ethylene to ethylidyne via ethylidene ( $=\text{CHCH}_3$ ) (Fig. 9) was monitored by SFG and a vibrational peak at  $2957\text{ cm}^{-1}$  ( $\nu_{\text{as}}(\text{CH}_3)$ )

provided strong evidence for the ethylidene intermediate [95Cre1]. A mixture of  $\pi$ -bonded and di- $\sigma$ -bonded ethylene can be obtained by exposing the Pt(111) surface to a near-saturation coverage of oxygen at room temperature, followed by exposure to ethylene at 120 K [82Ste]. IRAS spectra from the deuterium substituted ethenes,  $\text{H}_2\text{C}=\text{CD}_2$  and  $\text{D}_2\text{C}=\text{CD}_2$  on Pt(111) at 360 K were reported by Chesters et al. [90Che4]. The spectra from  $\text{H}_2\text{C}=\text{CD}_2$  indicated isotopic scrambling between the adsorbed ethylidyne species, possibly mediated by the coexisting Pt-H/Pt-D species.

Variable temperature STM was applied by Land et al. [92Lan] to image  $\text{C}_2\text{H}_4$  adsorption and decomposition on Pt(111). The conversion of  $\text{C}_2\text{H}_4$  to  $\text{C}_2\text{H}_3$  was directly observed, occurring in a "patchy" manner across the surface. As the reaction proceeded, well-defined islands of unreacted  $\text{C}_2\text{H}_4$  continued to be observed. Further dehydrogenation of ethylidyne up to 500 K produced randomly dispersed carbon containing particles. Annealing the carbon particle covered surface to above 700 K resulted in the formation of monolayer thick graphite islands, eventually accumulating at Pt steps.

Zaera et al. [96Zae] applied IRAS and isothermal kinetic measurements to study the simultaneous occurrence of several reactions, namely molecular desorption, dehydrogenation to ethylidyne, H-D exchange within the adsorbed molecules, and hydrogenation to ethane. The vinyl ( $-\text{CH}=\text{CH}_2$ ), ethyl ( $-\text{CH}_2\text{CH}_3$ ) and ethylidene ( $=\text{CHCH}_3$ ) species were prepared by thermal decomposition of their corresponding iodides and characterized by IRAS. The formation of ethylidene as an intermediate in the conversion of ethylene to ethylidyne was suggested but the complexity of the kinetics of that reaction (depending strongly on surface coverage) made a final proof difficult. A side ethylene-ethyl equilibrium at temperatures below those required for the formation of ethylidyne was responsible for H-D exchange in ethylene. The hydrogenation of ethylene to ethane also involved an ethyl intermediate, but only occurred at high ethylene coverage which was needed for the transition of the strongly bonded di- $\sigma$  species to a weak  $\pi$ -configuration.

Domen et al. [01Oht] reported the suppression of ethylidyne formation on Pt(111) by reversible adsorption of di- $\sigma$ -bonded ethylene in the presence of  $1.3 \times 10^2$  Pa  $\text{C}_2\text{H}_4$  using IRAS. Di- $\sigma$ -bonded ethylene was converted to ethylidyne at 260-300 K in  $1.3 \times 10^2$  Pa of ethylene, while it was converted already at 240-260 K in UHV. The vacant sites adjacent to di- $\sigma$ -bonded ethylene were suggested to be required for ethylidyne formation. These sites were occupied by di- $\sigma$ -bonded ethylene when the adsorbed molecules were in equilibrium with gaseous ethylene. The reversible adsorption of di- $\sigma$ -bonded ethylene was indicated by an IRAS peak at  $2906 \text{ cm}^{-1}$  even at 300 K, which was confirmed by the substitution of isotopically labeled ethylene at 200 K. The same group also studied  $\text{C}_2\text{H}_4$  hydrogenation on Pt(111) by DFT [00Miu] and IRAS [99Oht] and found that the rate did not depend on the coverage of di- $\sigma$ -bonded ethylene or ethylidyne, in agreement with SFG studies [96Cre2, 99Som, 03Fre].

IRAS studies of ethylidene ( $=\text{CH}-\text{CH}_3$ ) and ethylidyne ( $\equiv\text{C}-\text{CH}_3$ ) were also reported by Newell et al. [98New]. These species appeared during the decomposition of adsorbed ethyl ( $\text{C}_2\text{H}_5$ ) on Pt(111) produced by dissociative adsorption of ethane from a supersonic molecular beam at 150 K.

Lee and Wilson [03Lee] investigated the adsorption and decomposition of  $\text{C}_2\text{H}_4$  on Pt(111) by fast XPS. At 100 K ethylene exhibited a precursor-mediated adsorption kinetics, adopting a single environment with a saturation  $\text{C}_2\text{H}_4$  coverage of 0.25 ML and a binding energy of 283.2 eV. Thermal decomposition proceeded above 240 K via dehydrogenation to ethylidyne with an activation barrier of  $57 \pm 3 \text{ kJ mol}^{-1}$  and a preexponential factor  $\nu = 1 \times 10^{10 \pm 0.5} \text{ s}^{-1}$ . Site-blocking by preadsorbed  $\text{SO}_4$  reduced the ethylene saturation coverage but induced a new, less reactive  $\pi$ -bonded ethylene species centered around 283.9 eV, which in turn decomposed to ethylidyne at 350 K.

Sautet and Paul [91Sau] compared the different low temperature coordination modes of ethylene on Pt(111) and (110) by extended Hückel calculations, using a 49 or a 44 atoms cluster as model. The di- $\sigma$  coordination was found more stable on Pt(111) but on Pt(110) the  $\pi$ -coordination yielded the same adsorption energy. The  $\pi$ -mode was favoured by a decrease of the four electron repulsion caused by a smaller number of metal neighbours for the surface atom on Pt(110). Mittendorfer et al. [03Mit] carried out a comparative DFT study of the adsorption of ethylene, 1-butene, acetylene, and 1,3-butadiene on Pt(111), analyzing structural, electronic, energetic and spectroscopic properties. In another theoretical study Cortright et al. [99Cor] have used quantum chemical methods to estimate energetics for interactions of various  $\text{C}_2\text{H}_x$  species with platinum. It was suggested that the primary reaction pathways for cleavage

of the C-C bond take place through activated complexes based on ethyl ( $\text{C}_2\text{H}_5$ ) and ethylidene ( $=\text{CH}-\text{CH}_3$ ) species.

Brown et al. [99Bro2] measured the sticking probability and heat of adsorption for  $\text{C}_2\text{H}_4$  on the stepped Pt(211) and Pt(311)-(1 $\times$ 2) surfaces using microcalorimetry. Adsorption on Pt(211) leads to the formation of several different species as a function of coverage, whereas adsorption on Pt(311)-(1 $\times$ 2) produced only one species on the surface over the whole coverage range. The initial heats of adsorption for  $\text{C}_2\text{H}_4$  on Pt(211) and Pt(311)-(1 $\times$ 2) were 180 and 220 kJ/mol, respectively. The initial sticking probabilities were 0.84 for both surfaces. The most likely species to be formed on Pt(211) as a function of coverage were quad- $\sigma$  acetylene followed by ethylidyne whereas on Pt(311)-(1 $\times$ 2) ethylidyne forms at all coverages.

LEED studies on a variety of stepped Pt surfaces, Pt(S)-[4(111)  $\times$  (100)], Pt(S)-[6(111)  $\times$  (100)], Pt(S)-[7(111)  $\times$  (310)], Pt(S)-[9(111)  $\times$  (111)] and Pt(S)-[9(111)  $\times$  (100)] revealed (2 $\times$ 2), ( $\sqrt{19}\times\sqrt{19}$ )R22.4 $^\circ$ -C, disordered structures and graphite overlayers [72Lan, 74Bar, 75Lan1, 78Net1, 78Net2].

#### 3.8.6.4.1.11 Re

$\text{C}_2\text{H}_4$  adsorption on Re(0001) produced disordered and (2 $\times\sqrt{3}$ )R30 $^\circ$ -C structures [78Duc, 81Duc]. On various stepped Re surfaces, Re(S)-[14(0001)  $\times$  (10 $\bar{1}$ 0)], Re(S)-[6(0001)  $\times$  (16 $\bar{7}$ 1)], (2  $\times$   $\sqrt{3}$ )R30 $^\circ$ -C and disordered structures were observed [81Duc].

#### 3.8.6.4.1.12 Rh

LEED studies of  $\text{C}_2\text{H}_4$  on Rh(100) revealed c(2 $\times$ 2), c(2 $\times$ 2)- $\text{C}_2\text{H}+\text{C}_2\text{H}_3$ , (2 $\times$ 2)- $\text{C}_2\text{H}$ , c(2 $\times$ 2)-C and graphite overlayer structures [78Cas, 82Dub]. Slavin et al. [88Sla1, 88Sla2] demonstrated by HREELS that ethylidyne ( $\equiv\text{C}-\text{CH}_3$ ) was formed on Rh(100). Although the exact binding site was not determined, ethylidyne was identified for the first time on a surface which lacks three-fold hollow sites. The ethylidyne species was produced by preadsorbing  $\sim 0.5$  ML CO followed by adsorption of  $\text{C}_2\text{H}_4$  at 300 K. Adsorption of  $\text{C}_2\text{H}_4$  alone produced a mixture of hydrocarbon fragments which included ethylidyne. Ethylidyne was thermally stable up to 350 K. According to HREELS, the ethylidyne species stands approximately upright on the surface with its carbon-carbon bond along the surface normal, similar to the situation on Rh(111).

Kose et al. [99Kos] determined coverage dependent heats of adsorption and sticking probabilities for  $\text{C}_2\text{H}_4$  on Rh(100) by microcalorimetry. For  $\text{C}_2\text{H}_4$ , the initial heat of adsorption was  $175\pm 10$  kJ mol $^{-1}$ , and the initial sticking probability was  $0.88\pm 0.01$ . Ethylene adsorption on Rh(100) at 300 K produced  $\sigma$ -bonded CCH and the corresponding Rh-C bond energy was estimated as  $\sim 268$  kJ/mol.

Ethylidyne ( $\equiv\text{C}-\text{CH}_3$ ) on surfaces other than Pt(111) was first reported by Dubois et al. [80Dub], studying  $\text{C}_2\text{H}_4$  on Rh(111) by LEED, TPD and EELS. When ethylene adsorbs on Rh(111) [91Wan], it loses a hydrogen and rearranges (like on Pt) but on Rh ethylidyne occupies an hcp hollow site (i.e. a hexagonal close packed hollow site with a metal atom directly underneath the chemisorption site in the second metal layer) (Fig. 10). Contrary to Pt(111), the Rh metal atoms move away from the carbon atom bound to the hollow site to allow the carbon to better bond to the Rh atom directly underneath the carbon in the second layer. The adsorption-induced distortion in the top metal layers pulls the nearest neighbor metal atoms up out of the surface plane. Koestner et al. [82Koe2] determined by LEED crystallography that on Rh(111) the C-C bond of ethylidyne was anomalously short for an  $\text{sp}^3$  carbon ( $1.45\pm 0.10$  Å vs. 1.54 Å) and that the terminal carbon was located  $1.31\pm 0.10$  Å above a 3-fold hcp site. A  $\sigma$ - $\pi$  hyperconjugation of the ethylidyne orbitals was proposed as reason for bond shortening.

Koel et al. [84Koe] combined HREELS with a UHV-high-pressure system to study the structure of stable hydrocarbon species that form during catalytic reactions at atmospheric pressure. A monolayer of adsorbed ethylidyne ( $\equiv\text{C}-\text{CH}_3$ ) on Rh(111) at 310 K did not hydrogenate to ethylene or ethane in one



atmosphere D<sub>2</sub>. The exchange of H in the methyl group with deuterium was slow with the amount of exchange strongly dependent on the amount of uncovered, bare-metal surface (with little effect of the hydrogen pressure). A mechanism for H-D exchange involving an ethylidene (=CHCH<sub>3</sub>) intermediate was proposed. C<sub>2</sub>H<sub>4</sub> and C<sub>2</sub>H<sub>3</sub> on Rh(111) were also characterized via their vibrational fine structure in C1s core level XPS spectra by Andersen et al. [97And].

The chemisorption of C<sub>2</sub>H<sub>4</sub> was studied on stepped Rh(755) and (331) surfaces by LEED, AES and TDS [79Cas]. Several ordered surface structures were observed. The LEED patterns seen on the (755) surface were due to the formation of surface structures on the (111) terraces, while on the (331) surface the step periodicity played an important role in the determination of the unit cells of the observed structures. When heated in a low pressure of C<sub>2</sub>H<sub>4</sub> the (331) surface was more stable than the (755) surface which readily formed (111) and (100) facets. On the stepped Rh(S)-[6(111) × (100)] a disordered layer was observed [79Cas].

#### 3.8.6.4.1.13 Ru

Henderson et al. [88Hen] studied the adsorption and decomposition of C<sub>2</sub>H<sub>4</sub> on Ru(001) with HREELS, SIMS and TPD. Ethylene adsorbed molecularly on Ru(100) in a di-σ bonded structure and decomposed to ethylidyne (CCH<sub>3</sub>) above 150 K. IRAS studies were reported in [93Ran].

#### 3.8.6.4.1.14 Si

Jackman et al. [94Chu2, 95Jac] studied reactions of C<sub>2</sub>H<sub>4</sub> with atomic hydrogen on Si(100). Such reactions may be important for CVD diamond nucleation and growth. Without atomic hydrogen, C<sub>2</sub>H<sub>4</sub> displayed a simple surface chemistry, adsorbing molecularly at low temperatures and dissociating irreversibly to gaseous hydrogen and surface carbon as the temperature was raised. Atomic hydrogen stimulated C-H and C-C bond making/breaking processes. It was observed that adsorbed C<sub>2</sub>H<sub>4</sub> was converted to C<sub>2</sub>H<sub>2</sub> and ultimately to adsorbed CH<sub>2</sub> species in the presence of an atomic hydrogen flux. LEED studies of C<sub>2</sub>H<sub>4</sub> on Si(331) exhibited (1×1), (2×1) and (3×1) structures [70Hec].

#### 3.8.6.4.1.15 Ta

C<sub>2</sub>H<sub>4</sub> adsorption on Ta(100) was examined using LEED and AES [74Che3]. Carbon dissolution into the crystal was observed.

#### 3.8.6.4.1.16 W

The interaction of C<sub>2</sub>H<sub>4</sub> with W(100) was studied from 80-500 K by monitoring changes in the carbon Auger peak shape [74Che2, 74Che1, 79Che]. At 80 K decomposition to C<sub>2</sub>H<sub>2</sub> occurred followed by non-dissociative adsorption. Heating the adsorbate to 300 K resulted in further decomposition to C<sub>2</sub>H<sub>2</sub>. Decomposition to chemisorbed C atoms was detected above 300 K. (15×3)Rα-C and (15×12)Rα-C structures were observed for C<sub>2</sub>H<sub>4</sub> adsorption on W(110), and (1×1) for adsorption on W(111) [69Bou, 78Win].

#### 3.8.6.4.1.17 Alloys

Koel and coworkers [89Paf, 97Tsa] investigated the adsorption and decomposition of C<sub>2</sub>H<sub>4</sub> on Pt(111) and the (2×2) and (√3×√3)R30° Sn/Pt(111) surface alloys with TPD, LEED and sticking coefficient measurements. A (2√3×2√3)R30° ordered structure for C<sub>2</sub>H<sub>4</sub> chemisorbed on the (2×2)Sn/Pt(111) surface

alloy was reported. Chemisorption energies of  $C_2H_4$  over Pd and PdAu alloys were calculated from first-principles DFT calculations by Neurock et al. [02Neu, 03Mei]. Alloying the surface with Au reduced the activation barrier for hydrogenation (63 kJ/mol on Pd to 29-33 kJ/mol on PdAu) but increased the barriers for  $H_2$  dissociation and ethylidyne formation (Au reduces the number of sites that can activate hydrogen which decreases the rate of ethylene hydrogenation). These two effects balance each other out so that the primary influence of Au is to decrease ethylene decomposition that leads to ethylidyne and  $CH_x$  and deactivates the catalysts.

#### 3.8.6.4.2 Propene $C_3H_6$

##### 3.8.6.4.2.1 Mo

Vu and Tysøe [97Vu] reported that propene (propylene)  $C_3H_6$  adsorbed on Mo(100) and oxygen-covered Mo(100) either thermally decomposed to hydrogen and surface carbon, desorbed molecularly, self-hydrogenated to form propane, or ultimately decomposed to adsorbed  $C_1$  species, which hydrogenated to  $CH_4$ . Because the amount of hydrogen desorption decreased linearly with increasing oxygen coverage, it was proposed that propylene decomposition proceeded on the four-fold hollow sites of Mo(100). Predosing the surface with hydrogen increased the yield of self-hydrogenation to propane indicating that propylene reacted with surface hydrogen. It was proposed that propylene adsorbs on molybdenum by  $\pi$ -donation.

##### 3.8.6.4.2.2 Ni

Whelan et al. [01Whe, 02Whe] examined adsorption and decomposition of propene ( $C_3H_6$ ) on Ni(100) between 90 and 530 K using temperature-programmed C1s core level XPS with synchrotron radiation. At 105 K, C1s spectra indicated precursor mediated occupation of a single adsorption state from submonolayer to monolayer coverage with evidence of adsorbate-adsorbate interactions. High exposures lead to the formation of multilayers which desorbed above 105 K leaving a chemisorbed monolayer. Between 105 and 150 K, a shift of the binding energies in the C1s spectra was attributed to the transition from  $\pi$ - to di- $\sigma$ -bonded propene. The conversion of di- $\sigma$ -bonded propene to a  $C_3$  intermediate containing a methyl group occurred at 200 K. Formation of this  $-C_2H_xCH_3$  surface species was complete at 300 K and was followed by dehydrogenation to carbidic carbon which was the final decomposition product above 370 K.

##### 3.8.6.4.2.3 Pd

Reactions of propene on atomic oxygen-covered Pd(100)-p(2×2)-O were carried out by Guo and Madix [95Guo1] using TPRS. No partial oxidation products were observed, “combustion” yielded  $H_2O$ , CO and  $CO_2$ . Adsorbed O did not inhibit propene adsorption (while O inhibited both adsorption and reaction of ethylene). Isotope experiments showed that initial reactions occurred predominantly with the vinylic C-H bond. The same authors [95Guo2] also investigated the adsorption and reactions of  $C_3H_6$  on Pd(100)-p(1×1)-H and Pd(100)-p(1×1)-D. It was found that propene underwent efficient H-D exchange reactions below 300 K for all C-H bonds, whereas no hydrogenation products (alkanes) were observed. The exchange reaction was proposed to occur via reversible hydrogenation to a half-hydrogenated intermediate. The absence of alkene hydrogenation may be due to stronger metal-hydrogen bonds on Pd(100) than on other metals such as Pt and Rh. A possible effect of hydrogen dissolution in the Pd bulk on olefin hydrogenation was discussed by Rupprechter et al. [04Rup].

The adsorption of  $C_3H_6$  on clean and hydrogen-covered Pd(111) was studied by Stacchiola et al. [03Stac2] using TPD and IRAS. Propylene adsorbs in a di- $\sigma$  configuration on clean Pd(111) while pre-adsorption of hydrogen induced some  $\pi$ -bonded propylene (steric effects caused by the methyl group

seemed to limit the  $\pi$ -configuration). Upon heating, propylene desorbed molecularly at approx. 200 and 280 K and was subject to significant dehydrogenation to propylidyne and  $\eta_1$ -allyl species. Formation of propane was observed by reaction of hydrogen with propylene in TPD, with an activation energy of  $14 \pm 1.7$  kJ/mol.

#### 3.8.6.4.2.4 Pt

Koestner et al. [82Koe1] studied  $C_3H_6$  adsorption on Pt(111) by LEED, measuring intensity versus voltage (I-V) spectra. Two phases were detected. At low temperatures, the unsaturated C-C group formed a di- $\sigma$  bond to two Pt atoms. Upon warming to  $\sim 300$  K, a conversion took place to an alkylidyne species that was bonded to three Pt atoms and had its C-C bond nearest to the metal substrate oriented perpendicularly to the surface. At 300 K propylene formed ordered (2 $\times$ 2) structures and disordered structures of propylidyne ( $\equiv C-CH_2-CH_3$ ) [82Koe1, 83Koe, 86Ave1, 86Ogl].

Cremer et al. [96Cre1] studied  $C_3H_6$  hydrogenation on Pt(111) using SFG. Under UHV (in the absence of hydrogen) propylene adsorbed as di- $\sigma$  bonded propylene which dehydrogenated to propylidyne ( $\equiv C-CH_2-CH_3$ ) just below room temperature and to vinylmethylidyne ( $\equiv C-CH=CH_2$ ) at 450 K (and forming graphite at higher temperatures). In the presence of hydrogen at 295 K,  $C_3H_6$  hydrogenation proceeded from  $\pi$ -bonded propylene via a 2-propyl species (Pt-CH(CH<sub>3</sub>)<sub>2</sub>) to propane.

Koel et al. [97Tsa] studied the adsorption and decomposition of propylene on Pt(111) with TPD, LEED and sticking coefficient measurements. An adsorption energy of 73 kJ/mol was reported. Comparison with the (2 $\times$ 2) and ( $\sqrt{3} \times \sqrt{3}$ )R30° Sn/Pt(111) surface alloys (see 3.8.6.4.2.8) suggested that the Pt three-fold hollow sites were important for strong alkene chemisorption.

Zaera and Chrysostomou [00Zae] studied the thermal chemistry of propylene on Pt(111) by TPD. Besides molecular desorption and hydrogen production from propylene dehydrogenation (first to propylidyne and eventually to surface carbon), a small amount of propane from self-hydrogenation of the olefin was detected at  $\sim 280$  K. Hydrogen coadsorption weakened the adsorption of propylene on the surface, and enhanced the production of propane. Deuterium coadsorption with propylene lead to H-D exchange, in addition to deuteration to propane. Multiple H-D exchange was evidenced by the formation of all possible deuterium-substituted propylenes and propanes, including propylene-d<sub>6</sub> and propane-d<sub>8</sub>. Most of the propylene that remained on the surface above 350 K dehydrogenated to propylidyne (Pt<sub>3</sub>C-CH<sub>2</sub>-CH<sub>3</sub>). A small fraction of that species rehydrogenated to propane at 430 K, while the rest stepwise dehydrogenated to surface carbon.

#### 3.8.6.4.2.5 Rh

$C_3H_6$  adsorption on Rh(111) produced (2 $\times$ 2) and ( $2\sqrt{3} \times 2\sqrt{3}$ )R30° structures [82Van]. Hydrocarbon phases originating from propene adsorption on Rh(111) and subsequent annealing and those from direct adsorption at higher temperatures were characterized by HREELS [89Wan]. C<sub>x</sub>H species, ethylidyne, propylidyne and di- $\sigma$  adsorbed propene were observed.

#### 3.8.6.4.2.6 Ru

Propene adsorption on Ru(0001) [93Ran], studied by IRAS at 130 K, produced a physisorbed layer with a weak spectrum attributed to a di- $\sigma$  adsorbed species.  $C_3H_6$  converted to propylidyne at higher temperature and decomposed via the ethylidyne species. EELS and SIMS were used to investigate the adsorption and decomposition of propene on Ru(0001) [92Sak]. Propene was found to adsorb molecularly at 153 K but annealing to 203 K produced adsorbed propylidyne. At 233 K ethylidyne and propylidyne were found to coexist but by 293 K the propylidyne species had decomposed completely to ethylidyne and C<sub>x</sub>H.

#### 3.8.6.4.2.7 W

C<sub>3</sub>H<sub>6</sub> adsorption on W(100) and W(221) reported (5×1)-C and c(6×4)-C structures, respectively [84Ben].

#### 3.8.6.4.2.8 Alloys

Tsai et al. [97Tsa] studied propylene adsorption and decomposition on Pt(111) and the (2×2) and ( $\sqrt{3}\times\sqrt{3}$ )R30° Sn/Pt(111) surface alloys with TPD, LEED and sticking coefficient measurements. Little or no effect of alloyed Sn on either the initial sticking coefficient or the saturation coverage on the two Sn/Pt(111) ordered surface alloys was observed when compared with the clean Pt(111) surface at 100 K. Based on TPD peak temperatures, the propylene adsorption energy decreased from 73 to 62 and then to 49 kJ/mol as the substrate was changed from Pt(111) to the (2×2) and the ( $\sqrt{3}\times\sqrt{3}$ )R30° alloys. This implicates that the “Pt-only” three-fold hollow sites were important for strong alkene chemisorption, since removal of these sites on the ( $\sqrt{3}\times\sqrt{3}$ )R30° alloy caused a sharper decrease in the adsorption energy than expected based upon the changes observed for the (2×2) alloy. Even though propylene contains allylic C-H bonds that are much weaker than the vinylic C-H bonds in ethylene, only ca. 5-7% as much propylene decomposed on the (2×2) alloy compared to Pt(111) and no decomposition occurred on the ( $\sqrt{3}\times\sqrt{3}$ )R30° alloy. This shows the importance of adjacent “Pt-only” three-fold hollow sites for alkene decomposition.

#### 3.8.6.4.3 Butenes C<sub>4</sub>H<sub>10</sub>

##### 3.8.6.4.3.1 Ag

IRAS and TPD studies of cis- and trans-2-butenes adsorbed on Ag(111) were reported by Wu et al. [00Wu]. The surface infrared spectra of cis- and trans-2-butene were distinguishable, a monolayer of cis-2-butene/Ag(111) exhibited peaks at 1445, 1434 and 1030 cm<sup>-1</sup> whereas the trans isomer had features at 1429, 973 and 959 cm<sup>-1</sup>.

Pawela-Crew and Madix [95Paw1, 95Paw2] applied TPD, XPS, NEXAFS and IRAS to examine the desorption kinetics of butenes on Ag(110) (Fig. 14). The origin of repulsive intermolecular forces was revealed by NEXAFS, which showed a strong orientation of the double bond axis parallel to the surface, indicative of weak directional bonding between the surface and the alkene. It appears that this preferred orientation caused by the surface altered the intermolecular forces between colliding pairs of butenes, leading to the repulsive interactions that produced a decrease in the activation energy for desorption with increasing alkene coverage. Activation energies of desorption at zero coverage were 56±3 kJ/mol both for 1-butene and isobutylene. According to the observed vibrational modes (making use of the dipole selection rule) isobutylene lies flat on the surface. Unlike isobutylene, only three of the carbons in 1-butene are in a plane parallel to the surface; the methyl group was found tilted 110±10° away from the surface plane.

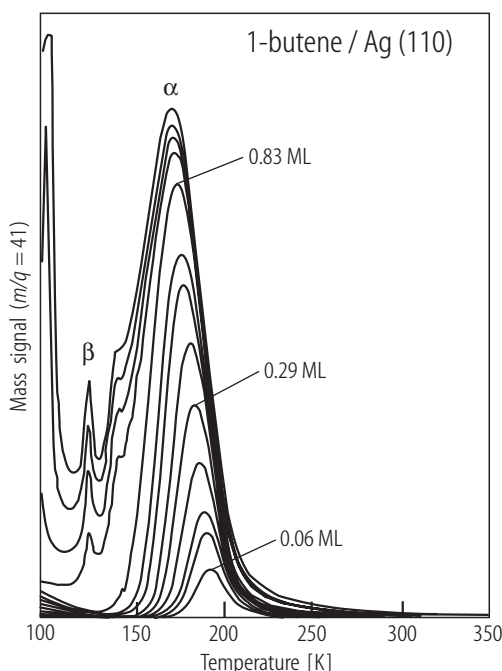


**Fig. 14** TPD spectra of 1-butene on Ag(110) for a broad coverage range exhibiting multiple state desorption for  $\theta > 0.8$  ML and repulsive lateral interaction over the entire coverage range observed, adapted from [95Paw1].

#### 3.8.6.4.3.2 Mo

2-butene adsorption on Mo(100) and oxygen-covered Mo(100) was studied by Wu and Tysøe [98Wu1]. The 2-butenes either thermally decomposed to yield hydrogen and adsorbed carbon, desorbed molecularly, self-hydrogenated to butane, or dissociated to form a  $C_2$  species which further decomposed to methane. It was proposed that 2-butenes thermally decomposed on the four-fold sites on Mo(100) since the hydrogen yield decreased linearly with oxygen coverage (oxygen blocks the four-fold sites). The butene desorption and self-hydrogenation activation energy increased with increasing oxygen coverage suggesting that 2-butenes bind to Mo(100) predominantly via donation of  $\pi$ -electrons to molybdenum. Methane formation was proposed to occur via the formation of methylene carbenes formed by direct carbon-carbon double-bond cleavage. The methane yield was much larger than that found following both ethylene and propylene adsorption on oxygen-modified molybdenum presumably due to differences in  $\pi$ -donation.

Kelly et al. [86Kel] investigated the chemisorption and reactions of 1-butene on clean Mo(100), and with sulfur or carbon overlayers, using TDS. The predominant reaction at low additive coverage (0-0.2 monolayers of S or C), and at low ambient pressure ( $10^{-10}$  Torr) was decomposition. As additive (S or C) coverage increased the amount of decomposition decreased, enabling other reaction pathways to become more probable. Hydrogenation, partial dehydrogenation, and isomerization reactions were detected. On sulfur overlayers the binding of the hydrocarbon was weak (physisorption), usually on the order of the heat of sublimation ( $\sim 40$  kJ/mol). However, molecular binding on carbon overlayers was stronger: the heat of desorption was 50-63 kJ/mol. In addition, isomerization of 1-butene to 2-butene occurred on the carbon overlayer. It was suggested that the metal sites control the reactions observed (except for isomerization). This explains why the difference in molecular hydrocarbon binding between the sulfur covered and carbon covered surface plays a minor role in these reactions.

Eng et al. [98Eng] studied the reaction pathways of cis- and trans-2-butene on clean Mo(110) and carbide-modified Mo(110) using TPD and HREELS. The vibrational data revealed that the decomposition pathways of cis- and trans-2-butene were different on clean Mo(110). In the case of cis-2-butene, the olefinic  $\alpha(C-H)$  bonds were cleaved at 80 K to produce surface hydrogen and 2-butyne. In contrast, the initial decomposition of trans-2-butene also involved  $\beta(C-H)$  bond scission, such that at least one of the methyl groups of the molecule was converted to a  $CH_2$  group at temperatures below 150 K. On carbide-

modified Mo(110), the initial decomposition step for both cis- and trans-2-butene involved  $\alpha(\text{C-H})$  bond cleavage to form 2-butyne. The difference in reactivity of Mo(110) and carbide-modified Mo(110) towards the 2-butenes provided evidence that the formation of the carbide overlayer enhanced the selective activation of  $\alpha(\text{C-H})$  bonds.

#### 3.8.6.4.3.3 Ni

Isobutene chemisorbed molecularly on Ni(111) in di- $\sigma$  configuration (below 150 K) [90Ham]. Both hydrogen atoms of the methylene group were bridge-bonded to the metal. These two weakly bound hydrogen atoms split off and the residual molecular fragment rehybridized towards  $\text{sp}^2$ . The new surface species was presumably a tilted di- $\sigma/\pi$  isobutenylidene complex. The adsorption and decomposition of 2,3-dimethyl-2-butene on Ni(111) was examined by HREELS and LEED between 80 and 400 K [92Fri]. Non-dissociated 2,3-dimethyl-2-butene showed no ordered superstructure. Partial decomposition around 170 K was accompanied by the development of a  $(2 \times 2)$ -LEED pattern, due to cleaved hydrogen atoms.

#### 3.8.6.4.3.4 Pd

1-butene adsorption on Pd(111), Pd(110) and Pd50Cu50(111) was investigated by NEXAFS, UPS and HREELS by Tourillon et al. [96Tou]. At 95 K, 1-butene was physisorbed on the different Pd single crystals (while being di- $\sigma$ -bonded on Pt(111)). The NEXAFS experiments revealed a decrease of the hydrocarbon-substrate interaction according to the sequence:  $\text{Pd}(111) > \text{Pd}(110) \geq \text{Pd50Cu50}(111)$ .

Katano et al. [02Kat1] applied STM and NEXAFS to examine the chemisorption of trans-2-butene on Pd(110). In STM trans-2-butene appeared as a dumbbell-shaped protrusion and the C=C bond was at the on-top site of the substrate atom. With increasing coverage, a short-range  $(3 \times 1)$ -1D ordered structure at 0.1 ML was formed and a  $c(4 \times 2)$  structure was observed at saturation coverage. NEXAFS experiments revealed the adsorption structure of trans-2-butene on Pd(110), where the direction in which the two methyl groups are connected is parallel to [001] at low coverage and the C=C double bond is parallel to [110] at high coverage.

Reactions of 1-butene on atomic oxygen-covered Pd(100)- $p(2 \times 2)$ -O were studied by Guo and Madix [95Guo1] using TPRS. No partial oxidation products were observed, combustion yielded  $\text{H}_2\text{O}$ , CO and  $\text{CO}_2$ . Adsorbed O did not inhibit 1-butene adsorption and reaction. Isotope experiments showed that initial reactions occurred predominantly with the vinylic C-H bond. The same authors [95Guo2] also investigated the adsorption and reactions of 1-butene on the Pd(100)- $p(1 \times 1)$ -H and Pd(100)- $p(1 \times 1)$ -D using TPRS. It was found that 1-butene underwent efficient H-D exchange below 300 K for all C-H bonds, whereas no hydrogenation products (alkanes) were observed. The exchange reaction was proposed to occur via reversible hydrogenation to a half-hydrogenated intermediate. The absence of alkene hydrogenation may be due to stronger metal-hydrogen bonds on Pd(100) than on other metals such as Pt and Rh, or to the effect of hydrogen bulk dissolution [04Rup]. Mittendorfer et al. [03Mit] carried out a DFT study of the adsorption of 1-butene on Pd(111) and Pt(111).

#### 3.8.6.4.3.5 Pt

Using LEED, different superstructures were observed for  $\text{C}_4\text{H}_8$  isomers on Pt(111), i.e.  $(2\sqrt{3} \times 2\sqrt{3})\text{R}30^\circ$  for cis-2- $\text{C}_4\text{H}_8$  and  $(8 \times 8)$  for trans-2- $\text{C}_4\text{H}_8$  [82Koe1]. At low temperature, the unsaturated C-C group formed a di- $\sigma$  bond to two Pt atoms. Upon warming to  $\sim 300$  K a conversion took place to a butylidyne species that was bonded to three Pt atoms and had its C-C bond nearest to the metal substrate oriented perpendicular to the surface. The butylidyne species was shown to order its ethyl group into an  $(8 \times 8)$  or  $(2\sqrt{3} \times 2\sqrt{3})\text{R}30^\circ$  superlattice when the hydrocarbon exposure was increased; this ordering was probably a natural consequence of the steric hindrance among neighbouring ethyl groups as the hydrocarbon

coverage increased slightly with larger exposures. Isobutene adsorption and hydrogenation on Pt(111) at 300 K was also studied by SFG by Cremer et al. [96Cre4].

Tourillon and coworkers [96Tou] characterized the chemisorption of 1-butene on Pt(111) by NEXAFS, UPS and HREELS. At 95 K, 1-butene was found to be di- $\sigma$ -bonded. Avery and Sheppard [86Ave3] applied TDS and EELS to study the adsorption of 1-butene and cis- and trans-2-butenes at 170 K on Pt(111). Each of the chemisorbed butenes produced a different EEL spectrum, corresponding to  $\eta_2$  di- $\sigma$  adsorbed species. At 300 K, TDS and EELS suggested an n-butyldiyne structure. Comparison with the spectrum of 2-butyne and the model cluster compound  $\text{Os}_3(\text{CO})_{10}(\text{CH}_3\text{CCCH}_3)$  lead to the assignment of a  $\mu_3$ - $\eta_2$   $\text{CH}_3\text{C}:\text{CCH}_3$  structure to the adsorbed species involving the central C:C bond in two  $\sigma$ -bonds and one  $\pi$ -bond to the metal surface.

Koel et al. [97Tsa] examined the adsorption and decomposition of isobutene on Pt(111) with TPD, LEED and sticking coefficient measurements. The isobutene adsorption energy was 72 kJ/mol, as estimated from TPD peak temperatures. Comparison with (2 $\times$ 2) and ( $\sqrt{3} \times \sqrt{3}$ )R30° Sn/Pt(111) surface alloys indicated that the Pt three-fold hollow sites were very important for strong alkene chemisorption and decomposition. Mittendorfer et al. [03Mit] reported a DFT study of the adsorption of 1-butene on Pt(111).

#### 3.8.6.4.3.6 Ru

Adsorption and decomposition of trans-2-butene on Ru(0001) were studied by Chesters et al. using IRAS [91Che]. IR spectra of submonolayer coverages at 90 K pointed to molecular adsorption as di- $\sigma$  species. Further exposure produced spectra assigned to a  $\pi$ -adsorbed species. Heating the monolayer to ~200 K produced a spectrum similar to that of 2-butyne bonded to the surface as a di- $\sigma/\pi$  complex. This behaviour of trans-2-butene contrasted with that of 1-butene and isobutene, which formed alkylidyne rather than alkyne species [90Che3]. At 90 K isobutene adsorbed as di- $\sigma$  bonded state. Annealing to 180 K decomposed the di- $\sigma$  bonded isobutene to isobutyldiyne. Heating of the substrate to 300 K produced ethylidyne as the only IR-detectable entity on the surface. 1-butene followed a similar decomposition pathway, with the corresponding alkylidyne, butylidyne, being formed at ~150 K which was replaced by ethylidyne at 300 K.

#### 3.8.6.4.3.7 Si

Kiskinova and Yates [95Kis] studied the adsorption, desorption and decomposition of the isomeric hydrocarbons, cis- and trans-2-butene, on Si(100)-(2 $\times$ 1) by means of a kinetic uptake method, TPD and AES. Both 2-butene molecules adsorbed molecularly on Si(100)-(2 $\times$ 1) at 120 K with an initial sticking coefficient of near unity. Measurements of the dependence of the adsorption rate on coverage indicated that for the precursor mediated adsorption process the conformational difference between the isomers was of minor importance. Di- $\sigma$  bonding was suggested for the chemisorption state where the molecule preserves its cis- or trans-structure. Upon heating of saturated 2-butene layers, 25% of trans-butene and 13% of cis-butene undergo dissociation, with steric conformational effects being presumably responsible for differences with respect to both desorption and decomposition. It was postulated that the intermediate surface species responsible for dissociation was a di- $\sigma$  (1,3) bonded butane which involved coupling of one methyl group to the substrate. The lack of a significant effect of conformation on the adsorption kinetics indicated that adsorption and desorption occurred by independent pathways.

#### 3.8.6.4.3.8 Alloys

1-butene adsorption on Pd(111), Pd(110) and Pd50Cu50(111) was investigated by NEXAFS, UPS and HREELS by Bertolini and coworkers [96Tou]. At 95 K, 1-butene was physisorbed on the different

Pd-based single crystals (while being di- $\sigma$ -bonded on Pt(111)). NEXAFS revealed a decrease of the hydrocarbon-substrate interaction according to the sequence: Pd(111) > Pd(110)  $\geq$  Pd50Cu50(111).

Tsai et al. [97Tsa] examined the adsorption and decomposition of isobutene on Pt(111) and the (2 $\times$ 2) and ( $\sqrt{3} \times \sqrt{3}$ )R30° Sn/Pt(111) surface alloys with TPD, LEED and sticking coefficient measurements. Little or no effect of alloyed Sn on either the initial sticking coefficient or the saturation coverage on the two Sn/Pt(111) ordered surface alloys was observed, as compared to Pt(111) at 100 K. The isobutene adsorption energy decreased from 72 to 62 and then to 45 kJ/mol as the substrate was changed from Pt(111) to the (2 $\times$ 2) and the ( $\sqrt{3} \times \sqrt{3}$ )R30° alloys, as estimated by TPD peak temperatures. This implicates that the “Pt-only” three-fold hollow sites are important for strong alkene chemisorption. Even though isobutene contains allylic C-H bonds that are much weaker than the vinylic C-H bonds in ethylene, only ca. 5-7% as much isobutene decomposed on the (2 $\times$ 2) alloy compared to the Pt(111) surface and no decomposition occurred on the ( $\sqrt{3} \times \sqrt{3}$ )R30° alloy.

#### 3.8.6.4.4 Pentenes C<sub>5</sub>H<sub>10</sub> and Hexenes C<sub>6</sub>H<sub>12</sub>

##### 3.8.6.4.4.1 Au

Scoles and coworkers [98Wet] used helium atom reflectivity to study the adsorption of 1-alkenes (C<sub>6</sub>H<sub>12</sub>-C<sub>11</sub>H<sub>22</sub>) on Au(111). The physisorption energies increased linearly with the chain length (~5-6 kJ/mol per additional methylene unit).

##### 3.8.6.4.4.2 Pd

The adsorption of trans-2-pentene, cis-2-pentene and 1-pentene on Pd(111) was studied by TPD by Doyle et al. [03Doy, 04Doy]. For all molecules, three distinct molecular desorption states were observed (130, 175 and 260 K), which were assigned to a multilayer,  $\pi$ -bonded pentene and interchanging di- $\sigma$ -bonded pentene/pentyl groups, with the latter species undergoing stepwise dehydrogenation. For trans-2-pentene on D<sub>2</sub> preadsorbed Pd(111), H-D exchange was observed, resulting in D-substituted pentene, which molecularly desorbed or dehydrogenated on heating.

Teschner et al. [05Tes] applied “high-pressure” XPS to study trans-2-pentene on Pd(111) and polycrystalline Pd foil. During hydrogenation a huge amount of carbon (up to 73%) was observed. Mainly graphite was present on Pd(111), whereas other components, C-H and C-Pd, were also formed on the foil to a greater extent. Differences found in the valence and the C1s region between Pd(111) and polycrystalline Pd foil were interpreted as indicators of different electronic structures. From UPS it was concluded that trans-2-pentene was hydrogenated in  $\sigma$ -bonded configuration.

Vasquez and Madix [98Vas] investigated the adsorption and reactivity of 1-hexene on clean Pd(111) and hydrogen (deuterium)-saturated Pd(111) using TPRS. The low-temperature adsorption configuration for the linear C<sub>6</sub> hydrocarbon was proposed to be a weakly  $\pi$ -bonded species. The adsorbed molecules first desorb molecularly with a fraction converting to a more tightly bonded half-hydrogenated state, which undergoes either  $\beta$ -hydride elimination to release the alkene or dehydrogenation to adsorbed carbon and hydrogen. Dehydrocyclization to benzene was observed on Pd(111), whereas it did not occur on Pd(100). H-D exchange was also observed which occurred through the reversible C-H bond formation via a half-hydrogenated intermediate.

##### 3.8.6.4.4.3 Pt

Using IRAS Chesters and coworkers [00Ilh] studied low temperature 1-hexene adsorption and thermal decomposition on Pt(111). A mixture of rotational conformers of hexylidyne was detected at 250 K. The decomposition path previously proposed for hexylidyne on Ru(0001), which involved the formation of metallocycles, was confirmed on Pt(111) by the observation of two types of metallocycle. One was



hydrogenated in C<sub>6</sub> [Pt<sub>3</sub>C-(CH<sub>2</sub>)<sub>5</sub>-Pt], forms at lower temperatures (270 K) and was identified by the symmetric stretching mode of the methylene group attached to the surface (at 2911 cm<sup>-1</sup>). The other, completely dehydrogenated [Pt<sub>3</sub>C-(CH<sub>2</sub>)<sub>4</sub>-CPt<sub>3</sub>], started to form around 370 K, and was identified by the antisymmetric stretching mode of methylenes on C<sub>3</sub> and C<sub>4</sub> and by the symmetric stretch of methylenes on C<sub>2</sub> and C<sub>5</sub>. The thermal decomposition of 1-hexene does not involve the formation of ethylidyne ( $\equiv\text{C}-\text{CH}_3$ ), in contrast with shorter 1-alkenes.

#### 3.8.6.4.4 Ru

1-Hexene adsorption and its thermal decomposition was studied by IRAS by Ilharco et al. [00Ilh]. A mixture of rotational conformers of hexylidyne was detected at 100 K on Ru(0001). The decomposition path for hexylidyne on Ru(0001) involved the formation of metallocycles, as confirmed by the observation of two types of metallocycle ([Ru<sub>3</sub>C-(CH<sub>2</sub>)<sub>5</sub>-Ru] and [RuC-(CH<sub>2</sub>)<sub>4</sub>-CRu]). The thermal decomposition of 1-hexene did not involve the formation of ethylidyne ( $\equiv\text{C}-\text{CH}_3$ ), in contrast with shorter 1-alkene chains on Ru(0001).

#### 3.8.6.5 Dienes

Dienes are even richer in  $\pi$ -electrons than alkenes and thus their bonding to the metal surface is stronger. Work function of the metal decreases upon adsorption of all of these organic molecules. However, the magnitude of the decline is in the order of alkanes < alkenes < dienes < alkynes. The dienes may dissociate/decompose at lower temperature than the alkenes and sequential dehydrogenation occurs as the temperature is increased.

At low temperature (~100 K), the binding of 1,3-butadiene depends on the type of metal and the crystallographic orientation of the substrate, being either di- $\pi$  bonded (e.g. on Pd(111)) or di- $\sigma$  bonded (e.g. on Pt(111); connected with a rehybridization from sp<sup>2</sup> to sp<sup>3</sup> of half of the carbon atoms). At ~300 K, 1,3-butadiene may dehydrogenate and/or transform into butylidyne, similar to butene. Hexadienes adsorb as weakly  $\pi$ -bonded species at low temperature and may undergo dehydrocyclization to benzene above 300 K. At high temperature benzene is a thermodynamically stable species that makes it an important product in free radical surface reactions.

##### 3.8.6.5.1 Propadiene C<sub>3</sub>H<sub>4</sub>

EELS and IRAS studies of propadiene adsorption (H<sub>2</sub>C=C=CH<sub>2</sub>, allene) were reported for Cu(110) [96Sho], Ni(111) [96Sho], Rh(111) [87Ben] and evaporated Ag films (transmission infrared spectroscopy) [96Sho]. Adsorption on Cu(110) and Ag films at low temperature produced a molecularly adsorbed species in which the orthogonal  $\pi$ -system of the molecule was retained and oriented so that one of the CH<sub>2</sub> units was oriented with its plane parallel to the surface, and the other with its plane perpendicular to the surface. The molecules adopted a preferential orientation with the C=C=C skeleton parallel to the surface. Adsorption of propadiene on Ni(111) was different, leading to hydrogen-transfer induced isomerisation in which the two original C=C double bonds were replaced by one single and one triple bond, resulting in the formation of a di- $\sigma$ /di- $\pi$  propyne species.

##### 3.8.6.5.2 Butadiene C<sub>4</sub>H<sub>6</sub>

###### 3.8.6.5.2.1 Ag

The orientation of butadiene on Ag(110) at submonolayer coverage was determined by NEXAFS [91Cou]. Butadiene was found to chemisorb with its  $\sigma$ -h plane parallel to the surface. The C=C and C-C

bond lengths were found to be identical to the gas phase values of 1.34 and 1.46 Å, respectively. There was ordering of the molecules such that the  $\pi$ -orbitals were perpendicular to the surface.

#### 3.8.6.5.2.2 Mo

Kelly et al. [86Kel] investigated the chemisorption and reactions of 1,3-butadiene on clean Mo(100), and with sulfur or carbon overlayers, using TDS. The predominant process at low additive coverage (0-0.2 monolayers of S or C), and at low ambient pressure ( $10^{-10}$  Torr) was decomposition. As additive (S or C) coverage increased the amount of decomposition decreased and other reaction pathways such as hydrogenation, partial dehydrogenation and isomerization became more probable. Molecular binding on the additive overlayers was found to be very different. On sulfur overlayers the binding of the hydrocarbon was weak (physisorption), usually on the order of the heat of sublimation ( $\sim 40$  kJ/mol). The binding on carbon overlayers was stronger: the heat of desorption was 71-97 kJ/mol.

#### 3.8.6.5.2.3 Pd

Reactions of 1,3-butadiene on atomic oxygen-covered Pd(100)-p(2 $\times$ 2)-O were studied by Guo and Madix [95Guo1] using TPRS. No partial oxidation products were observed, combustion yielded H<sub>2</sub>O, CO and CO<sub>2</sub>. Adsorbed O did not inhibit 1,3-butadiene adsorption. Isotope experiments showed that initial reactions occurred predominantly with the vinylic C-H bond. The same authors [95Guo2] also investigated the adsorption and reactions of 1,3-butadiene on the Pd(100)-p(1 $\times$ 1)-H and Pd(100)-p(1 $\times$ 1)-D surfaces using TPRS. It is found that 1,3-butadiene underwent selective hydrogenation to corresponding alkenes below or around 300 K, whereas no H-D exchange reaction was observed to occur. Strong bonding of a half-hydrogenated intermediate to the surface may be the reason for the irreversible hydrogenation of conjugated polyenes to alkenes.

The chemisorption of 1,3-butadiene on Pd(111), Pd(110) and Pd<sub>50</sub>Cu<sub>50</sub>(111) samples was studied by Bertolini et al. [96Ber, 96Tou, 02Ber] using NEXAFS, UPS and HREELS. Different chemisorption modes of 1,3-butadiene were observed on the various surfaces: At 95 K, 1,3-butadiene was physisorbed (di- $\pi$  mode) on the different Pd single crystals (while it was di- $\sigma$  bonded to Pt(111); see 3.8.6.5.2.4). At 300 K, 1,3-butadiene either dehydrogenated on Pd(110) and Pd<sub>50</sub>Cu<sub>50</sub>(111) or very probably transformed into butylidyne on Pd(111), similar to butene adsorbed on the (111) surface. NEXAFS revealed a decrease of the hydrocarbon-substrate interaction according to the sequence: Pd(111) > Pd(110)  $\geq$  Pd<sub>50</sub>Cu<sub>50</sub>(111). The activity for 1,3-butadiene hydrogenation should therefore obey the reverse sequence, what has been actually observed in reactivity measurements. 1,3-butadiene hydrogenation on Pd(111), Pd(110) and Pd<sub>50</sub>Cu<sub>50</sub>(111) displayed a very good selectivity in butenes and a higher activity as compared to Pt(111). Katano et al. [02Kat2] studied the adsorption of 1,3-butadiene on Pd(110) by HREELS, NEXAFS and STM. 1,3-butadiene was found  $\pi$ -bonded and the molecular plane was parallel to the surface, with the C-C single bond aligned toward  $[1\bar{1}0]$ .

Sautet and Paul [91Sau] studied the adsorption modes of butadiene on Pd(111) on the basis of extended Hückel calculations. For the Pd(111) face the  $\pi$ -coordination yielded about the same adsorption energy as the di- $\sigma$  one. This may provide a qualitative explanation of the better selectivity for butadiene partial hydrogenation on Pd(111) compared with Pt(111) (where the di- $\sigma$  coordination was found more stable). Mittendorfer et al. [03Mit] also reported a DFT study of the adsorption of 1,3-butadiene on Pd(111) and Pt(111), analyzing structural, electronic, energetic, and spectroscopic properties.

#### 3.8.6.5.2.4 Pt

Bertolini and coworkers [96Ber, 96Tou] studied the adsorption of 1,3-butadiene on Pt(111) by NEXAFS, UPS and HREELS. It was found that at 95 K 1-butene was di- $\sigma$  bonded to Pt(111) (while being  $\pi$ -bonded

to Pd(111)). At 300 K, a di- $\sigma$  interaction keeping one central carbon-carbon double bond was proposed on Pt(111) (while partial dehydrogenation was observed on Pd(111)). In the butadiene molecule half of the carbon atoms undergo a large rehybridization from  $sp^2$  to  $sp^3$ , as evidenced by HREELS. At 300 K, butadiene transformed into butylidyne on Pt(111). The differences between 1,3-butadiene adsorption on Pt(111) and Pd(111) could be related to differences in catalytic activities and selectivities in 1,3-butadiene hydrogenation. Sautet and Paul [91Sau] applied extended Hückel calculations to compare the different low temperature coordination modes of butadiene on Pt(111) and (110). The di- $\sigma$  coordination was more stable on Pt(111) but on the Pt(110) face the  $\pi$ -coordination yielded the same adsorption energy as the di- $\sigma$  one. A DFT study of 1,3-butadiene adsorption on Pd(111) and Pt(111) was reported in [03Mit].

#### 3.8.6.5.2.5 V

Chen [95Che] investigated the adsorption and decomposition of 1,3-butadiene on clean and carbide-modified V(110). By using HREELS and TDS it was observed that the formation of carbide significantly modified the reactivity of vanadium. While 1,3-butadiene strongly interacted with clean V(110) via the interaction between the d-band of vanadium and the  $\pi$ -orbitals of the adsorbate, on the carbide-modified surfaces the interaction was much weaker.

#### 3.8.6.5.3 Pentadiene $C_5H_8$ , Hexadiene $C_6H_{10}$

##### 3.8.6.5.3.1 Pd

Vasquez and Madix [98Vas] investigated the adsorption and reactivity of 1,5-hexadiene, 1,3-hexadiene, and 1,3,5-hexatriene on clean Pd(111) and hydrogen (deuterium)-saturated Pd(111) using TPRS. The low-temperature adsorption configuration for the linear  $C_6$  hydrocarbons was proposed to be a weakly  $\pi$ -bonded species. The adsorbed molecules desorbed molecularly with a fraction converting to a more tightly bonded half-hydrogenated state, which either  $\beta$ -hydride eliminated to release the alkene or dehydrogenated completely to adsorbed carbon and hydrogen. Dehydrocyclization to benzene was observed on Pd(111), whereas it did not occur on Pd(100). Cyclization of 1,3,5-hexatriene to benzene occurred at temperatures as low as 333 K on Pd(111). Hydrogenation of 1,3-hexadiene to hexene (self-hydrogenation) was observed on Pd(111). On H/Pd(111) 1,3-hexadiene and 1,5-hexadiene were hydrogenated to hexene, and hexatriene was hydrogenated to hexadiene and hexene. However, (total) hydrogenation to hexane did not occur for any of the unsaturated species. H-D exchange into all the adsorbed alkenes was observed though. The exchange reaction was proposed to occur via reversible C-H bond formation in a half-hydrogenated intermediate.

#### 3.8.6.6 Alkynes

Acetylene  $HC\equiv CH$  generally shows strong structural distortions when adsorbed on transition metals and the bonding is often described in terms of a  $\pi$ -donation- $\pi^*$ -backdonation process. At low temperature ( $\leq 200$ -300 K) acetylene forms a strong chemisorption bond to the substrate, creating a state of hybridization close to  $sp^3$ . On (111) planes,  $C_2H_2$  often stabilizes with its C-C axis parallel to the surface over a bridge site with the two C-centers pointing towards adjacent 3-fold hollow sites. The C-C distance of adsorbed  $C_2H_2$  is stretched by  $\sim 20\%$  with respect to that of the free molecule. The C-H axes are tilted by  $60^\circ$  with respect to the C-C axis, pointing away from the surface. Both ordered and disordered acetylene structures, as well as ordered carbon structures (resulting from acetylene decomposition), were observed by LEED.

In the temperature region  $\geq 200$ -300 K dehydrogenated fragments, possibly acetylide ( $-C\equiv CH$ ) and methylidyne ( $\equiv CH$ ), were found to co-exist with molecular acetylene. Further heating typically leads to

decomposition producing graphitic and carbidic carbon as final dehydrogenation products. Upon increasing the temperature, acetylene may also undergo cyclotrimerization to form benzene.

Propyne  $C_3H_4$  is also significantly perturbed upon adsorption, with the gas phase  $C\equiv C$  triple bond suffering a reduction in bond order to  $\sim 1$  and formation of a di- $\sigma$ /di- $\pi$ -bonded species. The strong correlation between the adsorption complexes of propyne and acetylene suggests that the surface chemistry is largely determined by the  $C\equiv C$  triple bond functionality. At higher temperature, propyne may trimerize to trimethylbenzene.

### 3.8.6.6.1 Acetylene $C_2H_2$

#### 3.8.6.6.1.1 Ag

Stuve and Madix studied  $C_2H_2$  adsorption on Ag(110) by EELS [82Stu]. At 100 K  $C_2H_2$  adsorbed without rehybridization and desorbed molecularly between 100 and 160 K. In contrast to interactions between acetylene and other metals the carbon-carbon triple bond was preserved, as determined by the CH stretching frequency of  $3270\text{ cm}^{-1}$ .

#### 3.8.6.6.1.2 Co

Chemisorption of  $C_2H_2$  on Co(0001) was studied by Ramsvik et al. [02Ram1] by high resolution XPS, XAS and LEED. Below 300 K,  $C_2H_2$  forms a strong chemisorption bond to the substrate, creating a hybridization state close to  $sp^3$  with the C-C axis of the molecules oriented parallel to the surface. The vibrational splitting in the XPS spectra due to excitation of the C-H stretch was determined to be  $389\pm 8\text{ meV}$ , which is  $\sim 6\%$  lower than the C-H stretch frequency for gaseous acetylene. The same group studied  $C_2H_2$  chemisorption and dissociation on Co( $11\bar{2}0$ ) [02Ram2] using XPS, NEXAFS, LEED and STM. Adsorbed  $C_2H_2$  dissociated at  $\sim 200\text{ K}$ , which was significantly lower than the dissociation onset for  $C_2H_2$ /Co(0001). NEXAFS showed that  $C_2H_2$  hybridized strongly on the Co( $11\bar{2}0$ ) surface, forming antibonding states below the ionisation limit, which were not present in the gas-phase. In the temperature region 200–300 K a dehydrogenated fragment, possibly  $C_2H$  or  $C_2$ , was found to co-exist with molecular  $C_2H_2$ . Heating to 450 K produced graphitic carbon, forming an ordered ( $5\times 2$ ) carbon overlayer at the expense of molecular  $C_2H_2$  (carbon overlayer was fully developed at 570 K). Above  $\sim 600\text{ K}$ , the amount of ordered carbon atoms decreased, leaving behind mainly graphitic carbon on Co( $11\bar{2}0$ ).

#### 3.8.6.6.1.3 Cu

Ho and coworkers [98Sti2, 99Lau, 00Lau2, 00Lau1, 02Ho, 02Ols] used a variable temperature STM to monitor the thermally induced rotation of single  $C_2H_2$  ( $C_2D_2$ ) molecules between two equivalent orientations on Cu(100) above 68 K. Acetylene adsorbed on a fourfold hollow site, with the C-H bonds bent away from the surface and the molecular plane perpendicular to the surface. Studies of the rotation rate at various temperatures indicated an energy barrier of  $169\pm 3\text{ meV}$  and a preexponential factor of  $10^{11.8\pm 0.2}\text{ s}^{-1}$ . By tracking single molecules above 178 K, measuring the hopping rate as a function of temperature, the thermal diffusion barrier of individual acetylene molecules was determined to be  $0.53\pm 0.01\text{ eV}$  with a preexponential factor of  $10^{13.6\pm 0.2}\text{ s}^{-1}$ . Molecule rotation could also be induced at 9 K with the help of electrons from the STM (Fig. 15). Furthermore, electrons were also used to produce ethynyl (CCH) by breaking a C-H bond in a single  $C_2H_2$  molecule with both  $C_2H_2$  and CCH being characterized via inelastic electron tunneling spectroscopy. HCCH dissociation was accompanied by significant changes in the vibrational spectra and bonding geometry. Electrons of 0–5 eV were also used to induce desorption, diffusion, and vibrational excitation of molecules.

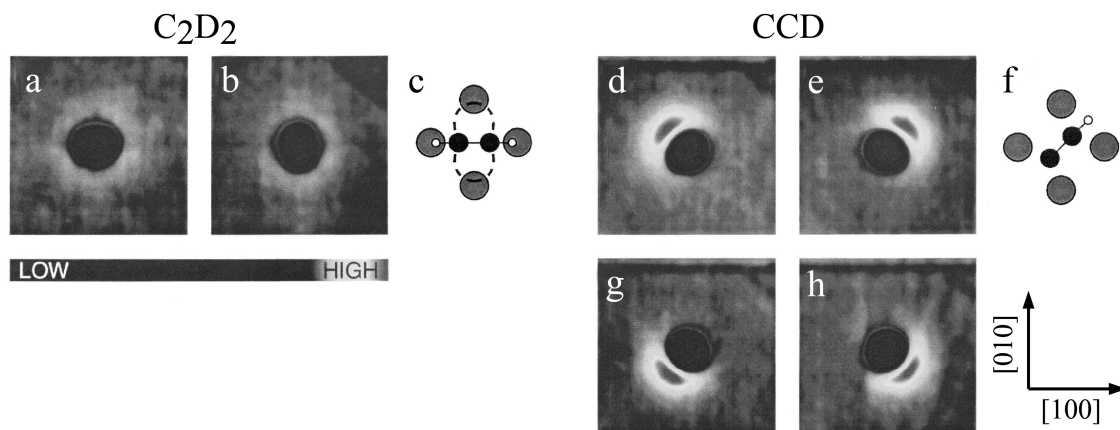


**Fig. 15** Constant current STM images of  $C_2D_2$  and CCD on Cu(100) at 9 K (image size  $38 \text{ \AA} \times 38 \text{ \AA}$ ). The color scheme was adjusted to emphasize the structure above the substrate surface.  $C_2D_2$  is imaged as elongated depression (a, b) and adsorbs above fourfold hollow sites in two equivalent orientations (the schematic in (c) represents image (b)). (d-h) show the four possible orientations of a CCD fragment, produced by breaking a single C-D bond by low-energy electrons from the STM tip. (f) shows the suggested orientation of CCD in image (e); adapted from [00Lau2].

PED [94Bao2] indicated that  $C_2H_2$  adsorption on Cu(111) was accompanied by major structural changes in the  $C_2H_2$  layer even though the overall adsorbate-substrate binding was weak (by contrast, experiments on ethylene-Cu(111) had identified a weakly physisorbed adsorbate without noticeable structural changes). These experimental findings were confirmed by Hermann and Witko [95Her] using cluster model calculations. Extended studies on a small  $Cu_7C_2H_2$  cluster (Fig. 16) revealed that  $C_2H_2$  stabilizes with its C-C axis parallel to the Cu(111) surface over a bridge site, with the two C centers pointing towards adjacent 3-fold hollow sites, as suggested PED. The calculated C-C distance of adsorbed  $C_2H_2$  increased by  $0.16 \text{ \AA}$  with respect to that of the free molecule which is close to the experimentally observed increase ( $0.28 \pm 0.10 \text{ \AA}$ ). The cluster model indicated that the C-H axes were pointing away from the surface, being tilted by  $60^\circ$  with respect to the C-C axis. The overall weak  $C_2H_2$ -Cu(111) interaction is determined by a competition between the energy required to change the geometry in the adsorbate molecule and the energy gained due to local bond formation of the distorted molecule. The same authors [98Wit] also reported potential energy curves  $E(z)$  which exhibited two minima (one referring to an undistorted physisorbed adsorbate and another yielding a strongly distorted adsorbate). It was rationalized why experiments for Cu(111)- $C_2H_2$  have reported only one adsorbate state so far. As mentioned,  $C_2H_2$  shows strong geometrical distortions when adsorbed on transition metals in a  $\pi$ -donation- $\pi^*$ -backdonation process. Triguero et al. [98Tri] demonstrated the importance of considering the available excited states of the free molecule in analyzing the bonding scheme of  $C_2H_2$  on cluster models on Cu(100), (110), and (111). By comparison to the structures of the triplet excited states in the gas phase it was shown that these must be considered as the states actually involved in the bonding.

Bandy et al. [84Ban] reported vibrational EELS spectra of  $C_2H_2$  on Cu(111), Ni(110) and Pd(110) at 110-120 K. Taking into account corresponding  $C_2D_2$  spectra the loss peaks were assigned to vibrational modes of the non-dissociatively adsorbed, but significantly rehybridized  $C_2H_2$  molecules.

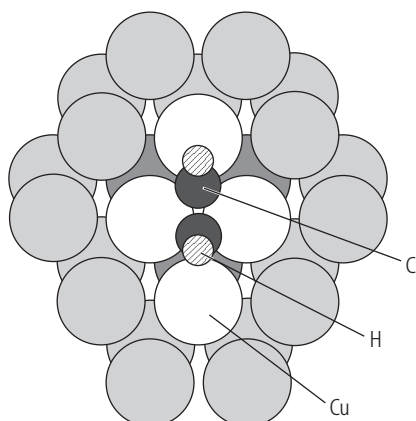


**Fig. 16** Structure model of the  $\text{Cu}_7(4,3)\text{C}_2\text{H}_2$  cluster used in [95Her]. The  $\text{C}_2\text{H}_2$  adsorbate is assumed to bend over a Cu(111) bridge site with the two C-centers pointing towards adjacent fcc and hcp hollow sites.

#### 3.8.6.6.1.4 Fe

Hung and Bernasek [95Hun] studied the adsorption of  $\text{C}_2\text{H}_2$  on clean, C- and O-covered Fe(100) using HREELS, TPD, AES and LEED.  $\text{C}_2\text{H}_2$  adsorbed on Fe(100) in a structure with hybridization similar to  $\text{sp}^3$ . At low exposure ( $<0.2$  L),  $\text{C}_2\text{H}_2$  decomposed to form  $\equiv\text{CH}$  and  $-\text{C}\equiv\text{CH}$  at 253 K. At higher exposure ( $>0.2$  L),  $\text{C}_2\text{H}_2$  partially dehydrogenated and hydrogenated to form  $\equiv\text{CH}$ ,  $-\text{C}\equiv\text{CH}$  and  $-\text{CH}=\text{CH}_2$  at the adsorption temperature of 100 K. When the surface was heated to 393 K, a  $=\text{C}=\text{CH}_2$  species was formed by dehydrogenation of  $-\text{CH}=\text{CH}_2$ . An ordered carbon overlayer with 0.81 ML coverage was obtained by heating the adsorbed  $\text{C}_2\text{H}_2$  layer to 553 K. Carbon overlayers hindered  $\text{C}_2\text{H}_2$  adsorption.

Anderson and Mehandru performed full structure determinations of  $\text{C}_2\text{H}_2$  on small and large cluster models of Fe(100), (110), and (111) surfaces using the atom superposition and electron delocalization molecular orbital theory. Four-fold sites were favored on the (100) and (110) surfaces and the di- $\sigma$  bridging site was favored on Fe(111). Using LEED, Yoshida et al. observed  $(2\times 2)$ ,  $(2\times 3)$  and coincidence structures of  $\text{C}_2\text{H}_2$  on Fe(110) [78Yos]. On Fe(111),  $(1\times 1)$ ,  $(5\times 5)$  and  $(3\times 3)$  was reported [78Yos].

#### 3.8.6.6.1.5 Ir

$\text{C}_2\text{H}_2$  adsorption on Ir(100) produced disordered structures or  $c(2\times 2)$ -C structures upon decomposition of  $\text{C}_2\text{H}_2$  [76Bro, 76Rho]. On Ir(111), Nieuwenhuys et al. [76Nie] reported  $(\sqrt{3} \times \sqrt{3})\text{R}30^\circ$  and  $(9\times 9)$ -C structures. On the stepped surface Ir(S)-[6(111)  $\times$  (100)], a  $(2\times 2)$  structure was observed.

#### 3.8.6.6.1.6 Ni

LEED studies of  $\text{C}_2\text{H}_2$  on Ni(100) reported  $c(2\times 2)$ ,  $(2\times 2)$ ,  $c(4\times 2)$  and  $(2\times 2)$ -C structures [77Cas, 78Hor, 81Cas]. Steinrück and coworkers [02Whe, 03Neu] studied the thermal chemistry of  $\text{C}_2\text{H}_2$  on Ni(100) in the temperature range 90-530 K by temperature-programmed XPS. The use of a third generation synchrotron light source allowed measurements of high-resolution C1s XPS spectra in “real-time” (i.e. within a few seconds), enabling to follow the thermal dehydrogenation in a quantitative and quasi-continuous manner. For  $\text{C}_2\text{H}_2$  decomposition, acetylide ( $-\text{C}\equiv\text{CH}$ ) and methylidyne ( $\equiv\text{CH}$ ) were observed as intermediates. Carbide carbon was formed as final dehydrogenation product.

On Ni(110), a  $c(2\times 2)$  structure was observed by LEED [84Str]. King et al. [99Bro1] measured the heats of adsorption and sticking probabilities for  $\text{C}_2\text{H}_2$  on Ni(110) at 300 K. The initial sticking probability and heat of adsorption for  $\text{C}_2\text{H}_2$  were 0.8 and  $190 \text{ kJ mol}^{-1}$ . CCH species were formed on the surface initially, and at higher exposure  $=\text{CH}_2$  and  $\equiv\text{CH}$  were produced. A value of the Ni-C bond strength of  $191 \text{ kJ mol}^{-1}$  was reported (calculated value  $204 \text{ kJ mol}^{-1}$ ). HREELS, LEED and TDS were

used to study the adsorption and decomposition of  $C_2H_2$  on Ni(110) [84Ban, 84Str].  $C_2H_2$  adsorbed molecularly at 80 K, but showed rehybridization to  $\sim sp^{2.5}$ . An ordered  $c(2\times 2)$  LEED pattern was formed. Steinrück and coworkers [95Wei, 96Ste, 01Whe, 02Whe] studied  $C_2H_2$  adsorption on Ni(110) by angle-resolved UPS. For a saturated  $c(2\times 2)$  layer (0.5 ML) the C-C axis was oriented parallel to surface, oriented along the substrate throughs ( $[1\bar{1}0]$  azimuth).

$C_2H_2$  on Ni(111) was frequently studied by LEED revealing  $(2\times 2)$ ,  $(\sqrt{3}\times\sqrt{3})R30^\circ$  and disordered layers [77Dem, 78Ber, 79Cat, 82Cas, 84Kob]. Using the same technique, Casalone et al. [82Cas] found that the  $C_2H_2$  molecules were adsorbed with the C-C bond parallel to the surface, with the center of the C-C bond over a bridge site. The C-C bond was perpendicular to the Ni-Ni bridge. The C-C bond length was 1.50 Å, the carbon atoms were  $2.1\pm 0.10$  Å above the surface. Hammer et al. [86Ham] performed combined LEED/EELS measurements to study the ordering of  $C_2H_2$  on Ni(111). Three different phases of long-range order structures were reported:  $(2\times 2)$ ,  $(\sqrt{3}\times\sqrt{3})R30^\circ$  and  $(2\sqrt{3}\times\sqrt{3})R30^\circ$ . Bridge positions were suggested as adsorption sites for the carbon atoms. Using EELS Lehwald and Ibach [79Leh] studied the  $C_2H_2$  adsorption at 150 K and its decomposition upon annealing to higher temperature. On Ni(111) acetylene formed a  $sp^3$ -type configuration which was stable up to 400 K. On the stepped Ni  $[5(111)\times(110)]$  surface, even at 150 K,  $C_2H_2$  instantaneously dehydrogenated to  $C_2$  which further decomposed into carbon atoms. Dalmai-Imelik and Bertolini [74Dal] measured the work function change upon adsorption of  $C_2H_2$  on Ni(111) by the retarding potential method. On the clean surface  $-0.6$  eV was obtained at  $3\times 10^{-9}$  Torr. For a pressure of  $10^{-8}$  Torr the change of work function was  $-1$  eV suggesting the polymerization of the hydrocarbon.

Bao et al. [95Bao] examined the local geometry of adsorbed ethylene on Ni(111) and its dehydrogenation to adsorbed  $C_2H_2$  using C1s scanned-energy mode PED. At 120 K  $C_2H_4$  adsorbed with its C-C axis parallel to the surface in an aligned bridge site such that the C atoms were approximately atop Ni atoms. Heating this surface lead to dehydrogenation of the adsorbed  $C_2H_4$  to adsorbed  $C_2H_2$ , and while the C-C axis remained parallel to the surface, the C-C bond length and C-Ni layer spacing were reduced, and the  $C_2H_2$  now occupied a cross-bridge site with the C atoms directly above fcc and hcp hollow sites on the surface.

In a theoretical study, Zhao et al. [97Zha] investigated  $C_2H_2$  adsorption on Ni(111), as well as its migration pathway from the aligned bridge site (the favoured adsorption site for  $C_2H_4$ ) to the cross-bridge site (the favoured adsorption site for  $C_2H_2$ ). The C-C bond length of  $C_2H_2$  was stretched by 20% compared with that of the gas phase, which is in good agreement with PED results [95Bao], and the corresponding bond order is much less than that of the gas phase. It was suggested that acetylene will migrate from the aligned bridge site to the cross-bridge site with a very small energy barrier, 0.02 eV. The favourite pathway of the migration was a translation to the nearest cross-bridge site, with a simultaneous rotation through  $30^\circ$ . In another theoretical study, Medlin and Allendorf [03Med] used plane-wave DFT and extended Hückel calculations to study the adsorption of  $C_2H_2$  and hydrogen on Ni(111). Atomic hydrogen was found to preferentially adsorb in a 3-fold hollow site, although the potential-energy surface for hydrogen binding was rather flat.  $C_2H_2$  was found to strongly adsorb above two contiguous hollow sites, with its molecular plane perpendicular to the surface and bisecting a Ni-Ni bond ("cross-bridge" configuration).

#### 3.8.6.6.1.7 Pd

IRAS studies of  $C_2H_2$  adsorption on Pd(100) by Camplin et al. [97Cam, 00Cam] indicated an adsorption geometry with the  $C\equiv C$  bond parallel to the surface, through a di- $\sigma$ /di- $\pi$  interaction. The rehybridization of the C-C bond caused the C-H bonds to tilt away from the surface plane. A configuration was suggested in which the HCCH plane was normal to the surface. Guo and Madix [95Guo2] investigated the adsorption and reactions of  $C_2H_2$  on Pd(100)- $p(1\times 1)$ -H and Pd(100)- $p(1\times 1)$ -D using TPRS.  $C_2H_2$  undergoes selective hydrogenation to the corresponding alkene below or around 300 K, whereas no H-D exchange reaction was observed.

Bandy et al. [84Ban] reported EELS spectra of  $C_2H_2$  chemisorbed on Pd(110) at 110 K indicating non-dissociative adsorption (but significant rehybridization). Yoshinobu et al. [90Yos] studied the

adsorption and thermal evolution of  $C_2H_2$  on Pd(110) by HREELS, TDS and LEED. At 90 K  $C_2H_2$  chemisorbed molecularly and was located in the  $\mu_2$ -site with its C-C bond axis inclined to the surface plane; one of the CH groups was hydrogen-bonded to the surface.

LEED studies of  $C_2H_2$  on Pd(111) indicated  $(\sqrt{3} \times \sqrt{3})R30^\circ$ -diffuse,  $(\sqrt{3} \times \sqrt{3})R30^\circ$ - $C_2H_2$ , disordered and  $(\sqrt{3} \times \sqrt{3})R30^\circ$ - $C_2H_3$  structures [82Gat1, 83Gat, 83Tys]. High-resolution XPS and LEED were applied by Sandell et al. [98San] to study  $C_2H_2$  (+H) on Pd(111). Adsorbing  $C_2H_2$  at 125 K produced two ordered phases, a  $(2 \times 2)$  and a  $(\sqrt{3} \times \sqrt{3})R30^\circ$  structure, with  $C_2H_2$  occupying hollow sites. When H was preadsorbed at 110-150 K, only the latter structure was observed. Heating the  $(\sqrt{3} \times \sqrt{3})R30^\circ$   $C_2H_2$  +H structure to 350 K produced a well-ordered  $(\sqrt{3} \times \sqrt{3})R30^\circ$  ethylidyne overlayer with  $C_2H_3$  in hollow sites. Baddeley et al. [98Bad] performed a scanned-energy mode PED study of the  $(2 \times 2)$  adsorption phase of  $C_2H_2$  on Pd(111). The carbon atoms in  $C_2H_2$  were found located almost over bridge sites with a C-C bond length of  $1.34 \pm 0.10$  Å. The center of the molecule was almost over a hollow site with the hcp site being favoured but the fcc site could not be excluded. The adsorption site for the  $(\sqrt{3} \times \sqrt{3})R30^\circ$  phase was basically identical.

Tysoe and coworkers [96Tys, 99Kal, 01Sta4, 01Sta3] described  $C_2H_2$  trimerization on Pd(111). Benzene was formed by reaction between adsorbed acetylene and a surface  $C_4$  metallocycle. The addition of hydrogen was found to increase the rate of cyclotrimerization even though this reaction does not involve hydrogen directly. This effect is presumably due to the removal of carbonaceous species from the Pd surface. The same group also investigated the hydrogenation of adsorbed  $C_2H_2$  and vinyl intermediates (formed by adsorbing vinyl iodide) on Pd(111) by TPD and IRAS [00Aza]. It was reported that vinyl species hydrogenated more rapidly than adsorbed acetylene, indicating that the rate-limiting step in acetylene hydrogenation was the addition of the first hydrogen to acetylene to form a vinyl species. IRAS revealed that vinyl species converted to ethylidyne above  $\sim 160$  K.

Sheth et al. [03She] examined the hydrogenation of  $C_2H_2$  on Pd(111) by DFT. The binding energies of  $C_2H_2$ , atomic hydrogen, vinyl, and  $C_2H_4$  at 25% (33%) coverage were computed to be  $-172$  ( $-136$ ),  $-260$  ( $-248$ ),  $-274$  ( $-235$ ), and  $-82$  ( $-62$ ) kJ/mol, respectively. Another DFT study of the acetylene adsorption on Pd(111) is described in [03Mit]. Medlin and Allendorf [03Med] used plane-wave DFT and extended Hückel calculations to study the adsorption of  $C_2H_2$  and hydrogen on Pd(111). Atomic hydrogen preferentially adsorbed in a 3-fold hollow site and the most stable adsorption structure was  $C_2H_2$  oriented above a 3-fold hollow site, with its axis parallel to the surface but tilted away from a metal-metal bond.

Chemisorption of  $C_2H_2$  on ultrathin (mono-, bi-, and trilayer) Pd films on Mo(100) was studied by Heitzinger et al. [93Hei] using a combination of AES, TPD and HREELS.  $C_2H_2$  was strongly rehybridized from sp in the gas phase toward  $sp^3$  on the Pd monolayer (as it is on Pd(100)). Chemisorption of  $C_2H_2$  on ultrathin Pd films (monolayer, bilayer, trilayer, etc.) deposited on Ta(110) [01Hei] was weaker than on bulk-terminated Pd surfaces, but was not as strongly perturbed as was seen for  $C_2H_4$ .  $C_2H_2$  was reversibly adsorbed on the 1st monolayer at 91 K, with thermal desorption peaks at 180 and 265 K.  $C_6H_6$  was formed via cyclotrimerization of  $C_2H_2$  and desorbed in a single peak at 407 K (yield  $\sim 1\%$  of an adsorbed benzene monolayer). On a thick Pd film ( $\theta_{Pd} = 5$ )  $C_2H_2$  adsorption at 175 K lead to  $C_2H_2$  desorption in a very broad peak near 330 K, and to benzene desorption at 250 and 500 K (yield twice of that on the Pd monolayer).

#### 3.8.6.1.8 Pt

LEED studies on Pt(100) reported  $c(2 \times 2)$  structures for  $C_2H_2$  adsorption [68Mor, 69Mor, 77Fis1, 77Fis2, 78Fis]. Panja et al. [01Pan] investigated the adsorption and reaction of  $C_2H_2$  on a hexagonally reconstructed  $(5 \times 20)$ -Pt(100) surface using TPD, AES, LEED and XPS, and compared them to those on two ordered Sn/Pt(100) alloy surfaces (see 3.8.6.1.14).  $C_2H_2$  nearly completely decomposed during TPD on Pt(100), forming hydrogen, which desorbed as  $H_2$ , and surface carbon. LEED studies of  $C_2H_2$  on Pt(111) reported  $(2 \times 1)$  and  $(2 \times 2)$  structures [69Mor, 74Wei, 77Kes, 77Sta, 82Koe1, 83Fre]. Stöhr et al. [84Stö] studied (disordered)  $C_2H_2$  on Pt(111) using NEXAFS and observed a C-C bond parallel to the surface with a bond length of  $1.45 \pm 0.03$  Å. Albert et al. [82Alb] used ARUPS to study  $C_2H_2$  on Pt(111). At low temperature acetylene adsorbed with the carbon-carbon bond parallel to the surface. In the high



temperature phase the carbon-carbon bond axis was normal or nearly normal to the surface, favoring the ethynidyne structure. DFT studies of  $C_2H_2$  and hydrogen adsorption on Pt(111) [03Med, 03Mit] reported that the most stable adsorption structure was  $C_2H_2$  oriented above a 3-fold hollow site, with its axis parallel to the surface but tilted away from a metal-metal bond.

#### 3.8.6.6.1.9 Re

LEED studies of  $C_2H_2$  on Re(0001) revealed disordered and  $(2 \times \sqrt{3})R30^\circ$ -C structures [78Duc, 81Duc]. On stepped surfaces Re(S)-[14(0001)  $\times$  (10 $\bar{1}$ 1)] and Re(S)-[6(0001)  $\times$  (16 $\bar{7}$ 1)] disordered structures were reported [81Duc].

#### 3.8.6.6.1.10 Rh

Using LEED,  $c(2 \times 2)$  and  $c(2 \times 2)$ - $C_2H+C_2H_3$  structures were reported for Rh(100) and  $c(4 \times 2)$  and  $(2 \times 2)$  for Rh(111) [78Cas, 80Dub]. Studies on Rh(331) were described in [79Cas]. On the stepped Rh(S)-[6(111)  $\times$  (100)] only a disordered layer was observed [79Cas]. Kose et al. [99Kos] determined coverage dependent heats of adsorption and sticking probabilities for  $C_2H_2$  on Rh(100) by microcalorimetry. For  $C_2H_2$ , the initial heat of adsorption was  $210 \pm 10$  kJ mol $^{-1}$ , and the initial sticking probability was  $0.86 \pm 0.01$ . According to a theoretical DFT study by Medlin and Allendorf [03Med]  $C_2H_2$  adsorbed above a 3-fold hollow site, with its C-C axis parallel to the surface but tilted away from a metal-metal bond.

#### 3.8.6.6.1.11 Ru

Adsorption of  $C_2H_2$  on Ru(001) and its coadsorption with CO were investigated by LEED, TPD and HREELS [86Par, 88Par, 92Sas]. On Ru(0001)- $p(2 \times 2)O$  and Ru(0001)- $p(1 \times 2)O$  decomposition to  $CCH_3$ ,  $CCH$ ,  $CH$  and  $CCH_2$  was observed between 200 and 350 K. CO and  $C_2H_2$  form an ordered mixed adlayer.

#### 3.8.6.6.1.12 Si

Jackman et al. [95Jac] studied the reactions of atomic hydrogen with  $C_2H_2$  adsorbed on Si(100). In the absence of atomic hydrogen,  $C_2H_2$  adsorbed molecularly at low temperature and dissociated irreversibly to gaseous hydrogen and surface carbon as the temperature was raised. Atomic hydrogen stimulated C-H and C-C bond making/breaking processes.  $CH_2$  species were found to react with acetylene to produce volatile  $C_3$  hydrocarbons. Dyson and Smith [97Dys] simulated the chemisorption of  $C_2H_2$  and  $CH_3$  on the dimerized Si(100) surface using the extended Brenner potential, Hartree-Fock and DFT. Various chemisorption sites were identified. Optimal  $C_2H_2$  chemisorption was found to occur in a cross-dimer configuration, parallel to the dimer rows. Optimal  $CH_3$  chemisorption occurred with the  $CH_3$  bonding directly to the surface dangling bonds. A second-layer chemisorption site for  $CH_3$  was also identified, which may be important in the formation of diamond films on a silicon substrate. On Si(111),  $C_2H_2$  adsorbed in a disordered fashion [76Chu] while on Si(311),  $c(1 \times 1)$ ,  $(2 \times 1)$  and  $(3 \times 1)$  layers were found [70Hec].

#### 3.8.6.6.1.13 W

Disordered as well as  $(5\times 1)$ -C,  $c(3\times 2)$ -C and  $c(2\times 2)$ -C structures were described upon  $C_2H_2$  adsorption on W(100) in [78Raw, 85Ste]. On W(110),  $(2\times 2)$ - $C_2H_2$ ,  $c(2\times 2)$ - $C_2H_2$  and  $(15\times 3)R14^\circ$ -C structures were observed [83Fou].

#### 3.8.6.6.1.14 Alloys

Panja et al. [01Pan] examined the adsorption and reaction of  $C_2H_2$  on two ordered Sn/Pt(100) alloy surfaces using TPD, AES, LEED and XPS, and compared them to a hexagonally reconstructed  $(5\times 20)$ -Pt(100) surface. Vapor deposition of Sn onto a Pt(100) single-crystal substrate was used to prepare two Pt-Sn alloys, the  $c(2\times 2)$  and  $(3\sqrt{2} \times \sqrt{2})R45^\circ$  Sn/Pt(100) structures with  $\theta_{Sn} = 0.5$  and 0.67 ML, respectively.  $C_2H_2$  nearly completely decomposed during TPD on Pt(100) in the absence of Sn, forming hydrogen, which desorbed as  $H_2$ , and surface carbon. The decomposition was strongly suppressed on the two Pt-Sn alloy surfaces, and a large  $C_2H_2$  desorption peak in TPD was observed. Additionally, 15% of the adsorbed acetylene monolayer was converted to gaseous benzene during TPD on the  $(3\sqrt{2}\times\sqrt{2})R45^\circ$  Sn/Pt(100) alloy. No benzene desorption occurred from the  $c(2\times 2)$  alloy. Alloyed Sn in the  $c(2\times 2)$  alloy decreased the initial sticking coefficient of acetylene on Pt(100) at 100 K by  $\sim 40\%$ , but additional Sn in the other alloy had no additional effect. The saturation coverage of  $C_2D_2$  in the chemisorbed monolayer at 100 K decreased from that on Pt(100) by 35% on the  $c(2\times 2)$  alloy and by 50% on the  $(3\sqrt{2}\times\sqrt{2})R45^\circ$  Sn/Pt(100) alloy. The effectiveness of Sn to “block” sites apparently depends on the location of Sn adatoms or alloyed Sn atoms on the Pt surface. The acetylene chemisorption bond energy, estimated by the acetylene desorption activation energy measured in TPD, also decreased (45-65%) as the alloyed Sn concentration increased. Multiple TPD peaks for  $C_2D_2$  desorption from both the  $c(2\times 2)$  and the  $(3\sqrt{2}\times\sqrt{2})R45^\circ$  Sn/Pt(100) alloy surfaces indicated either several energetically distinguishable adsorption sites for  $C_2H_2$  or the rate-limiting influence of more complex surface reactions on these surfaces.

#### 3.8.6.6.2 Propyne $C_3H_4$

##### 3.8.6.6.2.1 Cu

Roberts et al. [96Rob] reported IRAS data for propyne  $C_3H_4$  adsorbed on Cu(110) at low temperature, using molecules with targeted isotopic substitution, e.g. the partially deuterated molecule  $CD_3-C\equiv CH$ , which facilitated band assignments. The molecule was significantly perturbed upon adsorption, with the gas phase  $C\equiv C$  triple bond suffering a reduction in bond order to ca. 1 upon adsorption. Propyne was shown to be molecularly adsorbed with the formation of a di- $\sigma$ /di- $\pi$ -bonded species. A strong correlation between the adsorption complexes formed by propyne and those formed by acetylene on these surfaces was found and, therefore, concluded that the surface chemistry of these molecules was largely determined by the  $C\equiv C$  triple bond functionality. The di- $\sigma$ /di- $\pi$ -bonded surface species formed at low temperature was shown to be stable up to 300 K. At higher temperature, propyne trimerized to form trimethylbenzene on Cu(110).

Chesters and McCash [87Che] examined propyne adsorption on Cu(110) by IRAS and reported strongly rehybridized species (Fig. 17). Deuterium substitution of the acetylenic hydrogen allowed to assign bands at 1361 and 1353  $cm^{-1}$  to the  $C\equiv C$  stretch of  $CH_3CCH$  and  $CH_3CCD$ , respectively. Vibrational bands in the 2800-2950  $cm^{-1}$  range originated from acetylenic and methyl C-H stretches. Toomes et al. [00Too] applied scanned-energy PED to determine the adsorption site and internal structure of propyne ( $CH_3-C\equiv CH$ ) on Cu(111). Propyne binds to the surface via the acetylenic unit in a site analogous to that for acetylene on Cu(111). The acetylenic unit is parallel to the surface in a cross-bridging position such that one of the C atoms is above a fcc hollow site while the other is above a hcp hollow site, giving a C-C bond length of 1.47 Å. The methyl group was strongly tilted away from the

surface and was attached with equal probability to the C atoms in the fcc and hcp hollow sites. The molecular plane was found perpendicular to the surface.

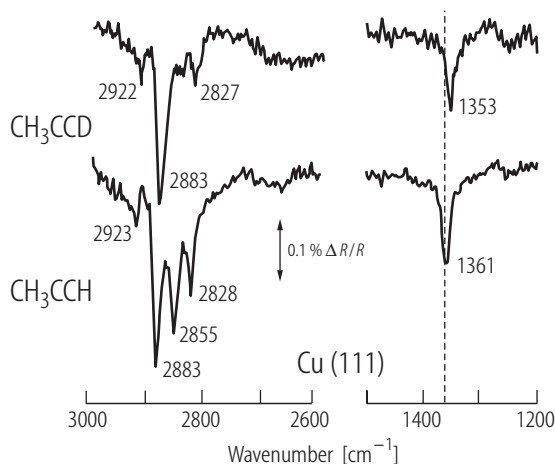


**Fig. 17:** IRAS spectra of propyne ( $\text{CH}_3\text{-C}\equiv\text{CH}$  and  $\text{CH}_3\text{-C}\equiv\text{CD}$ ) adsorption on Cu(111) at 150 K. With the help of isotopic substitution the bands at 1361 and 1353  $\text{cm}^{-1}$  were assigned to the  $\text{C}\equiv\text{C}$  stretch and the peaks in the 2800 -2950  $\text{cm}^{-1}$  range to acetylenic and methyl C-H stretch vibrations; adapted from Chesters and McCash [87Che].

Propyne adsorption on Cu(111) was studied by periodic and cluster model density functional theory by Valcarcel et al. [02Val]. A highly distorted propyne with C-1 and C-2 in nearly  $\text{sp}^2$  hybridization was suggested. Catalytic coupling of  $\text{C}_3\text{H}_4$  on Cu(111) was examined by Middleton and Lambert [99Mid]. Instead of trimerizing like acetylene, propyne undergoes coupling reactions in which two molecules react to yield either benzene, with elimination of hydrogen, or C-6 dienes. Propyne trimerization is most likely sterically inhibited by the methyl group.

#### 3.8.6.6.2.2 Ni

IRAS spectroscopy of  $\text{C}_3\text{H}_4$  adsorbed on Ni(111) at low temperatures was reported in [96Rob]. To facilitate band assignments molecules with targeted isotopic substitution, e.g.  $\text{CD}_3\text{-C}\equiv\text{CH}$  were employed.  $\text{C}_3\text{H}_4$  was significantly perturbed upon adsorption, with the gas phase  $\text{C}\equiv\text{C}$  triple bond suffering a reduction in bond order to ca. 1, and  $\text{CD}_3\text{-C}\equiv\text{CH}$  was molecularly adsorbed forming a di- $\sigma$ /di- $\pi$ -complex. The similarity of adsorption complexes formed by propyne and acetylene suggests that the adsorption properties of these molecules are largely determined by the  $\text{C}\equiv\text{C}$  triple bond. The di- $\sigma$ /di- $\pi$ -bonded surface species formed at low temperature was stable up to room temperature.

#### 3.8.6.6.2.3 Pd

IRAS studies of  $\text{C}_3\text{H}_4$  adsorption on Pd(100) by Camplin et al. [97Cam, 00Cam] indicated an adsorption geometry with the  $\text{C}\equiv\text{C}$  bond parallel to the surface (similar to acetylene). The rehybridization of the  $\text{C}\equiv\text{C}$  bond caused the H and  $\text{CH}_3$  groups to tilt away from the surface plane. For the propyne adsorption geometry a configuration was suggested in which the HCCC plane was normal or tilted with respect to the surface.

#### 3.8.6.6.2.4 Pt

Adsorption of  $\text{C}_3\text{H}_4$  on Pt(111) yielded  $(2\times 2)$  structures at 100 K, as shown by LEED [82Koe1]. Koestner et al. [82Koe1] studied  $\text{H}_3\text{C-C}\equiv\text{CH}$  adsorption on Pt(111) by LEED I-V analysis. At low temperature, the unsaturated C-C group forms a di- $\sigma$  bond to two Pt atoms. Upon warming to about room temperature and in the presence of hydrogen a conversion takes place to an alkylidyne species that is bonded to three Pt

atoms and has its C-C bond nearest to the metal substrate oriented perpendicularly to the surface. Peck et al. [98Pec] investigated the adsorption and reaction of  $C_3H_4$  on Pt(111) and Sn/Pt(111) surface alloys (see 3.8.6.6.2.5) with TPD, AES and LEED. Hydrogenation of  $C_3H_4$  to form propylene was the most favoured reaction pathway. No reversibly adsorbed  $C_3H_4$  was detected on Pt(111). Propyne adsorption and oxidation on Pt(111) at oxygen pressures up to 0.009 Torr were investigated by Gabelnick et al. [01Gab] using fluorescence yield ultrasoft X-ray adsorption methods which indicated that propyne adsorbed with its  $\pi$ -system nearly parallel to the surface and with a saturation coverage of  $1.45 \times 10^{15}$  C atoms/cm<sup>2</sup>.

#### 3.8.6.6.2.5 Alloys

Peck et al. [98Pec] investigated the adsorption and reaction of  $C_3H_4$  ( $H_3C-C\equiv CH$ ) on Pt(111) and the  $p(2\times 2)$  and  $(\sqrt{3} \times \sqrt{3})R30^\circ$ -Sn/Pt(111) surface alloys with TPD, AES and LEED. Hydrogenation of  $C_3H_4$  to form propylene ( $H_3C-CH=CH_2$ ) was the most favored reaction pathway on all three surfaces. Addition of Sn to the Pt(111) surface to form two ordered surface alloys suppressed the decomposition of  $C_3H_4$  to surface carbon. The alloy surfaces also greatly increased the amount of reversibly adsorbed  $C_3H_4$ , from zero on Pt(111) to 60% of the adsorbed layer on the  $(\sqrt{3} \times \sqrt{3})R30^\circ$ -Sn/Pt(111) surface alloy.  $C_3H_4$  reaction also lead to a small amount of benzene desorption, along with butane, butene, isobutylene and ethylene, depending the Sn concentration, with the  $(2\times 2)$ -Sn/Pt(111) surface alloy having the highest selectivity. Despite previous experiments showing cyclotrimerization of acetylene to form benzene on the Pt-Sn surface alloys, the analogous reaction of  $C_3H_4$  to form trimethylbenzene was not observed on the alloy surfaces. It was proposed that this and the high yield of propylene was due to facile dehydrogenation of  $C_3H_4$  because of the relatively weak  $H-CH_2-C\equiv CH$  bond compared to acetylene. Desorption of several  $C_4$  hydrocarbon products at low ( $<170$  K) temperature indicated some minor pathway involving C-C bond breaking.

#### 3.8.6.6.3 Butyne $C_4H_6$

EELS and IRAS studies of 2-butyne adsorption were reported for Cu(111) [87Che, 88Che1], Ni(111) [92Fri] and Pt(111) [86Ave2]. The adsorption of 2-butyne on Pd(100) at 80 K was studied by IRAS [00Cam]. 2-butyne chemisorbed directly via the  $C\equiv C$  bond at 80 K, and further addition of 2-butyne formed a disordered, physisorbed multilayer above the chemisorbed layer. For the 2-butyne adsorption geometry a configuration was suggested in which the CCCC plane was either normal or tilted with respect to the surface.

Table 3.8.6.7.1 Alkanes

Hydrocarbon	Substrate	Properties/remarks	Methods	References
<b>Methane</b> <b>CH<sub>4</sub></b>				
CH <sub>4</sub>	Cu(100)	physisorbed mono- and multi-layers at 24 K	IRAS	95Cam
CH <sub>4</sub>	Cu(111)	photodissociation into H, CH <sub>2</sub> , and CH <sub>3</sub> by 6.4 eV photons; photoreaction cross-section $\sim 2.0 \times 10^{-20} \text{ cm}^2$	TPD	00Watl
CH <sub>4</sub>	Cu, Ni, Pd, Pt cluster models (7-13 atoms)	$E_{ad}(\text{CH}_4)$ [eV] at top-sites for Cu <sub>10</sub> -0.09, Ni <sub>7</sub> 0.09, Pd <sub>7</sub> 0.08, Pt <sub>7</sub> 0.18	DFT	98Au
CH <sub>4</sub>	Co clusters (7- and 13-atoms)	adsorption of CH <sub>3</sub> , CH <sub>2</sub> , CH, C and H	DFT	95Bur
CH <sub>4</sub>	Co film on Cu(111)	more CH <sub>4</sub> dissociation than on (bulk) Co	molecular beams	98Lar
CH <sub>4</sub>	Ir(110)	dissociative chemisorption probability scaled approx. with $E_i \cos^2 \theta_i$	molecular beams	95Ver
CH <sub>4</sub>	Mo(100)	c(4×4)-C, c(2×2)-C, c(6√2 × 2√2)R45°-C, (1×1)-C	LEED	76Gui
CH <sub>4</sub>	Mo polycrystalline film	heat of adsorption 273 kJ mol <sup>-1</sup> at 295 K ( $\theta \rightarrow 0$ )	microcalorimetry	77Smu
CH <sub>4</sub>	Ni(100)	c(2×2), (2×2)	LEED	70Mai
CH <sub>4</sub>	Ni(100)	first CH <sub>4</sub> layer: 3000, 2884 and 1298 cm <sup>-1</sup> ; second CH <sub>4</sub> layer: 3017 and 1304 cm <sup>-1</sup> ; $T_{des}$ of the first layer 51 K, of the second layer ~34 K	IRAS, TPD, sticking coefficient measurements	95Nie, 96Yosl
CH <sub>4</sub>	Ni(100)	enhanced reaction probability ( $\times 100$ -10000) for highly vibrationally excited CH <sub>4</sub> ; $S_0^{2v3} 5 \times 10^{-4}$ (12 kJ/mol); $2 \times 10^{-2}$ (70 kJ/mol)	laser excitation, eigenstate- resolved measurements, molecular beams	02Sch, 87Ham, 00McC
CH <sub>4</sub>	Ni(110)	(2×2), (4×3), (4×5)-C, (2×3)-C no adsorption detected at 300 K carbon dissolution above 600 K	LEED, AES, ellipsometry	70Mai, 77Sch, 78Sch
CH <sub>4</sub>	Ni(111)	(2×2), (2×√3), (4×5), (2×2)-C, (16√3 × 16√3)R30°-C graphite overlayer	LEED, AES, TPD	70Mai, 79Sch, 84Ben
CH <sub>4</sub>	Ni(111)	dissociation to CH <sub>3</sub> , CH, formation of C <sub>2</sub> H <sub>2</sub> and C <sub>6</sub> H <sub>6</sub>	HREELS	86Lee, 87Lee, 88Cey, 95Yan
CH <sub>4</sub>	Ni(111)	CH <sub>3</sub> upon adsorption at 120 K; thermal decomposition to CH, C <sub>2</sub> H <sub>2</sub> and C between 120 and 450 K	XPS, molecular beams	05Den, 05Fuh2
CH <sub>4</sub>	Ni(111)	CH <sub>4</sub> dissociation into CH <sub>3</sub> and H preferentially on top of Ni atoms; dissociation barrier ~100 kJ/mol; C-H bond in transition state stretched to 1.6 Å and tilted relative to the CH <sub>3</sub> group	DFT	96Kra

Hydrocarbon	Substrate	Properties/remarks	Methods	References
CH <sub>4</sub>	Ni clusters (7- and 13-atoms)	adsorption of CH <sub>3</sub> , CH <sub>2</sub> , CH, C and H	DFT	95Bur
CH <sub>4</sub>	Pd(110) clean and oxygen modified	direct dissociation; probability decreases linearly with increasing O coverage	molecular beams	97Val
CH <sub>4</sub>	Pd(111) Pd(311) Pd(679)	structure sensitive C-H bond dissociation: Pd(111)>Pd(311)>Pd(679); effective activation energies 32-34 kJ/mol for Pd(111) and Pd(311), 44 kJ/mol for Pd(679)	TPD, TPO	97Kli
CH <sub>4</sub>	Pd flat, stepped, kinked	CH <sub>4</sub> dissociation to CH <sub>3</sub> and H; dissociation barrier reduced by ~0.3 eV on steps and kinks; association reaction structure- insensitive	DFT	03Liu
CH <sub>4</sub>	Pt(111)	trapping probability at 50 K decreased from 0.7 to 0 as $E_i$ increased from 3 to 20 kJ mol <sup>-1</sup> . CH <sub>4</sub> with kinetic energies 0.30-0.83 eV produced CH <sub>3</sub> at 120 K; CH formation for adsorption at 300 K.	IRAS, molecular beams, XPS, molecular dynamics simulations	93Oak, 95Yos, 99Yag, 00Car, 89Aru, 89Mul, 91Hea, 97Val, 01Car, 04Fuh, 05Fuhl
CH <sub>4</sub>	Pt(111)	symmetry of first layer degraded from T <sub>d</sub> to C <sub>3v</sub> ; symmetry of subsequent layers T <sub>d</sub> ; T <sub>des</sub> multilayer ~40 K, T <sub>des</sub> first layer ~70 K	IRAS	96Yos2
CH <sub>4</sub>	Pt polycrystalline film	heat of adsorption 151 kJ mol <sup>-1</sup> at 295 K ( $\theta \rightarrow 0$ )	microcalorimetry	84Pal
CH <sub>4</sub>	Rh flat, stepped, kinked	CH <sub>4</sub> dissociation to CH <sub>3</sub> and H dissociation barrier reduced by ~0.3 eV on steps and kinks; association reaction structure-insensitive	DFT	03Liu
CH <sub>4</sub>	Ru(0001) Ru(11 $\bar{2}$ 0)	on Ru(0001) dissociation to CH, CCH <sub>2</sub> ; on Ru(11 $\bar{2}$ 0) CH, CCH <sub>2</sub> and CCH <sub>3</sub>	HREELS, TPD, neutron vibrational spectroscopy (NVS)	94Wu, 02Cho
CH <sub>4</sub>	Si(100)	C <sub>1</sub> and C <sub>2</sub> hydrocarbons; dehydrogenation to C	TPD, AES	93Jac, 94Chu1
CH <sub>4</sub>	W(100)	(5×1)-C	LEED	69Bou
CH <sub>4</sub>	W(110)	T <sub>des</sub> ~50 K, activation energy ~8 kJ/mol	TPD, $\Delta\phi$	97Nah
CH <sub>4</sub>	W(111)	(6×6)-C	LEED	69Bou
<b>Ethane</b> <b>C<sub>2</sub>H<sub>6</sub></b>				
C <sub>2</sub> H <sub>6</sub>	Cu(110) Cu(111)	C-C bond parallel to surface	IRAS	75Hor, 88Che2
C <sub>2</sub> H <sub>6</sub>	Ir(110)	dissociative chemisorption probability scaled approx. $E_T$ ; S <sub>0</sub> ~0.03 at kinetic energies <62 kJ/mol; increases nearly linear to 0.40 at ~165 kJ/mol	molecular beams	95Ver, 95Sou
C <sub>2</sub> H <sub>6</sub>	Mo polycrystalline film	heat of adsorption 419 kJ mol <sup>-1</sup> at 295 K ( $\theta \rightarrow 0$ )	microcalorimetry	77Smu
C <sub>2</sub> H <sub>6</sub>	Ni(100)	c(2×2), (2×2)	LEED, molecular beams	70Mai, 87Ham

Hydrocarbon	Substrate	Properties/remarks	Methods	References
C <sub>2</sub> H <sub>6</sub>	Ni(110)	(2×2)	LEED	70Mai
C <sub>2</sub> H <sub>6</sub>	Ni(111)	(2×2), (2×√3), (√7 × √7)R19°-C, (2×2)-C disordered graphite	LEED	69Ber, 70Mai, 84Ben
C <sub>2</sub> H <sub>6</sub>	Pd(111)	trapping probability scales with $E_T \cos^{0.9} \theta$	molecular beams, stochastic trajectory simulations	02Kao
C <sub>2</sub> H <sub>6</sub>	Pt(110)-(1×2)	adsorption probability decreased from near unity ( $E_T$ 10 kJ/mol) to 0.5 ( $E_T$ 40 kJ/mol) for normal incidence	molecular beams, stochastic trajectory simulations	96Sti
C <sub>2</sub> H <sub>6</sub>	Pt(111)	non-dissociative adsorption at low $T$ ; C-C bond parallel to surface; dissociative adsorption at 150 K to C <sub>2</sub> H <sub>5</sub> , decomposition to ethylidene (CHCH <sub>3</sub> ) at 250 K, to ethylidyne (CCH <sub>3</sub> ) at 350 K	IRAS, TDS	89Che, 98New
C <sub>2</sub> H <sub>6</sub>	Pt(111) Pt(111)-p(2×2)-O	initial trapping probability at 100 K e.g. 0.85 for $E_T \cos^2 \theta = 10$ and 0.06 for $E_T \cos^2 \theta = 35$ ; total energy scaling $E_T \cos^{0.2} \theta$	molecular beams, stochastic trajectory simulations	90Aru, 92McM, 93McM1, 94Sou, 97Sti, 98Sti1, 00Kao
C <sub>2</sub> H <sub>6</sub>	Pt polycrystalline film	heat of adsorption 218 kJ mol <sup>-1</sup> at 295 K ( $\theta \rightarrow 0$ )	microcalorimetry	84Pal
C <sub>2</sub> H <sub>6</sub>	Ru(0001)	disordered at 80 K	LEED, TPD, ESDIAD	78Mad
C <sub>2</sub> H <sub>6</sub>	W(111)	(1×1)	LEED	78Win
<b>Propane</b>				
<b>C<sub>3</sub>H<sub>8</sub></b>				
C <sub>3</sub> H <sub>8</sub>	Ir(110)-(1×2)	precursor-mediated dissociative adsorption dominates over direct dissociation	molecular beams, LEED, AES	95Sou
C <sub>3</sub> H <sub>8</sub>	Mo polycrystalline film	heat of adsorption 558 kJ mol <sup>-1</sup> at 295 K ( $\theta \rightarrow 0$ )	microcalorimetry	77Smu
C <sub>3</sub> H <sub>8</sub>	Ni(100)	dissociative chemisorption only for $E_T > 10$ kJ/mol	molecular beams	87Ham
C <sub>3</sub> H <sub>8</sub>	Pt(110)	at 95 K $S_0$ increased linearly with coverage up to saturation (0.55 ML)	molecular beams, LEED, AES	93McM2, 93McM1
C <sub>3</sub> H <sub>8</sub>	Pt(111)	plane containing carbon chains aligned parallel to the surface; liquid-like multilayers	IRAS	89Che, 90Che2
C <sub>3</sub> H <sub>8</sub>	Pt(111) Pt(655)	initial trapping probability e.g. 0.28 for Pt(111), 0.38 for Pt(665), at 95 K for $E_T = 37.5$ kJ/mol and normal incidence	molecular-dynamics simulations	03Wan
C <sub>3</sub> H <sub>8</sub>	Pt polycrystalline film	heat of adsorption 248 kJ mol <sup>-1</sup> at 295 K ( $\theta \rightarrow 0$ )	microcalorimetry	84Pal

Hydrocarbon	Substrate	Properties/remarks	Methods	References
<b>Butane</b>				
<b>C<sub>4</sub>H<sub>10</sub></b>				
n- and isobutane	Ag(110)	weak attractive intermolecular interactions; $E_{des}$ (zero coverage): n-butane $44 \pm 1.2$ kJ/mol, isobutane $41 \pm 1.2$ kJ/mol	TPD, XPS, NEXAFS, IRAS	95Paw1, 95Paw2
C <sub>4</sub> H <sub>10</sub>	Mo(100) clean and with sulfur or carbon overlayers	95% molecular desorption; on S overlayers weak binding 38-42 kJ/mol; on C overlayers 46 kJ/mol	TDS	86Kel
C <sub>4</sub> H <sub>10</sub>	Pt(111)	chain axis aligned parallel to the surface and to Pt[1 $\bar{1}$ 0]; order-disorder transitions	LEED	77Fir
C <sub>4</sub> H <sub>10</sub>	Pt(111)	plane containing the carbon chains parallel to the surface	IRAS	89Che, 90Che2
C <sub>4</sub> H <sub>10</sub>	Pt(111)	<0.14 ML: disordered monolayer; 0.14-0.20 ML: ordered regions; C <sub>4</sub> H <sub>10</sub> preferentially oriented parallel to the surface; >0.20 ML: densely-packed ordered phase, C <sub>4</sub> H <sub>10</sub> probably tilted away from surface	molecular beams, TPD, LEED	01Wea
C <sub>4</sub> H <sub>10</sub>	Pt(111)	molecular plane parallel to the surface for submonolayers; close to 1 ML tilted structure with long axes oriented away from the surface	molecular-dynamics simulations	97Rau
C <sub>4</sub> H <sub>10</sub>	V(110) clean and carbide-modified	weak bonding; monolayer desorption at 145 K ( $E_{des}$ 39.3 kJ/mol), multilayer at 101 K ( $E_{des}$ 27.6 kJ/mol); reactivity enhanced on carbide-modified surfaces	HREELS, TDS	95Che
<b>Pentane C<sub>5</sub>H<sub>12</sub> and higher</b>				
(C <sub>n</sub> H <sub>2n+2</sub> , n = 5-12)	Au(111)	physisorption energy increased linearly chain length by $6.2 \pm 0.2$ kJ/mol per methylene unit	HAS	98Wet, 00Lib
C <sub>5</sub> H <sub>12</sub>	Ni(110)	(4×3), (4×5)	LEED	70Mai
C <sub>5</sub> H <sub>12</sub>	Pt(111)	chain axis aligned parallel to the surface and to Pt[1 $\bar{1}$ 0]; order-disorder transitions	LEED	77Fir
C <sub>5</sub> H <sub>12</sub> neopentane	Pt(111)	adsorption probability increased with coverage; enhanced trapping into second layer; dissociative chemisorption by direct collision and trapping-mediated mechanisms	molecular beams	97Wea, 98Wea
C <sub>5</sub> H <sub>12</sub> n- and neopentane C <sub>6</sub> H <sub>14</sub>	Pt(111)	plane of carbon chains parallel to the surface for monolayers; for multilayers plane of carbon atoms parallel to the substrate for hexane but inclined for pentane	IRAS	89Che, 90Che2



Hydrocarbon	Substrate	Properties/remarks	Methods	References
C <sub>7</sub> H <sub>16</sub>	Au(111)	not adsorbed	LEED, AES	75Che
C <sub>7</sub> H <sub>16</sub>	Au(S)-[6(111) × (100)]			
C <sub>7</sub> H <sub>16</sub>	Pt(111)	(2×2)	LEED	74Bar, 77Fir
C <sub>7</sub> H <sub>16</sub>	Pt(S)-[4(111) × (100)]	(4×2), (4×2)-C	LEED	74Bar
C <sub>7</sub> H <sub>16</sub>	Pt(S)-[6(111) × (100)]	(2×2), (9×9)-C	LEED	74Bar
C <sub>7</sub> H <sub>16</sub>	Pt(S)-[7(111) × (310)]	disordered	LEED	74Bar
C <sub>7</sub> H <sub>16</sub>	Pt(S)-[9(111) × (100)]	(2×2), (5×5)-C, (2×2)-C, 2(one-dimensional order)-C	LEED	74Bar
C <sub>8</sub> H <sub>18</sub>	Cu(111)	ordered, well-defined two-dimensional lattice with the molecular C-C-C planes parallel to the surface below 160 K; disordered liquid-like state at higher temperature	HAS	97Fuh
C <sub>9</sub> H <sub>20</sub>				
C <sub>10</sub> H <sub>22</sub>				
C <sub>8</sub> H <sub>18</sub>	Pt(111)	chain axis aligned parallel to the surface and to Pt[110]; order-disorder transitions	LEED	77Fir

**Table 3.8.6.7.2** Fragments

Hydrocarbon	Substrate	Properties/remarks	Methods	References
CH <sub>4</sub> , CH <sub>3</sub> , CH <sub>2</sub> , CH	Cu, Ni, Pd, Pt cluster models (7-13 atoms)	adsorption energies $E_{ads}(\text{CH}_3)$ [eV] at top-sites for Cu <sub>10</sub> 0.65, Ni <sub>7</sub> 2.21, Pd <sub>7</sub> 1.31, Pt <sub>7</sub> 1.75	DFT	98Au
CH <sub>3</sub> , CH <sub>2</sub>	Cu(111)	impinging CH <sub>3</sub> trapped as CH <sub>3</sub> at 300 K, partial decomposition to CH <sub>2</sub> ; impinging CH <sub>2</sub> trapped as CH <sub>2</sub> and formation of complex aromatic species	XPS, AES, HREELS	99Chu, 99Liv
CH <sub>3</sub> , CH <sub>2</sub>	Mo(100)	surface-CH <sub>3</sub> species 1106 cm <sup>-1</sup> surface-CH <sub>2</sub> 1061 cm <sup>-1</sup>	IRAS, TPD, HREELS, LEED	98Wu1, 99Wu, 97Par
C <sub>3</sub> -C <sub>6</sub> alkyl fragments	Ni(100)	iodo-precursors; C-I bond dissociated between 120 and 180 K to yield alkyl fragments; at higher temperatures decomposition to carbon and hydrogen at low coverage, to a mixture of alkanes and alkenes at saturation	TPD, XPS	95Tja
CH <sub>3</sub>	Ni(100) clean, with oxygen, and with NiO(111) overlayer	CH <sub>3</sub> dosing at 120-170 K produced C coverages >5 ML (adsorbed CH <sub>3</sub> ); C <sub>2</sub> -C <sub>4</sub> formation after very large CH <sub>3</sub> exposure	XPS, TPD	98Dic
CH <sub>3</sub> , CH <sub>2</sub> D, CD <sub>3</sub>	Ni(111)	CH <sub>3</sub> (C <sub>3v</sub> ) and CH (pyramidal Ni <sub>3</sub> -C-H) adsorbed on threefold hollow sites; >250 K C <sub>2</sub> H <sub>2</sub> formation and trimerization to benzene; relative stabilities CH <sub>3</sub> < CH+2H < 1/2 C <sub>2</sub> H <sub>2</sub> + 2H < 1/6 C <sub>6</sub> H <sub>6</sub> + H <sub>2(g)</sub>	HREELS	95Yan
CH <sub>3</sub>	Ni(111)	CH <sub>4</sub> dissociation into CH <sub>3</sub> and H on top of Ni atoms; dissociation barrier ~100 kJ/mol; active C-H bond in transition state stretched to 1.6 Å and tilted relative to CH <sub>3</sub>	DFT	96Kra

Hydrocarbon	Substrate	Properties/remarks	Methods	References
CH <sub>3</sub>	Ni(111)	adsorbed on 3-fold sites; activation energy for reaction with H to CH <sub>4</sub> 59 kJ/mol; activation energy of cleavage of C-I bond 12 kJ/mol	bond order conservation-Morse potential (BOC-MP) analysis	00Azi
CH <sub>x</sub> (x = 1, 2, 3)	Ni(111)	all CH <sub>x</sub> intermediates prefer threefold sites; calculated activation energy to form C-H bond 70-85 kJ/mol	DFT	00Wat2
CH <sub>n</sub> and C-CH <sub>n</sub> (n=1, 2, 3)	Pt(111)	carbon in CH <sub>n</sub> tries to complete tetra-valency; CH occupies three-fold hollow, CH <sub>2</sub> two-fold bridge and CH <sub>3</sub> a (one-fold coordinated) top site	cluster models, band structure calculations, EHT	83Min
CH <sub>3</sub>	Pt(111)	CH <sub>3</sub> I decomposes to CH <sub>3</sub> and I at ~250 K	HREELS, TPD, SIMS, AES	87Hen, 91Hen
C <sub>1</sub> -C <sub>6</sub> alkyl fragments	Pt(111)	alkyl surface moieties and their thermal chemistry	TPD, IRAS, ISS, XPS	95Zae, 99Zae, 02Zae1, 02Zae2
C <sub>2</sub> H <sub>5</sub>	Pt(111)	decomposition to ethylidene (CHCH <sub>3</sub> ) at 250 K and to ethylidyne (CCH <sub>3</sub> ) at 350 K	IRAS, TDS	98New
CH <sub>2</sub>	Rh(111)	dissociative adsorption of CH <sub>2</sub> I <sub>2</sub> at 90 K for submonolayer coverage, molecular adsorption on multilayers; CH <sub>2</sub> species stable up to 300 K	HREELS, XPS, AES, TPD	95Bol, 95Kli
CH <sub>2</sub>	Ru(001)	dissociative adsorption of CH <sub>2</sub> I <sub>2</sub> at 110 K; adsorbed CH <sub>2</sub> self-hydrogenates to CH <sub>4</sub> or couples to produce di-σ-bonded ethylene	XPS, UPS, TPD, AES, Δφ	00Kis
CH CCH <sub>2</sub> CCH <sub>3</sub>	Ru(0001) Ru(11 $\bar{2}$ 0)	methane dissociation on Ru(0001) to CH, CCH <sub>2</sub> ; on Ru(11 $\bar{2}$ 0) to CH, CCH <sub>2</sub> and CCH <sub>3</sub>	HREELS, TPD, AES	89Zho, 94Wu, 02Cho
hydrocarbon fragments (C <sub>1</sub> -C <sub>4</sub> )	various metal surfaces	C <sub>x</sub> H <sub>y</sub> fragments	UPS, XPS, HREELS, TPD, IRAS	97She, 98Sol
<b>Table 3.8.6.7.3 Alkenes</b>				
Hydrocarbon	Substrate	Properties/remarks	Methods	References
<b>Ethylene C<sub>2</sub>H<sub>4</sub></b>				
C <sub>2</sub> H <sub>4</sub>	Ag(100)	weak π-bonding at 100 K; oriented parallel to the surface at low coverage, reorientation involving rotation about the C-C axis with increasing coverage	IRAS, LEED	94Sla
C <sub>2</sub> H <sub>4</sub>	Ag(110)	no ordered adsorption at 293-423 K	LEED, AES	80Ron, 81Bar
C <sub>2</sub> H <sub>4</sub>	Ag(111)	on oxygen-activated Ag(111) reaction to acetaldehyde and ethylene oxide	IRAS	01Sla2

Hydrocarbon	Substrate	Properties/remarks	Methods	References
$C_2H_4$	Ag(410)	adsorption in a $\pi$ -bonded state at the step edge; steps remove the translational barrier for adsorption	molecular beam methods	05Sav
$C_2H_4$	Au(111)	not adsorbed	LEED	75Che
$C_2H_4$	Au(S)-[6(111) $\times$ (100)]	not adsorbed		75Che
$C_2H_4$	Co(0001)	complete decomposition below 300 K	UPS	84Alb
$C_2H_4$	Cr(100)	c(2 $\times$ 2)-C, ( $\sqrt{2} \times \sqrt{2}$ )R45°-C	LEED	82Gew
$C_2H_4$	Cr polycrystalline film	heat of adsorption ~422 kJ/mol at 296 K ( $\theta \rightarrow 0$ )	microcalorimetry	50Bee
$C_2H_4$	Cu(100)	(2 $\times$ 2)	LEED	77Ert
$C_2H_4$	Cu(100) clean, O-precovered, N-pre-covered	at 80 K parallel to the surface; $\pi$ -bonded; irradiation with low-energy ( $\leq 200$ eV) ethylene ions at 300 K produced hydrocarbon fragments or CN and NH	HREELS, LEED, TPD	82Nyb, 98Yu
$C_2H_4$	Cu(110)	one-dimensional order	LEED, EELS	77Ert, 92Jen, 94Kub
$C_2H_4$	Cu(110)	adsorbed atop on close-packed Cu rows (perpendicular height 2.08 $\pm$ 0.02 Å; C-C bond length 1.32 $\pm$ 0.09 Å) or in a short bridge site on the Cu rows (perpendicular height 2.09 $\pm$ 0.02 Å; C-C bond length 1.53 $\pm$ 0.13 Å); molecular plane parallel to the surface, but C-C axis may be out of the [110] direction	PED, STM	95Sch, 96Bui
$C_2H_4$	Cu(111)	$\pi$ -bonded at 91 K	LEED, EELS	77Ert, 90McC
$C_2H_4$	Cu (100), (110), (111)	excited states involved in bonding	cluster models	98Tri
$C_2H_4$	Cu(111)	undistorted physisorbed adsorbate and a strongly distorted adsorbate state	DFT cluster studies	98Wit
$C_2H_4$	Fe(100)	c(2 $\times$ 2)-C	LEED	77Bru, 85Vin
$C_2H_4$	Fe(111)	(1 $\times$ 1), (5 $\times$ 5), (3 $\times$ 3)	LEED	78Yos
$C_2H_4$	Fe(100) clean, C- and O-covered	molecularly adsorbed as di- $\sigma$ -bonded $C_2H_4$ ; decomposed to methylidyne ( $\equiv CH$ ) and ethynyl ( $-C\equiv CH$ ) upon heating to 523 K; finally c(2 $\times$ 2)-C; preadsorbed O blocked di- $\sigma$ -bonded $C_2H_4$ and induced physisorption of $\pi$ -bonded $C_2H_4$ at 100 K	HREELS, TPD, AES, LEED	95Hun
$C_2H_4$	Fe polycrystalline film	heat of adsorption 284 kJ mol <sup>-1</sup> at 296 K ( $\theta \rightarrow 0$ )	microcalorimetry	50Bee
$C_2H_4$	Ir(100)	disordered, decomposition, c(2 $\times$ 2)-C	UPS, LEED, AES	76Bro
$C_2H_4$	Ir(110)	disordered (1 $\times$ 1)-C	LEED, EELS	78Nie, 90Cha
$C_2H_4$	Ir(111)	( $\sqrt{3} \times \sqrt{3}$ )R 30°, (9 $\times$ 9)-C, ethynidyne formation at 180 K	LEED, EELS, SIMS, XPS	76Nie, 87Mar2, 87Mar1, 88Mar
$C_2H_4$	Ir(S)-[6(111) $\times$ (100)]	(2 $\times$ 2)	LEED	76Nie
$C_2H_4$	Mo(100)	c(2 $\times$ 2)-carbide, (1 $\times$ 1), (1 $\times$ 1) with streaks, c(2 $\times$ 2)-C	LEED	76Gui, 80Ko, 81Ko, 81Oya, 82Ove

Hydrocarbon	Substrate	Properties/remarks	Methods	References
C <sub>2</sub> H <sub>4</sub>	Mo(100)	at 80 K adsorption in four-fold hollow sites; substantial rehybridization to $\sim sp^3$ ; at 220 K dehydrogenation to distorted C <sub>2</sub> H <sub>2</sub> ; at 300 K C-C bond scission producing CH	ARUPS, AES, TDS	90Wan
C <sub>2</sub> H <sub>4</sub>	Mo(100) clean and oxygen-covered	binding predominantly via donation of $\pi$ -electrons; decomposition to H and adsorbed C on Mo(100) four-fold sites; adsorbed oxygen increases dissociation	XPS, TPD	97Wu
C <sub>2</sub> H <sub>4</sub>	Mo polycrystalline film	heat of adsorption 290 kJ mol <sup>-1</sup> at 296 K ( $\theta \rightarrow 0$ )	microcalorimetry	77Cer
C <sub>2</sub> H <sub>4</sub>	Ni(100)	c(2×2), (2×2), (2×2)-C(p4g), c(4×2), ( $\sqrt{7} \times \sqrt{7}$ )R 19°-C	LEED	70Dal, 77Ber, 78Hor, 79Omu, 81Kis, 83Lab, 83Rie, 84Ram
C <sub>2</sub> H <sub>4</sub>	Ni(100)	dehydrogenation species: vinyl (C <sub>2</sub> H <sub>3</sub> ), acetylene (C <sub>2</sub> H <sub>2</sub> ), acetylide (CCH), methylidyne (CH), carbidic carbon	XPS	02Whe, 03Neu
C <sub>2</sub> H <sub>4</sub>	Ni(100)	molecular adsorption at 90 K, little rehybridization; at higher temperature decomposition to vinyl C <sub>2</sub> H <sub>3</sub>	EELS, TPD	86Hall1, 87Zae1, 87Zae2
C <sub>2</sub> H <sub>4</sub>	Ni(110)	initial sticking probability 0.78	microcalorimetry, sticking coefficient measurements	99Bro1
C <sub>2</sub> H <sub>4</sub>	Ni(110)	heat of adsorption 120 kJ mol <sup>-1</sup> . Ni-C bond strength 191 kJ/mol	HREELS, LEED, TDS	79Leh, 83Ans2, 84Str, 86Ban
C <sub>2</sub> H <sub>4</sub>	Ni(110)	molecular adsorption at 80 K, rehybridization to $\sim sp^3$ ; ordered complex LEED pattern; >200 K decomposition to CCH and CH; at 500 K (4×5)-C	PED	99Gie
C <sub>2</sub> H <sub>4</sub>	Ni(110)	c(2×4) phase at 0.5 ML and at 0.2 ML (no long-range order): the two molecules per unit cell occupy low-symmetry sites approx. midway between short-bridge and atop; C-C axis tilted $\sim 10^\circ$ with respect to surface plane; C-C axes preferentially aligned along close-packed Ni rows		
C <sub>2</sub> H <sub>4</sub>	Ni(110)	di- $\sigma$ or $\pi$ -coordination on top of ridges, weak binding over the troughs	angle resolved inverse photoemission (ARIPe), DFT	96Gut
C <sub>2</sub> H <sub>4</sub>	Ni(110)	(2×1)-C, (4×5)-C, c(2×4)-C <sub>2</sub> H <sub>4</sub> , c(2×2)-CCH, graphite overlayer	LEED	75McC, 77Abb, 77McC, 84Str
C <sub>2</sub> H <sub>4</sub>	Ni(110)	for $\theta = 0.25$ : molecular plane coplanar to the surface, C-C axis preferentially aligned along the [1 $\bar{1}$ 0]; similar bonding predicted for $\pi$ - and di- $\sigma$ coordination; optimized geometry parameters for $\pi$ -bonded species: C-C: 1.42 Å, Ni-C: 2.01 Å; tilting of CH <sub>2</sub> relative to the (110) crystal plane: 23°	ARUPS, TPD, LEED, DFT	92Wei1, 92Wei2
C <sub>2</sub> H <sub>4</sub>	Ni(110)	c(2×4) (0.5 ML): C-C axis parallel to surface, oriented along [1-10]	ARUPS, LEED, NEXAFS, DFT	92Wei2, 96Ste

Hydrocarbon	Substrate	Properties/remarks	Methods	References
C <sub>2</sub> H <sub>4</sub>	Ni(111)	(2×2)	LEED, TPD	69Ber, 94Dal
C <sub>2</sub> H <sub>4</sub>	Ni(111)	di-σ complex, comparison to vibrational data of [Os <sub>2</sub> (CO) <sub>8</sub> (u <sub>2</sub> -η <sub>2</sub> -(C <sub>2</sub> H <sub>4</sub> )]	IRAS	95Coo
C <sub>2</sub> H <sub>4</sub>	Ni(111) Ni[5(111) × (-110)]	c(4×2), (2×2); carbon atoms adsorb on bridge positions; dehydrogenation to C <sub>2</sub> H <sub>2</sub> > 230 K; on the stepped surface partial dehydrogenation and decomposition to H and CH	LEED, EELS	79Ber, 79Leh, 86Ham
C <sub>2</sub> H <sub>4</sub>	Ni(111)	work function change -0.3 eV at 3×10 <sup>-9</sup> and 10 <sup>-8</sup> Torr	Δφ	74Dal
C <sub>2</sub> H <sub>4</sub>	Ni(111)	C-C axis parallel to the surface at 120 K, in an aligned bridge site, C atoms approximately atop Ni atoms	PED	94Bao1, 95Bao
C <sub>2</sub> H <sub>4</sub>	Ni polycrystalline film	heat of adsorption 251 kJ mol <sup>-1</sup> at 296 K (θ → 0)	microcalorimetry	50Bee
C <sub>2</sub> H <sub>4</sub>	monolayer Ni films on Pt(111), W(110), Ru(0001)	1 ML Ni/Pt(111) inactive for ethylene decomposition; 1 ML Ni/Ru(0001) active	TPD	03Kha
C <sub>2</sub> H <sub>4</sub>	Pd(100) Pd(100)-p(2×2)-O Pd(100)-p(1×1)-H Pd(100)-p(1×1)-D	di-σ and π-bonded C <sub>2</sub> H <sub>4</sub> at 80 K, reactions predominantly with vinylic C-H bonds	TPRS, HREELS, isotope exchange	85Stu2, 85Stu1, 95Guo1, 95Guo2
C <sub>2</sub> H <sub>4</sub>	Pd(110)	C-C bond aligned along [110]	NEXAFS, STM	01Oga
C <sub>2</sub> H <sub>4</sub>	Pd(110) Pd(110)(2×1)-H	one-dimensional (3×1) and c(2×2) domains; π-bonded at on-top	TDS, HREELS, STM, LEED	85Che, 89Nis, 90Sek, 90Yos, 91Nis, 92Sek, 98Ich, 00Ich
C <sub>2</sub> H <sub>4</sub>	Pd(100), (110), (111)	binding energies for ethylene (π), ethylene (di-σ), ethyl, vinyl, ethylidyne, atomic oxygen, and atomic carbon on Pd-19 cluster (and Pd(111) slab): -30 (-27), -60 (-62), -130 (-140), -237 (-254), -620 (-636), -375 (-400), and -610 (-635) kJ/mol, respectively	DFT	00Han, 00Neu2, 00Neu1, 02Ge, 02Pal, 03Mit
C <sub>2</sub> H <sub>4</sub>	Pd(111), clean and O- precovered	at 100 K di-σ bonded ethylene; on Pd(111)2×2-O π-bonded; HREELS vibrational frequencies: di-σ bonded: ~363, 177, 136, 108 meV; π-bonded: ~364, 177, 136, 108 meV; C <sub>2</sub> H <sub>3</sub> : ~366, 167, 135, 46 meV; C1s binding energies: di-σ: 283.08 eV; C <sub>2</sub> H <sub>3</sub> : 283.70, 284.05 eV; DFT adsorption energies: di-σ bonded: -0.84 eV; π-bonded: -0.65 eV	EELS, HREELS, XPS, TDS, DFT	81Kes, 82Gat1, 83Gat, 03Soc
C <sub>2</sub> H <sub>4</sub>	Pd(111)	at 300 K ethylidyne CCH <sub>3</sub> formation	ARUPS	83Llo
C <sub>2</sub> H <sub>4</sub>	Pd(111)	1329 cm <sup>-1</sup> , 1089 cm <sup>-1</sup> <i>E<sub>des</sub></i> 28 kJ/mol for π-bonded ethylene	IRAS, TPD, LEED	84Tys, 97Cam, 97Kal, 00Sta, 01Sta1, 02Sta1, 02Sta2, 03Sta1, 04Zhe

Hydrocarbon	Substrate	Properties/remarks	Methods	References
C <sub>2</sub> H <sub>4</sub>	Pd(111)	di-σ bonded at 90 K; ethylidyne at 300 K; hydrogen preadsorption favors π-bonding	SFG	03Fre, 05Mor
C <sub>2</sub> H <sub>4</sub>	PdAu	Au reduces ethylene decomposition to ethylidyne and CH <sub>x</sub>	DFT	02Neu, 03Mei
C <sub>2</sub> H <sub>4</sub>	Pd films mono-, bi-, and trilayers on Mo(100)	weakly chemisorbed; less rehybridized toward sp <sup>3</sup> as compared to Pd(100)	AES, TPD, HREELS	93Hei
C <sub>2</sub> H <sub>4</sub>	Pt(100)	c(2×2) graphite overlayer	LEED	68Mor, 69Mor, 75Lan1, 75Lan2, 77Fis1, 78Fis
C <sub>2</sub> H <sub>4</sub>	Pt(100)	heat of adsorption 200 kJ mol <sup>-1</sup> at 300 K (θ → 0)	microcalorimetry	95Yeo
C <sub>2</sub> H <sub>4</sub>	Pt(100)	molecular adsorption at 120 K; vibrational bands at 3000 (w), 1468 (w), 1162 (s), 879 (w) and 403 cm <sup>-1</sup> (s)	IRAS, EELS	83Ans1, 87Hat
C <sub>2</sub> H <sub>4</sub>	Pt(100) hex	heat of adsorption 250 kJ mol <sup>-1</sup> at 300 K (θ → 0)	microcalorimetry	95Yeo
C <sub>2</sub> H <sub>4</sub>	Pt(100)-hex-R0.7°	reconstruction lifted upon ethylene adsorption; heterogeneous nucleation of highly anisotropic (1×1) domains	STM, LEED	01Ron
C <sub>2</sub> H <sub>4</sub>	Pt(110)	di-σ and π-bound ethylene; little di-σ ethylene on surface preexposed to 100 L H <sub>2</sub>	EELS, TDS	90Yag1, 88Win, 89Yag, 90Bac, 90Yag2
C <sub>2</sub> H <sub>4</sub>	Pt(110)	same adsorption energy for di-σ- and π-coordination	EHT	91Sau
C <sub>2</sub> H <sub>4</sub>	Pt(110)-(1×2)	heat of adsorption 202-205 kJ mol <sup>-1</sup> at 300 K (θ → 0) (see also Fig. 2 and 3.8.6.4.1.10)	microcalorimetry, EELS, TPD	90Yag3, 90Yag1, 95Stu
C <sub>2</sub> H <sub>4</sub>	Pt(111)	di-σ bonded C <sub>2</sub> H <sub>4</sub> , sp <sup>3</sup> hybridization (see also Fig. 13)	EELS, UPS	77Iba2, 77Iba1, 82Iba1, 82Iba2, 82Ste, 91Cas
C <sub>2</sub> H <sub>4</sub>	Pt(111)	(2×2), (2×2)-C <sub>2</sub> H <sub>3</sub> , (2×1) one-dimensional order-C disordered graphite overlayer	LEED	78Kes, 79Kes, 88Van, 94Sta, 97Döl, 69Mor, 70Smi, 74Bar, 74Wei, 75Lan1, 77Sta, 78Kes, 79Kes, 82Koe1, 82Ste, 83Fre
C <sub>2</sub> H <sub>4</sub>	Pt(111)	disordered, parallel to surface, C-C bond 1.49±0.03 Å	NEXAFS	84Stö
C <sub>2</sub> H <sub>4</sub>	Pt(111)	carbon-carbon bond parallel to the surface at low temperature; at ~250 K ethylidyne with carbon-carbon bond normal or nearly normal to the surface	ARUPS	82Alb
C <sub>2</sub> H <sub>4</sub>	Pt(111)	at 100 K 0.25 ML C <sub>2</sub> H <sub>4</sub> saturation coverage; binding energy 283.2 eV; decomposition above 240 K to ethylidyne with an activation barrier of 57±3 kJ mol <sup>-1</sup> and a preexponential factor $\nu = 1 \times 10^{10 \pm 0.5} \text{ s}^{-1}$ ; π-bonded ethylene 283.9 eV	XPS	03Lee

Hydrocarbon	Substrate	Properties/remarks	Methods	References
$\text{H}_2\text{C}=\text{CD}_2$ and $\text{D}_2\text{C}=\text{CD}_2$	Pt(111)	at 360 K isotopic scrambling between ethylidyne species	IRAS	90Che4
$\text{C}_2\text{H}_4$	Pt(111)	carbon to hydrogen ratio 2:3 for ethylidyne	TPD	79Dem1, 82Ste
$\text{C}_2\text{H}_4$	Pt(111)	$2880\text{ cm}^{-1} \nu_s(\text{CH}_3)$ of ethylidyne ( $\text{M}\equiv\text{CCH}_3$ ), $2910\text{ cm}^{-1} \nu_s(\text{CH}_2)$ of di- $\sigma$ bonded ethylene, $\sim 3000\text{ cm}^{-1} \nu_s(\text{CH}_2)$ of $\pi$ -bonded ethylene, $2957\text{ cm}^{-1} \nu_{as}(\text{CH}_3)$ of ethylidene ( $=\text{CHCH}_3$ )	IRAS, SFG	81Ski, 88Moh, 92Rek, 94Kub, 95Cre2, 95Crel, 96Cre2, 96Cre3, 96Cre4, 96Zae, 99Oht, 99Som
$\text{C}_2\text{H}_4$	Pt(111)	adsorption and decomposition: ethylene, ethylidyne, carbon particles, graphite	STM	92Lan
$\text{C}_2\text{H}_4$	Pt(111) Sn/Pt(111)	di- $\sigma$ -bonded below 150 K on ordered Sn/Pt(111) surface alloys; increasing the Sn concentration decreases $E_{des}$ ( $\text{C}_2\text{H}_4$ ) from 285 K on Pt(111) to 240 K and to 184 K on the alloys	TPD, UPS, EELS, LEED, sticking coefficient measurements	89Paf, 97Tsa
$\text{C}_2\text{H}_4$	Pt(111)	di- $\sigma$ coordination more stable than $\pi$ -coordination	EHT, DFT	91Sau, 00Min, 03Mit
$\text{C}_2\text{H}_4$	Pt(111)	various $\text{C}_2\text{H}_x$ species, activated complexes of ethyl ( $\text{C}_2\text{H}_5$ ) and ethylidene ( $=\text{CH}-\text{CH}_3$ )	quantum chemical methods	99Cor
$\text{C}_2\text{H}_4$	Pt(111)	heat of adsorption $174\text{ kJ mol}^{-1}$ at 300 K ( $\theta \rightarrow 0$ )	microcalorimetry	95Stu
$\text{C}_2\text{H}_4$	Pt(210)	molecular adsorption at 100 K; $\pi$ -bonded; desorption at 250 K and decomposition to various hydrocarbon species	TPD, EELS	88Win, 90Bac, 90Yag2
$\text{C}_2\text{H}_4$	Pt(211)	initial heat of adsorption $180\text{ kJ/mol}$ ; initial sticking probability 0.84	microcalorimetry	99Bro2
$\text{C}_2\text{H}_4$	Pt(311)-(1 $\times$ 2)	initial heat of adsorption $220\text{ kJ mol}^{-1}$ ; initial sticking probability 0.84; ethylidyne at all coverages	microcalorimetry	99Bro2
$\text{C}_2\text{H}_4$	Pt(S)-[4(111) $\times$ (100)]	disordered graphite overlayer facets	LEED	74Bar
$\text{C}_2\text{H}_4$	Pt(S)-[6(111) $\times$ (100)]	ordered graphite overlayer ( $\sqrt{19 \times \sqrt{19}}$ )R22.4°-C	LEED	74Bar, 75Lan1
$\text{C}_2\text{H}_4$	Pt(S)-[7(111) $\times$ (310)]	disordered graphite overlayer	LEED	74Bar
$\text{C}_2\text{H}_4$	Pt(S)-[9(111) $\times$ (100)]	adsorbed	LEED	74Bar
$\text{C}_2\text{H}_4$	Pt(S)-[9(111) $\times$ (111)]	disordered graphite overlayer (2 $\times$ 2)	LEED	72Lan, 78Net1, 78Net2

Hydrocarbon	Substrate	Properties/remarks	Methods	References
C <sub>2</sub> H <sub>4</sub>	Pt(S)-[9(111) × (100)]	graphite overlayer (511), (311), (731) facetting	LEED	75LanI
C <sub>2</sub> H <sub>4</sub>	Pt polycrystalline film	heat of adsorption 148 kJ mol <sup>-1</sup> at 296 K ( $\theta \rightarrow 0$ )	microcalorimetry	84Pal
C <sub>2</sub> H <sub>4</sub>	Re(0001)	disordered (2 × √3)R30°-C		78Duc, 81Duc
C <sub>2</sub> H <sub>4</sub>	Re(S)-[14(0001) × (10-10)]	(2 × √3)R30°	LEED	81Duc
C <sub>2</sub> H <sub>4</sub>	Re(S)-[6(0001) × (16-71)]	disordered	LEED	81Duc
C <sub>2</sub> H <sub>4</sub>	Rh(100)	ethylidyne species (≡C-CH <sub>3</sub> ) formed by preadsorbing ~0.5 ML CO followed by C <sub>2</sub> H <sub>4</sub> at 300 K; oriented upright with carbon-carbon bond approx. along surface normal	HREELS	88Sla2, 88SlaI
C <sub>2</sub> H <sub>4</sub>	Rh(100)	initial heat of adsorption 175 ± 10 kJ mol <sup>-1</sup> , initial sticking probability 0.88 ± 0.01	microcalorimetry	99Kos
C <sub>2</sub> H <sub>4</sub>	Rh(100)	c(2×2), c(2×2)-C <sub>2</sub> H + C <sub>2</sub> H <sub>3</sub> , (2×2)-C <sub>2</sub> H, c(2×2)-C graphite overlayer	LEED, AES, TDS	78Cas, 82Dub
C <sub>2</sub> H <sub>4</sub>	Rh(111)	c(4×2), (2×2)-C <sub>2</sub> H <sub>3</sub> , (8×8)-C, (2×2)R30°-C, (√19 × √19) R23.4°-C (2√3 × 2√3) R30°-C, (12×12)-C	LEED, TPD, EELS	78Cas, 80Dub, 82Koe2, 82Van, 84Koe
C <sub>2</sub> H <sub>4</sub>	Rh(111)	ethylidyne (≡C-CH <sub>3</sub> ) on hep hollow sites; adsorbate-induced restructuring; C-C bond 1.45 ± 0.10 Å; terminal carbon located 1.31 ± 0.10 Å above hep site	LEED, TPD, EELS, isotope exchange	80Dub, 84Koe, 82Koe2, 91Wan
C <sub>2</sub> H <sub>4</sub>	Rh(111)	analysis of vibrational fine structure in C1s core level spectra	high-resolution XPS	97And
C <sub>2</sub> H <sub>4</sub>	Rh(755) Rh(331) Rh(S)-[6(111) × (100)]	several ordered surface structures; LEED patterns on (755) due to formation of surface structures on (111) terraces; when heated in C <sub>2</sub> H <sub>4</sub> (331) more stable than (755) (which formed (111) and (100)); disordered layer on Rh(S)-[6(111) × (100)]	LEED, AES, TDS	79Cas
C <sub>2</sub> H <sub>4</sub>	Rh polycrystalline film	heat of adsorption 205 kJ mol <sup>-1</sup> at 296 K ( $\theta \rightarrow 0$ )	microcalorimetry	50Bee
C <sub>2</sub> H <sub>4</sub>	Ru(0001)	C <sub>2</sub> H <sub>4</sub> adsorbed molecularly in a di-σ structure and decomposed to ethylidyne (CCH <sub>3</sub> ) above 150 K	HREELS, SSIMS, TPD, IRAS	86Hil, 87Sak, 87Hill, 87Hil2, 88Hen, 93Ran
C <sub>2</sub> H <sub>4</sub>	Si(100)	an atomic hydrogen flux converted adsorbed C <sub>2</sub> H <sub>4</sub> to C <sub>2</sub> H <sub>2</sub> and CH <sub>2</sub> ; H stimulates C-H and C-C bond making/breaking	TDS	94Chu2, 95Jac
C <sub>2</sub> H <sub>4</sub>	Si(331)	c(1×1), (2×1), (3×1)	LEED	70Hec
C <sub>2</sub> H <sub>4</sub>	Ta(100)	decomposition and carbon solution	LEED, AES	74Che3
C <sub>2</sub> H <sub>4</sub>	Ta polycrystalline film	heat of adsorption 577 kJ mol <sup>-1</sup> at 296 K ( $\theta \rightarrow 0$ )	microcalorimetry	50Bee
C <sub>2</sub> H <sub>4</sub>	W(100)	at 80 K decomposition to C <sub>2</sub> H <sub>2</sub> followed by non-dissociative adsorption; decomposition to C <sub>2</sub> H <sub>2</sub> around 300 K and chemisorbed C atoms above 300 K	AES	74Che2, 74Chel, 79Che



Hydrocarbon	Substrate	Properties/remarks	Methods	References
$C_2H_4$	W(110)	$(15 \times 3)R\alpha-C$ , $(15 \times 12)R\alpha-C$	LEED	69Bou
$C_2H_4$	W(111)	(1×1)	LEED	78Win
$C_2H_4$	W polycrystalline film	heat of adsorption $422 \text{ kJ mol}^{-1}$ at $296 \text{ K}$ ( $\theta \rightarrow 0$ )	microcalorimetry	50Bee
<b>Ethylidyne</b>				
<b><math>C_2H_3</math></b>				
$C_2H_3$	Pd(111)	$(\sqrt{3} \times \sqrt{3})R30^\circ$ overlayer with $C_2H_3$ in hollow sites; HREELS vibrational frequencies: $C_2H_3$ : ~366, 167, 135, 46 meV C1s binding energies: $C_2H_3$ : 283.70, 284.05 eV	EELS, HREELS, high-resolution XPS, TDS, DFT	03Soc, 81Kes, 82Gat1, 83Gat, 98San
$C_2H_3$	Pd(111)	di- $\sigma$ bonded $C_2H_4$ at 90 K, ethylidyne at 300 K	SFG	03Fre, 05Mor
$C_2H_3$	Pt(111)	disordered, perpendicular to surface, C-C bond $1.47 \pm 0.03 \text{ \AA}$	NEXAFS	85Hor
$C_2H_3$	Pt(111)	disordered; perpendicular to surface; C-C bond $1.49 \pm 0.02 \text{ \AA}$	NMR	85Wan
$C_2H_3$	Pt(111)	(2×2) bonded perpendicular to surface in fcc sites; C-C bond $1.50 \pm 0.05 \text{ \AA}$ ; C-surface distance $1.20 \pm 0.05 \text{ \AA}$	LEED	79Kes
$C_2H_3$	Pt(111)	$C_2H_3$ decomposition into ethylidyne ( $CHCH_3$ ) at 250 K and into ethylidyne ( $CCH_3$ ) at 350 K	IRAS, TPD	98New
$C_2H_3$	Pt(111)	ethylidyne formation near 300 K with rate constants of $3 \times 10^{16} \text{ exp}(-22.4(\text{kcal/mol})/RT) \text{ s}^{-1}$ for $C_2H_4$ and $2 \times 10^{16} \text{ exp}(-23.0(\text{kcal/mol})/RT) \text{ s}^{-1}$ for $C_2D_4$	TPRS	95Yat
$C_2H_3$	Rh(111)	(2×2) C-C bond perpendicular to surface with $1.45 \pm 0.10 \text{ \AA}$ ; terminal carbon $1.31 \pm 0.10 \text{ \AA}$ above hcp site	LEED	82Koe2, 91Wan
$C_2H_3$	Rh(111)	analysis of vibrational fine structure in C1s core level spectra	high-resolution XPS	97And
<b>Propene</b>				
<b><math>C_3H_6</math></b>				
$C_3H_6$	Mo(100) clean and O-covered	molecular desorption; decomposition to C and H, self-hydrogenation to propane, $CH_4$ formation; decomposition on four-fold hollow sites	UPS, TPD	97Vu
$C_3H_6$	Mo polycrystalline film	heat of adsorption $328 \text{ kJ mol}^{-1}$ at $296 \text{ K}$ ( $\theta \rightarrow 0$ )	microcalorimetry	77Cer

Hydrocarbon	Substrate	Properties/remarks	Methods	References
$C_3H_6$	Ni(100)	precursor mediated adsorption at 105 K; transition from $\pi$ - to di- $\sigma$ -bonded between 105 and 150 K; at 200 K conversion of di- $\sigma$ -bonded to $C_3H_5CH_3$ ; dehydrogenation to carbidic carbon	high-resolution XPS	01Whe, 02Whe
$C_3H_6$	Pd(100)-p(2 $\times$ 2)-O, Pd(100)-p(1 $\times$ 1)-H, Pd(100)-p(1 $\times$ 1)-D	di- $\sigma$ -bonded to $C_3H_5CH_3$ ; dehydrogenation to carbidic carbon no partial oxidation; $H_2O$ , CO and $CO_2$ as products; adsorbed O does not inhibit propene adsorption; efficient H-D exchange; no hydrogenation	TPRS, isotope exchange	95Guo1, 95Guo2
$C_3H_6$	Pd(111), clean and H-covered	di- $\sigma$ on Pd(111); some $\pi$ -bonded $C_3H_6$ on hydrogen-precovered Pd(111); molecular desorption at approx. 200 and 280 K; dehydrogenation to propylidyne and allyl species	TPD, IRAS	03Stac2
$C_3H_6$	Pt polycrystalline film	heat of adsorption 176 kJ mol <sup>-1</sup> at 296 K ( $\theta \rightarrow 0$ )	microcalorimetry	84Pal
$C_3H_6$	Pt(111)	disordered (2 $\times$ 2) di- $\sigma$ bonded at low $T$ ; around 300 K conversion to propylidyne ( $\equiv C-CH_2-CH_3$ ); at 300 K (2 $\times$ 2) and disordered structures of propylidyne	LEED, STM, EELS	80Hub, 82Gar, 82Koe1, 83Koe, 86Ave1, 86Ogl
$C_3H_6$	Pt(111)	di- $\sigma$ bonded at 90 K; dehydrogenation to propylidyne ( $\equiv C-CH_2-CH_3$ ) at $\sim$ 300 K and to vinylmethylidyne ( $\equiv C-CH=CH_2$ ) at 450 K; hydrogenation at 295 K from $\pi$ -bonded $C_3H_6$ via 2-propyl species (Pt-CH(CH <sub>3</sub> ) <sub>2</sub> ) to $C_3H_8$	SFG, IRAS	96Cre1, 90Che1, 96Cre1
$C_3H_6$	Pt(111)	molecular desorption; dehydrogenation to propylidyne and surface C; self-hydrogenation to propane at $\sim$ 280 K; H-D exchange	TPD	00Zae
$C_3H_6$	Pt(111) Sn/Pt(111)	adsorption energy 73 kJ/mol	TPD, LEED, sticking coefficient measurements	97Tsa
$C_3H_6$	Rh(111)	(2 $\times$ 2) + (2 $\sqrt{3} \times 2\sqrt{3}$ )R30°, (2 $\sqrt{3} \times 2\sqrt{3}$ )R30°	LEED	82Van
$C_3H_6$	Rh(111)	molecular di- $\sigma$ adsorption at 80 K; above 200 K propylidyne $\equiv CCH_2CH_3$ p(2 $\times$ 2); at 300 K ethylidyne $CCH_3$ and $CH_x$ fragments	HREELS, TDS, LEED	87Ben, 89Wan
$C_3H_6$	Ru(0001)	physisorbed layer at 130 K, weak spectrum of di- $\sigma$ adsorbed species; propylidyne upon annealing to 203 K	EELS, IRAS	92Sak, 93Ran
$C_3H_6$	W(100)	(5 $\times$ 1)-C	LEED	84Ben
$C_3H_6$	W(221)	c(6 $\times$ 4)-C	LEED	84Ben

Hydrocarbon	Substrate	Properties/remarks	Methods	References
<b>Butenes</b>				
<b>C<sub>4</sub>H<sub>8</sub></b>				
C <sub>4</sub> H <sub>8</sub>	Ag(110)	$\pi$ -bonded, repulsive intermolecular, double bond axis parallel to the surface; $E_{des}$ (zero coverage) 65 $\pm$ 3 kJ/mol for 1-butene and isobutylene	TPD, XPS, NEXAFS, IRAS	92Ayr, 95Paw1, 95Paw2
C <sub>4</sub> H <sub>8</sub> cis- and trans-2- butenes	Ag(111)	cis-2-butene/Ag(111): 1445, 1434, 1030 cm <sup>-1</sup> trans-isomer: 1429, 973, 959 cm <sup>-1</sup>	IRAS, TPD	00Wu
C <sub>4</sub> H <sub>8</sub> 2-butene	Mo(100) clean and O-covered	binding via $\pi$ -electrons; thermal decomposition to H and C on four-fold sites; molecular desorption; self-hydrogenation to butane, dissociation to C <sub>2</sub> species and methane	UPS, TPD	98Wul
C <sub>4</sub> H <sub>8</sub> cis- and trans-2- butene	Mo(110) clean and carbide-modified	decomposition of cis-2-butene via cleavage of olefinic $\alpha$ (C-H) bonds to surface H and 2-butyne; decomposition of trans-2-butene via $\beta$ (C-H) bond scission, one of the CH <sub>3</sub> groups converts to CH <sub>2</sub>	TPD, HREELS	98Eng
C <sub>4</sub> H <sub>8</sub>	Mo(100) clean and with S or C overlayers	weak binding on sulfur overlayers (physisorption) 38-42 kJ/mol; molecular binding on C overlayers, heat of desorption 50-63 kJ/mol	TDS	86Kel
C <sub>4</sub> H <sub>8</sub> isobutene	Ni(111)	isobutene: molecularly adsorbed in di-sigma configuration below 150 K; hydrogen atoms of the methylene group bridge-bonded to the metal 2,3-dimethyl-2-butene: no ordered superstructure; partial decomposition at $\sim$ 170 K	HREELS, LEED	90Ham, 92Fri
C <sub>4</sub> H <sub>8</sub>	Pd(111)	physisorbed at 95 K; $\pi_1^*$ , $\pi_2^*$ splitting variations 2.0 eV	NEXAFS, UPS HREELS, DFT	96Tou, 03Mit, 04Val
C <sub>4</sub> H <sub>8</sub>	Pd(110)	physisorbed at 95 K $\pi_1^*$ , $\pi_2^*$ splitting variations ca. 2.4 eV	NEXAFS, UPS HREELS	96Tou
trans-2-C <sub>4</sub> H <sub>8</sub>	Pd(110)	C=C bond located at on-top sites; short-range (3 $\times$ 1)-1D ordered structure; c(4 $\times$ 2); C=C double bond parallel to [001] at low coverage and parallel to [110] at high coverage	STM, NEXAFS	02Kat1
C <sub>4</sub> H <sub>8</sub> 1-butene	Pd(100)-p(2 $\times$ 2)-O Pd(100)-p(1 $\times$ 1)-H Pd(100)-p(1 $\times$ 1)-D	adsorbed O does not inhibit 1-butene adsorption; initial reactions occurred with the vinylic C-H bond; efficient H-D exchange below 300 K for all C-H bonds; no hydrogenation (alkanes) observed	TPRS, isotope exchange	95Guo1, 95Guo2

Hydrocarbon	Substrate	Properties/remarks	Methods	References
$C_4H_8$	Pd50Cu50(111)	physisorbed at 95 K $\pi_1^*, \pi_2^*$ splitting variations $\sim 2.4$ eV	NEXAFS, UPS, HREELS	96Tou
cis-2- $C_4H_8$	Pt(111)	$(2\sqrt{3} \times 2\sqrt{3})R30^\circ$	LEED	82Koe1
trans-2- $C_4H_8$	Pt(111)	$(8 \times 8)$	LEED	82Koe1
$C_4H_8$	Pt(111)	di- $\sigma$ -bonded at 95 K	NEXAFS, UPS HREELS, DFT	86Ave1, 86Ave2, 96Ber, 96Tou, 03Mit, 04Val
$C_4H_8$	Pt(111)	$\eta^2$ di- $\sigma$ adsorbed species: at 300 K $\mu_3-\eta^2$ $CH_3C\equiv CCH_3$ structure; central CC bond in two $\sigma$ -bonds and one $\pi$ -bond to the surface	IRAS, EELS, SFG, TPD	86Ave3, 86Ave1, 90Che1, 95Cre2
1-butene and cis- and trans-2- butenes				
$C_4H_8$	Pt(111)	$(2\sqrt{3} \times 2\sqrt{3})R30^\circ$ for cis-2- $C_4H_8$ $(8 \times 8)$ for trans-2- $C_4H_8$ at low $T$ di- $\sigma$ bonding; around 300 K butyldiyne formation; bonded to 3 Pt atoms, C-C bond nearest to the metal oriented perpendicular	LEED	82Koe1
$C_4H_8$	Pt(111)	adsorption energy 72 kJ/mol	TPD, LEED, sticking coefficient measurements	97Tsa
2-butene	Sn/Pt(111)		IRAS	90Che3, 91Che
$C_4H_8$	Ru(0001)	at 90 K molecular adsorption as di- $\sigma$ species; decomposition pathways different		
trans-2-butene				
1-butene				
isobutene)				
cis- and trans-2- butene	Si(100)-(2 $\times$ 1)	molecular adsorption at 120 K; initial sticking near unity, saturation coverages at 120 K $1.4 \times 10^{14}$ molecules $cm^{-2}$ for trans-butene, $1.6 \times 10^{14}$ molecules $cm^{-2}$ for cis-butene; $E_{des} \sim 142$ kJ/mol for trans-2-butene and $\sim 125$ kJ/mol for cis-2-butene	kinetic uptake, TPD, AES	95Kis
<b>Pentenes <math>C_5H_{10}</math> and Hexenes <math>C_6H_{12}</math> and higher</b>				
1-alkenes ( $C_6H_{12}$ - $C_{11}H_{22}$ )	Au(111)	physisorption energies increased linearly with chain length ( $\sim 5$ -6 kJ/mol per methylene unit)	HAS	98Wet

Hydrocarbon	Substrate	Properties/remarks	Methods	References
$C_3H_{10}$ <i>trans</i> -2-pentene, <i>cis</i> -2-pentene, and 1-pentene	Pd(111)	three distinct molecular desorption states at 130, 175 and 260 K, due to a multilayer, $\pi$ -bonded pentene and interchanging di- $\sigma$ -bonded pentene/pentyl groups	TPD	03Doy, 04Doy
$C_3H_{10}$ <i>trans</i> -2-pentene	Pd(111)	up to 73% carbon observed during hydrogenation (graphite, C-H and C-Pd components); <i>trans</i> -2-pentene hydrogenated via $\sigma$ -bonded configuration	XPS, UPS	05Tes
$C_3H_{10}$	Pt(111)		EELS	86Ave1
$C_6H_{12}$	Ni(111)	2,3-dimethyl-2-butene: no ordered superstructure; partial decomposition at $\sim 170$ K	HREELS, LEED	90Ham, 92Fri
$C_6H_{12}$ 1-hexene	Pd(111) clean and H(D)-saturated	weak $\pi$ -bonded species, dehydrocyclization	TPRS	98Vas
$C_6H_{12}$	Pt(111)	mixture of rotational conformers of hexylidyne; thermal decomposition of 1-hexene does not involve formation of ethylidyne ( $\mu(3)$ -CCH <sub>3</sub> )	IRAS	00Ilh
$C_6H_{12}$	Ru(0001)	mixture of rotational conformers of hexylidyne; thermal decomposition of 1-hexene does not involve the formation of ethylidyne ( $\mu(3)$ -CCH <sub>3</sub> )	IRAS	00Ilh

**Table 3.8.6.7.4 Dienes**

Hydrocarbon	Substrate	Properties/remarks	Methods	References
<b>Propadiene</b> <b><math>C_3H_4</math></b>				
$C_3H_4$	Ag films Cu(110)	orthogonal $\pi$ -system retained; one CH <sub>2</sub> group with its plane parallel to the surface, the other with its plane perpendicular to the surface; preferential orientation with the C=C=C skeleton parallel to the surface	IRAS	96Sho
$C_3H_4$	Ni(111)	isomerization, original C=C double bonds replaced by one single and one triple bond; formation of a di- $\sigma$ /di- $\pi$ propyne species	IRAS	96Sho
$C_3H_4$	Rh(111)	molecular adsorption at 80 K; above 200 K p(2 $\times$ 2) structure; at 300 K decomposition to CCH <sub>3</sub> and C <sub>x</sub> H	EELS	87Ben

Hydrocarbon	Substrate	Properties/remarks	Methods	References
<b>Butadiene</b>				
$C_4H_6$	Ag(110)	sigma-h plane parallel to the surface; C=C and C-C bond lengths identical to the gas phase values of 1.34 and 1.46 Å	NEXAFS	91Cou
$C_4H_6$	Mo(100) clean and with S or C overlayers	decomposition on clean surface, on S overlayers weak physisorption 40 kJ/mol; on C overlayers 71–97 kJ/mol	TDS	86Kel
$C_4H_6$	Pd(100)-p(2×2)-O	$O_{ads}$ did not inhibit 1,3-butadiene adsorption; initial reactions with the vinylic C-H bond	TPRS, isotope exchange	95Guo1
$C_4H_6$	Pd(100)-p(1×1)-H Pd(100)-p(1×1)-D	selective hydrogenation to alkenes ≤300 K, no H-D exchange	TPRS, isotope exchange	95Guo2
$C_4H_6$	Pd(110)	π-bonding with the molecular plane parallel to the surface; C-C single bond aligned towards [110]	HREELS, NEXAFS, STM	02Kat2
$C_4H_6$	Pd(110)	physisorbed (di-π mode) at 95 K, at 300 K dehydrogenation	NEXAFS, UPS, HREELS	96Tou, 02Ber
$C_4H_6$	Pd(111)	at 95 K di-σ bonded; at 300 K di-σ interaction, keeping one central carbon-carbon double bond (probably transformed into butylidyne)	NEXAFS, UPS, HREELS	96Ber, 96Tou, 02Ber
$C_4H_6$	Pd(111)	π-bonded and di-σ species have about the same adsorption energy	EHT, DFT	91Sau, 03Mit, 04Val
$C_4H_6$	Pd50Cu50(111)	physisorbed (di-π mode) at 95 K, at 300 K dehydrogenation	NEXAFS, UPS, HREELS	96Tou, 02Ber
$C_4H_6$	Pt(110)	same adsorption energy for di-σ and π-coordination	EHT	91Sau
$C_4H_6$	Pt(111)	di-σ coordination more stable	EHT, DFT	91Sau, 03Mit, 04Val
$C_4H_6$	Pt(111)	at 95 K π-bonded; at 300 K di-π bonded	NEXAFS, UPS, HREELS, IRAS	86Ave2, 96Tou, 05Jug
$C_4H_6$	V(110) clean and carbide-modified	monolayer desorption at ~150 K, multilayer at 110 K	HREELS, TPD	95Che
<b>Pentadiene</b>				
$C_5H_8$				
<b>Hexadiene</b>				
$C_6H_{10}$				
1,5-hexadiene	Ni(100)	formation of benzene during TPD	XPS, TPD	99Tja

Hydrocarbon	Substrate	Properties/remarks	Methods	References
1,5-hexadiene	Pd(111)	weak $\pi$ -bonded adsorption configuration at low-temperature; dehydrocyclization to benzene; H-D exchange	TPRS, isotope exchange	98Vas
1,3-hexadiene	clean and H(D)-saturated			
(1,3,5-hexatriene)				
<b>Table 3.8.6.7.5 Alkynes</b>				
Hydrocarbon	Substrate	Properties/remarks	Methods	References
<b>Acetylene</b>				
<b>C<sub>2</sub>H<sub>2</sub></b>				
C <sub>2</sub> H <sub>2</sub>	Ag(110)	at 100 K molecular adsorption; carbon-carbon triple bond preserved; CH stretching frequency of 3270 cm <sup>-1</sup> ; desorption between 100 and 160 K	LEED, EELS	81Pas, 82Mad, 82Stu
C <sub>2</sub> H <sub>2</sub>	Co(0001)	strong chemisorption bond $\leq 300$ K, hybridization close to sp <sup>3</sup> ; C-C axis parallel to the surface; vibrational splitting in XPS due to excitation of C-H stretch 389 $\pm$ 8 meV	XPS, XAS, LEED, UPS	84Alb, 02Ram1
C <sub>2</sub> H <sub>2</sub>	Co(11-20)	C <sub>2</sub> H <sub>2</sub> dissociates at $\sim 200$ K; at 200-300 K C <sub>2</sub> H or C <sub>2</sub> coexisting with molecular C <sub>2</sub> H <sub>2</sub> ; at 450 K decomposition to graphitic carbon and formation of a (5 $\times$ 2) C overlayer; mainly graphitic carbon $\geq 600$ K	XPS, NEXAFS, LEED, STM	02Ram2
C <sub>2</sub> H <sub>2</sub>	Cu(100)	pre-adsorbed oxygen facilitates CH bond scission to form CCH species	EELS, XPS	87Mar3, 89Mar
C <sub>2</sub> H <sub>2</sub>	Cu(100)	adsorbed on fourfold hollow site, C-H bond bent away from surface, molecular plane perpendicular to surface; energy barrier for molecule rotation 169 $\pm$ 3 meV, preexponential factor 10 <sup>11.8<math>\pm</math>0.2</sup> s <sup>-1</sup> ; thermal diffusion barrier of individual molecules 0.53 $\pm$ 0.01 eV, preexponential factor 10 <sup>13.6<math>\pm</math>0.2</sup> s <sup>-1</sup>	STM-IETS	99Lau, 00Lan2, 00Lau1, 02Ho, 02Ols
C <sub>2</sub> H <sub>2</sub>	Cu(110)	molecular adsorption $< 200$ K; trimerization to benzene which desorbs at $\sim 325$ K	EELS, TPD	85Ave
C <sub>2</sub> H <sub>2</sub>	Cu(111)	non-dissociative adsorption; C-C axis parallel to Cu(111), over fcc (111) bridge site; C-C 1.48 $\pm$ 0.10 Å	PED, EELS, IRAS	84Ban, 87Che, 94Bao2
C <sub>2</sub> H <sub>2</sub>	Cu(111) Cu(110)	C-C axis parallel to Cu(111); on bridge site with the two C centers point towards adjacent 3-fold hollow sites; C-C distance increased by 0.16 Å with respect to free molecule; C-H axes tilted by 60° with respect to the C-C axis, pointing away from the surface	cluster model DFT	95Her 98Wit, 87Che, 98Tri

Hydrocarbon	Substrate	Properties/remarks	Methods	References
$C_2H_2$	Fe(100) clean, C- and O-covered	hybridization $\sim sp^3$ ; <0.2 L: decomposition to $\equiv CH$ and $-C\equiv CH$ at 253 K; >0.2 L: $C_2H_2$ partial dehydrogenation/hydrogenation to $\equiv CH$ , $-C\equiv CH$ and $-CH=CH_2$ at 100 K; $=C=CH_2$ species at 393 K via dehydrogenation of $-CH=CH_2$	HREELS, TPD, AES, LEED	95Hun
$C_2H_2$	Fe(110)	(2 $\times$ 2), (2 $\times$ 3) coincidence	LEED, EELS	78Yos, 82Erl
$C_2H_2$	Fe(111)	(1 $\times$ 1), (5 $\times$ 5), (3 $\times$ 3)	LEED, EELS	78Yos, 84Ste
$C_2H_2$	Fe(100), (110), and (111) cluster models	four-fold sites favored on (100) and (110); di- $\sigma$ bridging favored on (111)	molecular orbital theory	84And
$C_2H_2$	Ir(100)	disordered c(2 $\times$ 2)-C	LEED	76Bro, 76Rho
$C_2H_2$	Ir(111)	( $\sqrt{3} \times \sqrt{3}$ )R30°, (9 $\times$ 9)-C at 180 K adsorbed CCH and ethynidyne species	LEED, HREELS, SIMS, XPS	76Nie, 87Kos, 87Marl
$C_2H_2$	Ir(S)-[6(111) $\times$ (100)]	(2 $\times$ 2)	LEED	76Nie
$C_2H_2$	Mo polycrystalline film	heat of adsorption 261 kJ mol <sup>-1</sup> at 295 K ( $\theta \rightarrow 0$ )	microcalorimetry	77Cer
$C_2H_2$	Ni(100)	c(2 $\times$ 2), (2 $\times$ 2), c(4 $\times$ 2), (2 $\times$ 2)-C	LEED, EELS	77Cas, 78Hor, 81Cas, 83Din1, 83Din2, 87Zael
$C_2H_2$	Ni(100)	dehydrogenation species: acetylide (CCH), methynidyne (CH), carbide carbon	high-resolution XPS	02Whe, 03Neu
$C_2H_2$	Ni(110)	C-C bond parallel to surface; bonded to two metal atoms on adjacent ridges; for c(2 $\times$ 2) C-C axis oriented along the substrate troughs ([1 $\bar{1}$ 0] azimuth)	(AR)UPS, LEED, NEXAFS, TPD, DFT	95Wei, 96Ste
$C_2H_2$	Ni(110)	adsorbed molecularly at 80 K, rehybridization to $\sim sp^{2.5}$ ; c(2 $\times$ 2); C-C bond parallel to surface	HREELS, LEED, TDS	79Leh, 83Ans2, 84Ban, 84Str
$C_2H_2$	Ni(110)	c(2 $\times$ 2) initial sticking probability 0.8; heat of adsorption 190 kJ mol <sup>-1</sup> ; Ni-C bond strength 191 kJ/mol	LEED, microcalorimetry molecular beams	84Str, 99Bro1
$C_2H_2$	Ni(111)	(2 $\times$ 2), ( $\sqrt{3} \times \sqrt{3}$ )R30° disordered C-C bond parallel to the surface, center of the C-C bond over bridge site; C-C bond perpendicular to Ni-Ni bridge; C-C bond length 1.50 Å, carbon atoms 2.1 $\pm$ 0.10 Å above surface	LEED, AES	82Cas, 77Dem, 78Ber, 79Cat, 82Cas, 84Kob



Hydrocarbon	Substrate	Properties/remarks	Methods	References
$C_2H_2$	Ni(111)	(2x2), ( $\sqrt{3} \times \sqrt{3}$ )R30° and ( $2\sqrt{3} \times \sqrt{3}$ )R30°; bridge positions suggested as adsorption sites for the C atoms	LEED, EELS, IRAS	78Ber, 78Dem, 79Ber, 79Dem2, 79Leh, 81Iba, 84Ban, 86Ham, 89Rud
$C_2H_2$	Ni (111)	change of work function -0.6 eV was obtained at $3 \times 10^{-9}$ Torr; -1 eV at $10^{-8}$ Torr; possibly polymerization	$\Delta\Phi$	74Dal
$C_2H_2$	Ni(111)	preferably adsorbed in cross-bridge site; C-C bond length 20% stretched compared with that of gas phase; energy barrier for migration from aligned bridge site to cross-bridge site 0.02 eV	DFT, EHT	97Zha, 03Med
$C_2H_2$	Ni (111)	C-C axis parallel to the surface; on cross-bridge site with C atoms directly above inequivalent hollow sites; C-C bondlength larger than gas-phase molecule, indicating a significant reduction of C-C bond order	PED	95Bao
$C_2H_2$	Ni(111) Ni [5 (111) × (110)]	on Ni(111) sp <sup>3</sup> -type configuration at 150 K; on the stepped surface $C_2H_2$ dehydrogenated to $C_2$ which further decomposed into C atoms	EELS	79Leh
$C_2H_2$	Pd(100)	adsorption geometry with C≡C bond parallel to the surface; C-H bonds tilted away from surface plane	IRAS, TPD, EELS	83Kes, 93Hei, 97Cam, 00Cam
$C_2H_2$	Pd(100)-p(1x1)-H Pd(100)-p(1x1)-D	selective hydrogenation to alkene around 300 K; no H-D exchange	TPRS, isotope exchange	95Guo2
$C_2H_2$	Pd(110)	non-dissociative adsorption; significant rehybridisation; at 90 K molecular adsorption in $\mu$ 2-site with C-C bond inclined to the surface	HREELS, TDS, LEED	84Ban, 90Yos, 90Yos, 94Tak
$C_2H_2$	Pd(111)	( $\sqrt{3} \times \sqrt{3}$ )R30°-diffuse, ( $\sqrt{3} \times \sqrt{3}$ )R30°- $C_2H_2$ disordered ( $\sqrt{3} \times \sqrt{3}$ )R30°- $C_2H_3$	LEED	82Gat1, 83Gat, 83Tys, 03Zhe
$C_2H_2$	Pd(111)	at 125 K two ordered phases, (2x2) and ( $\sqrt{3} \times \sqrt{3}$ )R30°; $C_2H_2$ in hollow sites; ( $\sqrt{3} \times \sqrt{3}$ )R30° with preadsorbed H; ( $\sqrt{3} \times \sqrt{3}$ )R30° ethyldiyne overlayer upon heating ( $\sqrt{3} \times \sqrt{3}$ )R30° $C_2H_2$ +H to 350 K; $C_2H_3$ in hollow sites	high-resolution XPS, LEED	98San
$C_2H_2$	Pd(111)	(2x2); C atoms located almost over bridge sites; C-C bond length 1.34±0.10 Å; molecule center over (presumably) hcp hollow site; adsorption site for the ( $\sqrt{3} \times \sqrt{3}$ )R30° identical	PED	98Bad
$C_2H_2$	Pd(111)	C=CH <sub>2</sub> species, C-C bond length of 0.146 nm, 50° tilted	UPS, NEXAFS	94Ome
$C_2H_2$	Pd(111)	$C_2H_2$ trimerization to benzene via reaction of adsorbed $C_2H_2$ and a surface $C_4$ metallocycle	TPD, IRAS, NMR	96Tys, 99Kal, 01Sta4, 01Sta3

Hydrocarbon	Substrate	Properties/remarks	Methods	References
C <sub>2</sub> H <sub>2</sub>	Pd(111)	adsorbed acetylene, vinyl intermediates (from vinyl iodide), vinylidene	TPD, IRAS, EELS	82Gat2, 83Kat, 83Kes, 85Mar, 92Nas, 00Aza
C <sub>2</sub> H <sub>2</sub>	Pd(111)	binding energy at 25% (33%) coverage -172 (-136) kJ/mol; C <sub>2</sub> H <sub>2</sub> oriented above a 3-fold hollow site, with its axis parallel to the surface but tilted away from a metal-metal bond	DFT	03Med, 03Mit, 03She
C <sub>2</sub> H <sub>2</sub>	Pd(111)	at 4.7 K three equivalent rotational states on (both fcc and hcp) 3-fold hollow adsorption sites, with the fcc adsorption site being more stable	STM	05Mat
C <sub>2</sub> H <sub>2</sub>	Pd films on Mo(100)	C <sub>2</sub> H <sub>2</sub> strongly rehybridized toward sp <sup>3</sup>	AES, TPD, HREELS	93Hei
C <sub>2</sub> H <sub>2</sub>	Pd films on Ta(110)	weaker chemisorption than on bulk-terminated Pd; not as strongly perturbed as for C <sub>2</sub> H <sub>4</sub> ; C <sub>2</sub> H <sub>2</sub> reversibly adsorbed on 1 <sup>st</sup> monolayer ( <i>T<sub>des</sub></i> at 180 and 265 K); on a thick Pd film ( <i>θ</i> (Pd) = 5) C <sub>2</sub> H <sub>2</sub> desorption in a broad peak near 330 K	TPD	01Hei
C <sub>2</sub> H <sub>2</sub>	Pt(100)	c(2×2)	LEED	68Mor, 69Mor, 77Fis1, 77Fis2, 78Fis
C <sub>2</sub> H <sub>2</sub>	Pt(100), (110), (100)	most stable adsorption sites are three-fold hollow on (111), four-fold-hollow on (100); on (110) four-fold and di-σ bridging comparable	molecular orbital theory	84Meh
C <sub>2</sub> H <sub>2</sub>	(5×20)-Pt(100), hexagonally reconstructed	decomposition into hydrogen and surface C	TPD, AES, LEED, XPS	01Pan
C <sub>2</sub> H <sub>2</sub>	Pt(111)	at 140 K non-dissociative adsorption; rehybridization to ~sp <sup>2</sup> ; di-σ bonded with additional π contribution; bridging ethynylidyne and C <sub>2</sub> H formed between 330 and 400 K	EELS, TDS	77Iba1, 78Iba, 88Ave
C <sub>2</sub> H <sub>2</sub>	Pt(111)	(2×1), (2×2)	LEED	77Kes check 82Koe1 69Mor, 74Wei, 77Kes, 77Sta, 82Koe1, 83Fre
C <sub>2</sub> H <sub>2</sub>	Pt(111)	carbon-carbon bond axis parallel to the surface	ARUPS	82Alb
C <sub>2</sub> H <sub>2</sub>	Pt(111)	C <sub>2</sub> H <sub>2</sub> oriented above a 3-fold hollow site, with its axis parallel to the surface but tilted away from a metal-metal bond	quantum chemical methods, DFT	99Cor, 03Mit, 03Med
C <sub>2</sub> H <sub>2</sub>	Pt(111)	disordered; bond parallel to surface; C-C bond length 1.45±0.03 Å	NEXAFS	84Stö
C <sub>2</sub> H <sub>2</sub>	Pt polycrystalline film	heat of adsorption 188 kJ mol <sup>-1</sup> at 295 K ( <i>θ</i> → 0)	microcalorimetry	84Pal

Hydrocarbon	Substrate	Properties/remarks	Methods	References
$C_2H_2$	Sn/Pt(100) Pt-Sn alloys: $c(2 \times 2)$ $\theta(Sn) = 0.5$ ; $(3\sqrt{2} \times \sqrt{2})R45^\circ$ $\theta(Sn) = 0.67$ ML	alloyed Sn decreased initial sticking coefficient at 100 K by ~40%; saturation coverage of $C_2D_2$ at 100 K decreased by 35-50% on the alloys; $C_2H_2$ decomposition into H and surface C strongly suppressed on alloys	TPD, AES, LEED, XPS	01Pan
$C_2H_2$	Re(0001)	disordered $(2 \times \sqrt{3})R30^\circ-C$	LEED	78Duc, 81Duc
$C_2H_2$	Re(S)-[14(0001) $\times$ (10-11)] Re(S)-[6(0001) $\times$ (16-71)]	disordered	LEED	81Duc
$C_2H_2$	Rh(100)	$c(2 \times 2)$ , $c(2 \times 2)-C_2H + C_2H_3$	LEED	78Cas
$C_2H_2$	Rh(100)	initial heat of adsorption $210 \pm 10$ kJ mol <sup>-1</sup> ; initial sticking probability $0.86 \pm 0.01$	microcalorimetry	99Kos
$C_2H_2$	Rh(111)	$c(4 \times 2)$ , $(2 \times 2)$	LEED, EELS	78Cas, 80Dub, 88Mat
$C_2H_2$	Rh(111)	oriented above a 3-fold hollow site, with C-C axis parallel to the surface but tilted away from a metal-metal bond	DFT	03Med
$C_2H_2$	Rh(755) Rh(331) Rh(S)-[6(111) $\times$ (100)]	several ordered and disordered structures; refacetting into (111) and (100) facets	LEED, AES, TDS	79Cas
$C_2H_2$	Ru(0001) Ru(0001)-p(2 $\times$ 2)O Ru(0001)-p(1 $\times$ 2)O	molecularly adsorbed; nearly sp <sup>3</sup> hybridized; between 200 and 350 K decomposition to CCH <sub>3</sub> , CCH, CH, CCH <sub>2</sub>	LEED, TPD, HREELS	86Par, 87Jak, 88Par, 92Sas
$C_2H_2$	Si(111)	disordered	EELS	76Chu
$C_2H_2$	Si(100)	molecular adsorption at low temperature; dissociation as temperature is raised; $C_2H_2$ converted to CH <sub>2</sub> , which reacts with $C_2H_2$ to C <sub>3</sub> hydrocarbons	TDS, reactive beam scattering	95Jac
$C_2H_2$	dimerized Si(001)	optimal $C_2H_2$ chemisorption in a cross-dimer configuration, parallel to the dimer rows	DFT	97Dys
$C_2H_2$	Si(111)	$c(1 \times 1)$ , $(2 \times 1)$ , $(3 \times 1)$	LEED	70Hec
$C_2H_2$	W(100)	disordered $(5 \times 1)-C$ , $c(3 \times 2)-C$ $c(2 \times 2)-C$	LEED, EELS	78Raw, 81Ham, 85Ste
$C_2H_2$	W(110)	$(2 \times 2)-C_2H_2$ , $c(2 \times 2)-C_2H_2$ , $(15 \times 3)R14^\circ-C$	LEED, EELS	77Bac2, 78Bac, 83Fou
$C_2H_2$	W(100), (110), (111)	distorted rehybridized molecular complexes; dissociative chemisorption	EELS	77Bac1, 77Bac2

Hydrocarbon	Substrate	Properties/remarks	Methods	References
<b>Propyne</b> <b>C<sub>3</sub>H<sub>4</sub></b>				
CD <sub>3</sub> CCH	Cu(110)	significant perturbation upon adsorption; molecularly adsorbed as di-σ/di-π-bonded species, stable up to 300 K; at higher <i>T</i> propyne trimerized to trimethylbenzene	IRAS	96Rob
C <sub>3</sub> H <sub>4</sub>	Cu(111)	strong rehybridization; νC≡C 1361 cm <sup>-1</sup>	IRAS	87Che, 88Che1
C <sub>3</sub> H <sub>4</sub>	Cu(111)	adsorption via the acetylenic unit, parallel to the surface in a cross-bridging position, one C atom above a fcc hollow site, the other above a hcp hollow site; C-C bond length 1.47 Å, methyl group tilted away from surface	PED	00Too
C <sub>3</sub> H <sub>4</sub>	Cu(111)	highly distorted propyne with C-1 and C-2 in nearly sp <sup>2</sup> hybridization	DFT	02Val
C <sub>3</sub> H <sub>4</sub>	Mo polycrystalline film	heat of adsorption 293 kJ mol <sup>-1</sup> at 295 K (θ → 0)	microcalorimetry	77Cer
C <sub>3</sub> H <sub>4</sub>	Ni(111)	significant perturbation upon adsorption; molecularly adsorbed as di-σ/di-π-bonded species, stable up to 300 K	IRAS	96Rob
C <sub>3</sub> H <sub>4</sub>	Pd(100)	adsorption geometry with the C≡C bond parallel to the surface, H and CH <sub>3</sub> groups tilted away from surface plane	IRAS, TPD	97Cam, 00Cam
C <sub>3</sub> H <sub>4</sub>	Pt(111)	(2×2)	LEED, IRAS	82Koe1
C <sub>3</sub> H <sub>4</sub>	Pt(111)	hydrogenation of methyl-acetylene to form propylene favoured	TPD, AES, LEED	98Pec
methyl- acetylene (H <sub>3</sub> C-C≡CH)				
C <sub>3</sub> H <sub>4</sub>	Pt(111)	adsorbed with π-system nearly parallel to the surface; saturation coverage 1.45 × 10 <sup>15</sup> C atoms/cm <sup>2</sup>	XAS	01Gab
C <sub>3</sub> H <sub>4</sub>	Pt polycrystalline film	heat of adsorption 186 kJ mol <sup>-1</sup> at 295 K (θ → 0)	microcalorimetry	84Pal
C <sub>3</sub> H <sub>4</sub>	Sn/Pt(111)	hydrogenation to propylene favored; alloys suppress decomposition to carbon; small amount of benzene desorption, no cyclotrimerization to trimethylbenzene; C-C bond scission minor pathway	TPD, AES, LEED	98Pec
acetylene (H <sub>3</sub> C-C≡CH)				
C <sub>3</sub> H <sub>4</sub>	Rh(111)	molecular adsorption at 80 K; p(2×2); at 300 K decomposition to CCH <sub>3</sub> and C <sub>x</sub> H	HREELS, LEED, TDS	87Ben

Hydrocarbon	Substrate	Properties/remarks	Methods	References
Butyne <b>C<sub>4</sub>H<sub>6</sub></b>				
C <sub>4</sub> H <sub>6</sub>	Cu(111)	strong rehybridization; $\nu\text{C}\equiv\text{C}$ 1392 cm <sup>-1</sup>	IRAS	87Che, 88Che1
C <sub>4</sub> H <sub>6</sub>	Ni(111)	(3×2√3)rect.; stable up to 300 K; 2-butyne with two flat lying molecules per unit cell	EELS	92Fri
C <sub>4</sub> H <sub>6</sub>	Pd(100)	chemisorbed via the C≡C bond; CCCC plane either normal or tilted to the surface	IRAS	00Cam
C <sub>4</sub> H <sub>6</sub>	Pt(111)	adsorption via C≡C bond	EELS, IRAS	86Ave2

## 3.8.6.8 References for 3.8.6

- 34Hor Horiuti, I., Polanyi, M.: *Trans. Faraday Soc.* **30** (1934) 1164.
- 50Bee Beeck, O., Cole, W.A., Wheeler, A.: *Discuss. Faraday Soc.* **8** (1950) 314.
- 68Mor Morgan, A.E., Somorjai, G.A.: *Surf. Sci.* **12** (1968) 405.
- 69Ber Bertolini, J.C., Dalmai-Imelik, G.: *Rapport Institute de Recherche sur la Catalyse, Villeurbanne*, 1969.
- 69Bou Boudart, M., Ollis, D.F., in: *The structure and chemistry of solid surfaces*, Somorjai, G.A. (ed.), New York: John Wiley & Sons, 1969.
- 69Mor Morgan, A.E., Somorjai, G.A.: *J. Chem. Phys.* **51** (1969) 3309.
- 70Dal Dalmai-Imelik, G., Bertolini, J.C.: *C. R. Acad. Sci. (Paris)* **270** (1970) 1079.
- 70Hec Heckingbottom, R., Wood, P.R.: *Surf. Sci.* **23** (1970) 437.
- 70Mai Maire, G., Anderson, J.R., Johnson, B.B.: *Proc. R. Soc. (London) A* **320** (1970) 227.
- 70Smi Smith, D.L., Merrill, R.F.: *J. Chem. Phys.* **52** (1970) 5861.
- 72Lan Lang, B., Joyner, R.W., Somorjai, G.A.: *Surf. Sci.* **30** (1972) 454.
- 74Bar Baron, K., Blakely, D.W., Somorjai, G.A.: *Surf. Sci.* **41** (1974) 45.
- 74Che1 Chesters, M.A., Hopkins, B.J., Jones, A.R., Nathan, R.: *J. Phys. C* **7** (1974) 4486.
- 74Che2 Chesters, M.A., Hopkins, B.J., Jones, A.R., Nathan, R.: *Surf. Sci.* **45** (1974) 740.
- 74Che3 Chesters, M.A., Hopkins, B.J., Leggett, M.R.: *Surf. Sci.* **43** (1974) 1.
- 74Dal Dalmai-Imelik, G., Bertolini, J.C.: *Jpn. J. Appl. Phys. Suppl. Vol. 2, Pt. 2* **2** (1974) 205.
- 74Wei Weinberg, W.H., Deans, H.A., Merrill, R.P.: *Surf. Sci.* **41** (1974) 312.
- 75Che Chesters, M.A., Somorjai, G.A.: *Surf. Sci.* **52** (1975) 21.
- 75Hor Horn, K., Pritchard, J.: *Surf. Sci.* **52** (1975) 437.
- 75Lan1 Lang, B.: *Surf. Sci.* **53** (1975) 317.
- 75Lan2 Lang, B., Legare, P., Maire, G.: *Surf. Sci.* **47** (1975) 89.
- 75McC Mccarty, J., Madix, R.J.: *J. Catal.* **38** (1975) 402.
- 76Bro Broden, G., Rhodin, T., Capehart, W.: *Surf. Sci.* **61** (1976) 143.
- 76Chu Chung, Y., Siekhaus, W., Somorjai, G.A.: *Surf. Sci.* **58** (1976) 341.
- 76Gui Guillot, G., Riwan, R., Lecante, J.: *Surf. Sci.* **59** (1976) 581.
- 76Nie Nieuwenhuys, B.E., Hagen, D.I., Rovida, G., Somorjai, G.A.: *Surf. Sci.* **59** (1976) 155.
- 76Pea Pearce, H.A., Sheppard, N.: *Surf. Sci.* **59** (1976) 205.
- 76Rho Rhodin, T.N., Broden, G.: *Surf. Sci.* **60** (1976) 466.
- 77Abb Abbas, N., Madix, R.J.: *Surf. Sci.* **62** (1977) 739.
- 77Bac1 Backx, C., Fuerbacher, B.F., Fitton, B., Willis, R.F.: *Surf. Sci.* **63** (1977) 193.
- 77Bac2 Backx, C., Willis, R.F., Fuerbacher, B.F., Fitton, B.: *Surf. Sci.* **68** (1977) 516.
- 77Ber Bertolini, J.C., Dalmai-Imelik, G., Rousseau, J.: *Surf. Sci.* **67** (1977) 478.
- 77Bru Bruckner, C., Rhodin, T.: *J. Catal.* **47** (1977) 214.
- 77Cas Casalone, C., Cattania, M.G., Simonetta, M., Tescari, M.: *Surf. Sci.* **62** (1977) 321.
- 77Cer Cerny, S., Smutek, M., Buzek, F.: *J. Catal.* **47** (1977) 159.
- 77Dem Demuth, J.E.: *Surf. Sci.* **69** (1977) 365.
- 77Ert Ertl, G.: *Surf. Sci.* **7** (1977) 309.
- 77Fir Firmet, L.E., Somorjai, G.A.: *J. Chem. Phys.* **66** (1977) 2901.
- 77Fis1 Fischer, T.E., Kelemen, S.R.: *Surf. Sci.* **69** (1977) 485.
- 77Fis2 Fischer, T.E., Kelemen, S.R., Bonzel, H.P.: *Surf. Sci.* **64** (1977) 85.
- 77Iba1 Ibach, H., Hopster, H., Sexton, B.: *Appl. Phys.* **14** (1977) 21.
- 77Iba2 Ibach, H., Hopster, H., Sexton, B.: *Appl. Surf. Sci.* **1** (1977) 1.
- 77Kes Kesmodel, L.L., Dubois, L.H., Somorjai, G.A.: *Surf. Sci.* **66** (1977) 299.
- 77McC Mccarty, J., Madix, R.J.: *J. Catal.* **48** (1977) 422.
- 77Sch Schouten, F., Kaleveld, E., Bootsma, G.: *Surf. Sci.* **63** (1977) 460.
- 77Smu Smutek, M., Cerny, S.: *J. Catal.* **47** (1977) 178.
- 77Som Somorjai, G.A.: *Adv. Catal.* **26** (1977) 1.
- 77Sta Stair, P.C., Somorjai, G.A.: *J. Chem. Phys.* **66** (1977) 573.
- 78Bac Backx, C., Willis, R.F.: *Chem. Phys. Lett.* **53** (1978) 471.

- 78Ber Bertolini, J.C., Massardier, J., Dalmai-Imelik, G.: *J. Chem. Soc. Faraday Trans. I* **74** (1978) 1720.
- 78Cas Castner, D.G., Sexton, B.A., Somorjai, G.A.: *Surf. Sci.* **71** (1978) 519.
- 78Dem Demuth, J.E., Ibach, H.: *Surf. Sci.* **78** (1978) L238.
- 78Duc Ducros, R., Housley, M., Alnot, M., Cassuot, A.: *Surf. Sci.* **71** (1978) 433.
- 78Fis Fischer, T.E., Kelemen, S.R.: *J. Vac. Sci. Technol.* **15** (1978) 607.
- 78Hor Horn, K., Bradshaw, A.M., Jacobi, K.: *J. Vac. Sci. Technol.* **15** (1978) 575.
- 78Iba Ibach, H., Lehwald, S.: *J. Vac. Sci. Technol.* **15** (1978) 407.
- 78Kes Kesmodel, L.L., Dubois, L.H., Somorjai, G.A.: *Chem. Phys. Lett.* **56** (1978) 267.
- 78Mad Madey, T.E., Yates, J.T.: *Surf. Sci.* **76** (1978) 397.
- 78Net1 Netzer, F.P., Willie, R.: *J. Catal.* **51** (1978) 18.
- 78Net2 Netzer, F.P., Willie, R.: *Surf. Sci.* **74** (1978) 547.
- 78Nie Nieuwenhuys, B.E., Somorjai, G.A.: *Surf. Sci.* **72** (1978) 8.
- 78Raw Rawlings, K.J., Hopkins, B., Foulis, S.: *Surf. Sci.* **77** (1978) 561.
- 78Sch Schouten, F., Brake, E., Gijzeman, O.L.J., Bootsma, G.: *Surf. Sci.* **74** (1978) 1.
- 78She Sheppard, N., Nguyen, T.T.: *Adv. Infrared Raman Spectrosc.* **5** (1978) 67.
- 78Win Winters, H.: *IBM J. Res. Dev.* **22** (1978) 260.
- 78Yos Yoshida, K., Somorjai, G.A.: *Surf. Sci.* **75** (1978) 46.
- 79Ber Bertolini, J.C., Rousseau, J.: *Surf. Sci.* **83** (1979) 531.
- 79Cas Castner, D.G., Somorjai, G.A.: *Surf. Sci.* **83** (1979) 60.
- 79Cat Cattania, M.G., Simonetta, M., Tescari, M.: *Surf. Sci.* **82** (1979) L615.
- 79Che Chesters, M.A., Hopkins, B.J., Taylor, P.A., Winton, R.I.: *Surf. sci.* **83** (1979) 181.
- 79Dem1 Demuth, J.E.: *Surf. Sci.* **80** (1979) 367.
- 79Dem2 Demuth, J.E., Ibach, H.: *Surf. Sci.* **85** (1979) 365.
- 79Kes Kesmodel, L.L., Dubois, L.H., Somorjai, G.A.: *J. Chem. Phys.* **70** (1979) 2180.
- 79Leh Lehwald, S., Ibach, H.: *Surf. Sci.* **89** (1979) 425.
- 79Onu Onuferko, J.H., Woodruff, D.P., Holland, B.: *Surf. Sci.* **87** (1979) 357.
- 79Sch Schouten, F., Gijzeman, O.L.J., Bootsma, G.: *Surf. Sci.* **87** (1979) 1.
- 79Som Somorjai, G.A., Hove, M.A.V., in: *Structure and bonding*, Dunitz, J.D., Goodenough, J.B., Hemmerich, P., Albers, J.A., Jørgensen, C.K., Neilands, J.B., Reinen, D., Williams, R.J.P. (eds.), Springer-Verlag, Berlin, 1979.
- 80Dub Dubois, L.H., Castner, D.G., Somorjai, G.A.: *J. Chem. Phys.* **72** (1980) 5234.
- 80Hub Hubbard, A.T.: *J. Vac. Sci. Technol.* **17** (1980) 49.
- 80Ko Ko, E., Madix, R.J.: *Surf. Sci.* **100** (1980) L449.
- 80Ron Roviida, G., Pratesi, F., Ferroni, E.: *Appl. Surf. Sci.* **5** (1980) 121.
- 81Bar Barteau, M.A., Madix, R.J.: *Surf. Sci.* **103** (1981) L171.
- 81Cas Casalone, G., Cattania, M.G., Simonetta, M.: *Surf. Sci.* **103** (1981) L121.
- 81Duc Ducros, R., Housley, M., Piquard, G., Alnot, M.: *Surf. Sci.* **108** (1981) 235.
- 81Ham Hamilton, J.C., Swanson, N., Waelawski, B.J., Cellota, R.J.: *J. Chem. Phys.* **74** (1981) 4156.
- 81Iba Ibach, H., Lehwald, S.: *J. Vac. Sci. Technol.* **18** (1981) 625.
- 81Kes Kesmodel, L.L., Gates, J.A.: *Surf. Sci.* **111** (1981) L747.
- 81Kis Kiskinova, M.P., Goodman, D.W.: *Surf. Sci.* **109** (1981) L555.
- 81Ko Ko, E., Madix, R.J.: *Surf. Sci.* **109** (1981) 221.
- 81Oya Oyama, T., Ohi, S., Kawazu, A., Tominaga, G.: *Surf. Sci.* **109** (1981) 82.
- 81Pas Passler, M.A., Lin, T.H., Ignatiev, A.: *J. Vac. Sci. Technol.* **18** (1981) 481.
- 81Ski Skinner, P., Howard, M.W., Oxtan, I.A., Kettle, S.F.A., Powell, D.B., Sheppard, N.: *J. Chem. Soc. Faraday Trans. II* **77** (1981) 1203.
- 82Alb Albert, M.R., Sneddon, L.G., Eberhardt, W., Greuter, F., Gustafsson, T., Plummer, E.W.: *Surf. Sci.* **120** (1982) 19.
- 82Cas Casalone, G., Cattania, M.G., Merati, F., Simonetta, M.: *Surf. Sci.* **120** (1982) 171.
- 82Dub Dubois, L.H.: *J. Chem. Phys.* **77** (1982) 5228.
- 82Erl Erley, W., Baro, A.M., Ibach, H.: *Surf. Sci.* **120** (1982) 273.
- 82Gar Garwood, G., Hubbard, A.: *Surf. Sci.* **118** (1982) 223.
- 82Gat1 Gates, J.A., Kesmodel, L.L.: *Surf. Sci.* **120** (1982) L461.

- 82Gat2 Gates, J.A., Kesmodel, L.L.: *J. Chem. Phys.* **76** (1982) 4281.
- 82Gew Gewinner, G., Peruchetti, J.C., Jaegle, A.: *Surf. Sci.* **122** (1982) 383.
- 82Iba1 Ibach, H.: *Surf. Sci.* **117** (1982) 685.
- 82Iba2 Ibach, H., Mills, D.L.: *Electron energy loss spectroscopy and surface vibration*, New York: Academic Press, 1982.
- 82Koe1 Koestner, R.J., Frost, J.C., Stair, P.C., Van Hove, M.A., Somorjai, G.A.: *Surf. Sci.* **116** (1982) 85.
- 82Koe2 Koestner, R.J., Van Hove, M.A., Somorjai, G.A.: *Surf. Sci.* **121** (1982) 321.
- 82Mad Madix, R.J.: *Appl. Surf. Sci.* **14** (1982) 41.
- 82Nyb Nyberg, C., Tengstal, C.G., Andersson, S., Holmes, M.W.: *Phys. Chem. Lett.* **87** (1982) 87.
- 82Ove Overbury, S., Stair, P.C.: *J. Vac. Sci. Technol. A* **1** (1982) 1055.
- 82Ste Steiniger, H., Ibach, H., Lehwald, S.: *Surf. Sci.* **117** (1982) 685.
- 82Stu Stuve, E.M., Madix, R.J., Sexton, B.A.: *Surf. Sci.* **123** (1982) 491.
- 82Van Van Hove, M.A., Koestner, R.J., Somorjai, G.A.: *J. Vac. Sci. Technol.* **20** (1982) 886.
- 83Ans1 Anson, C.E., Keiller, B.T., Oxtton, I.A., Powell, D.B., Sheppard, N.: *J. Chem. Soc. Chem. Commun.* **8** (1983) 470.
- 83Ans2 Anson, C.E., Bandy, B.J., Chesters, M.A., Keiller, B., Oxtton, I.A., Sheppard, N.: *J. Electron Spectrosc. Relat. Phenom.* **29** (1983) 315.
- 83Din1 Dinardo, N.J., Demuth, J.E., Avouris, P.: *J. Vac. Sci. Technol. A* **1** (1983) 1244.
- 83Din2 Dinardo, N.J., Demuth, J.E., Avouris, P.: *Phys. Rev. B* **27** (1983) 5832.
- 83Fou Foulas, S., Rawlings, K.J., Hopkins, B.: *Surf. Sci.* **133** (1983) 377.
- 83Fre Freyer, N., Pirug, G., Bonzel, H.P.: *Surf. Sci.* **125** (1983) 327.
- 83Gat Gates, J.A., Kesmodel, L.L.: *Surf. Sci.* **124** (1983) 68.
- 83Hof Hoffmann, F.M.: *Surf. Sci. Rep.* **3** (1983) 103.
- 83Kes Kesmodel, L.L.: *J. Chem. Phys.* **79** (1983) 4646.
- 83Koe Koestner, R.J., Van Hove, M.A., Somorjai, G.A.: *J. Phys. Chem.* **87** (1983) 203.
- 83Lab Labohm, F., Engelen, C., Gijzeman, O.L.J., Geus, J.W., Bootsma, G.: *Surf. Sci.* **126** (1983) 429.
- 83Llo Lloyd, D.R., Netzer, F.P.: *Surf. Sci.* **129** (1983) 1249.
- 83Min Minot, C., Van Hove, M.A., Somorjai, G.A.: *Surf. Sci.* **127** (1983) 441.
- 83Rie Rieder, K., Wilsch, H.: *Surf. Sci.* **131** (1983) 245.
- 83Tys Tysoe, W.T., Nyberg, G.L., Lambert, R.M.: *Surf. Sci.* **135** (1983) 128.
- 84Alb Albert, M.R., Sneddon, L.G., Plummer, E.W.: *Surf. Sci.* **147** (1984) 127.
- 84And Anderson, A.B., Mehandru, S.P.: *Surf. Sci.* **136** (1984) 398.
- 84Ban Bandy, B., Chesters, M.A., Pemble, M., McDougall, G., Sheppard, N.: *Surf. Sci.* **139** (1984) 87.
- 84Ben Benziger, J.B., Preston, R.E.: *Surf. Sci.* **141** (1984) 567.
- 84Kob Kobayashi, H., Teramae, H., Yamabe, T., Yamaguchi, M.: *Surf. Sci.* **141** (1984) 580.
- 84Koe Koel, B.E., Bent, B.E., Somorjai, G.A.: *Surf. Sci.* **146** (1984) 211.
- 84Meh Mehandru, S.P., Anderson, A.B.: *Appl. Surf. Sci.* **19** (1984) 116.
- 84Pal Palfi, S., Lisowski, W., Smutek, M., Cerny, S.: *J. Catal.* **88** (1984) 300.
- 84Ram Ramanathan, R., Quinlan, M., Wise, H.: *Chem. Phys. Lett.* **106** (1984) 87.
- 84Ste Steip, U., Tsai, M.-C., Küppers, J., Ertl, G.: *Surf. Sci.* **147** (1984) 65.
- 84Stö Stöhr, J., Sette, F., Johnson, A.L.: *Phys. Rev. Lett.* **53** (1984) 1684.
- 84Str Strosio, J.A., Bare, S.R., Ho, W.: *Surf. Sci.* **148** (1984) 499.
- 84Tys Tysoe, W.T., Nyberg, G.L., Lambert, R.M.: *J. Phys. Chem.* **88** (1984) 1960.
- 85Ave Avery, N.R.: *J. Am. Chem. Soc.* **107** (1985) 6711.
- 85Bee Beebe, T.P., Albert, M.R., Yates, J.T.: *J. Catal.* **96** (1985) 1.
- 85Che Chesters, M.A., McDougall, G., Pemble, M., Sheppard, N.: *Appl. Surf. Sci.* **22/23** (1985) 369.
- 85Hor Horsley, J.A., Stöhr, J., Koestner, R.J.: *J. Chem. Phys.* **83** (1985) 3146.
- 85Koe Koel, B.E.: *Scanning Electron Microsc.* **4** (1985) 1421.
- 85Mar Marchon, B.: *Surf. Sci.* **162** (1985) 382.
- 85Ste Stefan, P.M., Shek, M.L., Spicer, W.E.: *Surf. Sci.* **149** (1985) 423.



- 85Stu1 Stuve, E.M., Madix, R.J.: *J. Phys. Chem.* **89** (1985) 105.  
 85Stu2 Stuve, E.M., Madix, R.J.: *Surf. Sci.* **160** (1985) 293.  
 85Vin Vink, T.J., Gijzeman, O.L.J., Geus, J.W.: *Surf. Sci.* **150** (1985) 14.  
 85Wan Wang, P.-K., Slichter, C.P., Sinfelt, J.J.: *J. Phys. Chem.* **89** (1985) 3606.  
 86Ave1 Avery, N.R., Sheppard, N.: *Proc. R. Soc. (London) A* **405** (1986) 1.  
 86Ave2 Avery, N.R., Sheppard, N.: *Proc. R. Soc. (London) A* **405** (1986) 27.  
 86Ave3 Avery, N.R., Sheppard, N.: *Surf. Sci.* **169** (1986) L367.  
 86Ban Bandy, B., Chesters, M.A., James, D.I., McDougall, G., Pemble, M., Sheppard, N.: *Philos. Trans. R. Soc. (London) A* **318** (1986) 141.  
 86Hall1 Hall, R., Bare, S., Desantolo, A., Zaera, F.: *J. Vac. Sci. Technol. A* **4** (1986) 1493.  
 86Ham Hammer, L., Hertlein, T., Müller, K.: *Surf. Sci.* **178** (1986) 693.  
 86Hil Hills, M.M., Parmeter, J.E., Mullins, C.B., Weinberg, W.H.: *J. Am. Chem. Soc.* **108** (1986) 3554.  
 86Kel Kelly, D.G., Salmeron, M., Somorjai, G.A.: *Surf. Sci.* **175** (1986) 465.  
 86Lee Lee, M.B., Yang, Q.Y., Tang, S.L., Ceyer, S.T.: *J. Chem. Phys.* **85** (1986) 1693.  
 86Ogl Ogle, K.M., Creighton, J.R., Akter, S., White, J.M.: *Surf. Sci.* **169** (1986) 246.  
 86Par Parmeter, J.E., Hills, M.M., Weinberg, W.H.: *J. Am. Chem. Soc.* **108** (1986) 3563.  
 86Ste Steinrück, H.-P., Hamza, A.V., Madix, R.J.: *Surf. Sci.* **173** (1986) L571.  
 87Ben Bent, B.E., Mate, C.M., Crowell, J.E., Koel, B.E., Somorjai, G.A.: *J. Phys. Chem.* **91** (1987) 1493.  
 87Che Chesters, M.A., McCash, E.: *J. Electron Spectrosc. Relat. Phenom.* **44** (1987) 99.  
 87Ham Hamza, A.V., Madix, R.J.: *Surf. Sci.* **179** (1987) 25.  
 87Hat Hatzikos, G.H., Masel, R.J.: *Surf. Sci.* **185** (1987) 479.  
 87Hen Henderson, M.A., Mitchell, G.E., White, J.M.: *Surf. Sci. Lett.* **184** (1987) L325.  
 87Hil1 Hills, M.M., Parmeter, J.E., Weinberg, W.H.: *J. Am. Chem. Soc.* **109** (1987) 4224.  
 87Hil2 Hills, M.M., Parmeter, J.E., Weinberg, W.H.: *J. Am. Chem. Soc.* **109** (1987) 597.  
 87Jak Jakob, P., Cassuto, A., Menzel, D.: *Surf. Sci.* **187** (1987) 407.  
 87Kos Kostov, K.L., Marinova, T.S.: *Surf. Sci.* **184** (1987) 359.  
 87Lee Lee, M.B., Yang, Q.Y., Ceyer, S.T.: *J. Chem. Phys.* **87** (1987) 2724.  
 87Mar1 Marinova, T.S., Kostov, K.L.: *Surf. Sci.* **181** (1987) 573.  
 87Mar2 Marinova, T.S., Chakarov, D.V.: *Surf. Sci.* **192** (1987) 275.  
 87Mar3 Marinova, T.S., Stefanov, P.K.: *Surf. Sci.* **191** (1987) 66.  
 87Sak Sakakini, B., Swift, A.J., Vickermann, J.C., Harendt, C., Christmann, K.: *J. Chem. Soc. Faraday Trans.* **83** (1987) 1975.  
 87Zae1 Zaera, F., Hall, R.B.: *J. Phys. Chem.* **91** (1987) 4318.  
 87Zae2 Zaera, F., Hall, R.: *Surf. Sci.* **180** (1987) 1.  
 88Ave Avery, N.R.: *Langmuir* **4** (1988) 445.  
 88Cey Ceyer, S.T.: *Annu. Rev. Phys. Chem.* **39** (1988) 479.  
 88Che1 Chesters, M.A.: *J. Molec. Struct.* **173** (1988) 405.  
 88Che2 Chesters, M.A., in: *Analytical applications of spectroscopy*, Creaser, C.S., Davies, A.M.C. (eds.), London: Royal Soc. Chem., 1988, p. 201.  
 88Hen Henderson, M.A., Mitchell, G.E., White, J.M.: *Surf. Sci.* **203** (1988) 378.  
 88Mar Marinova, T.S., Chakarov, D.V.: *Surf. Sci.* **200** (1988) 309.  
 88Mat Mate, C.M., Kao, C.T., Bent, B., Somorjai, G.A.: *Surf. Sci.* **197** (1988) 183.  
 88Moh Mohsin, S., Trenary, M., Robota, H.: *J. Phys. Chem.* **92** (1988) 5229.  
 88Par Parmeter, J.E., Hills, M.M., Weinberg, W.H.: *J. Am. Chem. Soc.* **110** (1988) 7952.  
 88She Sheppard, N.: *Annu. Rev. Phys. Chem.* **39** (1988) 589.  
 88Sla1 Slavin, A.J., Bent, B.E., Kao, C.T., Somorjai, G.A.: *Surf. Sci.* **202** (1988) 388.  
 88Sla2 Slavin, A.J., Bent, B.E., Kao, C.T., Somorjai, G.A.: *Surf. Sci.* **206** (1988) 124.  
 88Van Van Hove, M.A., Bent, B.E., Somorjai, G.A.: *J. Phys. Chem.* **92** (1988) 973.  
 88Win Windham, R.G., Bartram, M.E., Koel, B.E.: *J. Phys. Chem.* **92** (1988) 2862.  
 89Aru Arumainayagam, C.R., McMaster, M.C., Schoofs, G.R., Madix, R.J.: *Surf. Sci.* **222** (1989) 213.  
 89Che Chesters, M.A., Gardner, P., McCash, E.M.: *Surf. Sci.* **209** (1989) 89.

- 89Mar Marinova, T.S., Stefanov, P.K.: *Surf. Sci.* **219** (1989) 490.
- 89Mul Mullins, C., Rettner, C.T., Auerbach, D.J., Weinberg, W.H.: *Chem. Phys. Lett.* **163** (1989) 111.
- 89Nis Nishijima, M., Yoshinobu, J., Sekitani, T., Onchi, M.: *J. Chem. Phys.* **90** (1989) 5114.
- 89Paf Paffett, M.T., Gebhard, S.C., Windham, R.G., Koel, B.E.: *Surf. Sci.* **223** (1989) 449.
- 89Rud Rudolf, P., Astaldi, G., Modesti, S., Rosei, R.: *Surf. Sci.* **220** (1989) L714.
- 89Wan Wang, D., Wu, K., Cao, Y., Zhai, R., Guo, X.: *Surf. Sci.* **223** (1989) L927.
- 89Yag Yagasaki, E., Masel, R.I.: *Surf. Sci.* **222** (1989) 430.
- 89Zho Zhou, Y., Henderson, M.A., Feng, W.M., White, J.M.: *Surf. Sci.* **224** (1989) 386.
- 90Aru Arumainayagam, C.R., McMaster, M.C., Madix, R.J.: *Surf. Sci.* **237** (1990) L424.
- 90Bac Backmann, A.L., Masel, R.I.: *J. Phys. Chem.* **94** (1990) 5300.
- 90Cha Chakarov, D.V., Marinova, T.S.: *Surf. Sci.* **227** (1990) 297.
- 90Che1 Chesters, M.A., De La Cruz, C., Gardner, P., McCash, E., Pudney, P., Shahid, G., Sheppard, N.: *J. Chem. Soc. Faraday Trans.* **86** (1990) 2757.
- 90Che2 Chesters, M.A., Gardner, P.: *Spectrochim. Acta A* **46** (1990) 1011.
- 90Che3 Chesters, M.A., Horn, A.B., Ilharco, L.M., Ransley, I.A., Sakakini, B., Vickermann, J.C.: *J. Electron Spectrosc. Relat. Phenom.* **54/55** (1990) 677.
- 90Che4 Chesters, M.A., De La Cruz, C., Gardner, P., McCash, E.M., Prentice, J.D., Sheppard, N.: *J. Electron Spectrosc. Relat. Phenom.* **54-55** (1990) 739.
- 90Ham Hammer, L., Dötsch, B., Brandenstein, F., Fricke, A., Müller, K.: *J. Electron Spectrosc. Relat. Phenom.* **54/55** (1990) 687.
- 90McC McCash, E.M.: *Vacuum* **40** (1990) 423.
- 90Sek Sekitani, T., Yoshinobu, J., Onchi, M., Nishijima, M.: *J. Phys. Chem.* **94** (1990) 6847.
- 90Wan Wang, L., Tysoe, W.T.: *Surf. Sci.* **236** (1990) 325.
- 90Yag1 Yagasaki, E., Backmann, A.L., Masel, R.I.: *J. Phys. Chem.* **94** (1990) 1066.
- 90Yag2 Yagasaki, E., Masel, R.J.: *Surf. Sci.* **226** (1990) 51.
- 90Yag3 Yagasaki, E., Backmann, A.L., Masel, R.I.: *J. Vac. Sci. Technol. A* **8** (1990) 2610.
- 90Yos Yoshinobu, J., Sekitani, T., Onchi, M., Nishijima, M.: *J. Electron Spectrosc. Relat. Phenom.* **54** (1990) 697.
- 90Yos Yoshinobu, J., Sekitani, T., Onchi, M., Nishijima, M.: *J. Phys. Chem.* **94** (1990) 4269.
- 91Cas Cassuto, A., Kiss, J., White, J.M.: *Surf. Sci.* **255** (1991) 289.
- 91Che Chesters, M.A., Horn, A.B., Ilharco, L.M., Ransley, I.A., Sakakini, B.H., Vickerman, J.C.: *Surf. Sci.* **251-252** (1991) 291.
- 91Cou Coulman, D., Solomon, J.L., Madix, R.J., Stöhr, J.: *Surf. Sci.* **257** (1991) 97.
- 91Hea Head-Gordon, M., Tully, J.C., Rettner, C.T., Mullins, B., Auerbach, D.J.: *J. Chem. Phys.* **94** (1991) 1516.
- 91Hen Henderson, M.A., Mitchell, G.E., White, J.M.: *Surf. Sci.* **248** (1991) 279.
- 91Nis Nishijima, M., Sekitani, T., Yoshinobu, J., Onchi, M.: *Surf. Sci.* **242** (1991) 493.
- 91Sau Sautet, P., Paul, J.: *Catal. Lett.* **9** (1991) 245.
- 91Wan Wander, A., Van Hove, M.A., Somorjai, G.A.: *Phys. Rev. Lett.* **67** (1991) 626.
- 92Ayr Ayre, C., Madix, R.: *Surf. Sci.* **262** (1992) 51.
- 92Fri Fricke, A., Graupner, H., Hammer, L., Müller, K.: *Surf. Sci.* **272** (1992) 182.
- 92Jen Jenks, C.J., Bent, D.E., Bernstein, N., Zaera, F.: *Surf. Sci.* **277** (1992) L89.
- 92Lan Land, T.A., Michely, T., Behm, R.J., Hemminger, J.C., Comsa, G.: *J. Chem. Phys.* **97** (1992) 6774.
- 92McM McMaster, M.C., Madix, R.J.: *Surf. Sci.* **275** (1992) 265.
- 92Nas Nascente, P.A.P., Van Hove, M.A., Somorjai, G.A.: *J. Vac. Sci. Technol. A* **10** (1992) 2342.
- 92Rek Rekoske, J.E., Cortright, R.D., Goddard, S.A., Sharma, S.B., Dumesic, J.A.: *J. Phys. Chem.* **96** (1992) 1880.
- 92Sak Sakakini, B., Ransley, I.A., Odnoza, C.F., Vickermann, J.C., Chesters, M.A.: *Surf. Sci.* **271** (1992) 227.
- 92Sas Sasaki, T., Kawada, F., Aruga, T., Iwasawa, Y.: *Surf. Sci.* **278** (1992) 291.
- 92Sek Sekitani, T., Takaoka, T., Fujisawa, M., Nishijima, M.: *J. Phys. Chem.* **96** (1992) 8462.

- 92Wei1 Weinelt, M., Huber, W., Zebisch, P., Steinrück, H.-P., Pabst, M., Rösch, N.: *Surf. Sci.* **271** (1992) 539.
- 92Wei2 Weinelt, M., Huber, W., Zebisch, P., Steinrück, H.-P., Reichert, B., Birkenheuer, U., Rösch, N.: *Phys. Rev. B* **46** (1992) 1675.
- 93Hei Heitzinger, J.M., Gebhard, S.C., Koel, B.E.: *J. Phys. Chem.* **97** (1993) 5327.
- 93Jac Jackman, R.B., Chua, L.H., Foord, J.S.: *Surf. Sci.* **292** (1993) 47.
- 93McM1 McMaster, M.C., Madix, R.J.: *Surf. Sci.* **294** (1993) 420.
- 93McM2 McMaster, M.C., Schroeder, S.L.M., Madix, R.J.: *Surf. Sci.* **297** (1993) 253.
- 93Nie Niemantsverdriet, J.W.: *Spectroscopy in catalysis*, Weinheim, New York: VCH, 1993.
- 93Oak Oakes, D.J., McCoustra, M.R.S., Chesters, M.A.: *Faraday Discuss. Chem. Soc.* **96** (1993) 325.
- 93Ran Ransley, I.A., Ilharco, L.M., Bateman, J.E., Sakakini, B.H., Vickermann, J.C., Chesters, M.A.: *Surf. Sci.* **298** (1993) 187.
- 93Sta Starke, U., Barbieri, A., Materer, N., Van Hove, M.A., Somorjai, G.A.: *Surf. Sci.* **286** (1993) 1.
- 94Bao1 Bao, S., Hofmann, P., Schindler, K.M., Fritzsche, V., Bradshaw, A.M., Woodruff, D.P., Casado, C., Asensio, M.C.: *J. Phys. Condens. Matter* **6** (1994) L93.
- 94Bao2 Bao, S., Schindler, K.M., Hofmann, P., Fritzsche, V., Bradshaw, A.M., Woodruff, D.P.: *Surf. Sci.* **291** (1994) 295.
- 94Chu1 Chua, L.H., Jackman, R.B., Kingsley, C.J., Foord, J.S.: *Diamond Relat. Mater.* **3** (1994) 706.
- 94Chu2 Chua, L.H., Jackman, R.B., Foord, J.S.: *Surf. Sci.* **315** (1994) 69.
- 94Dal Daley, S.P., Utz, A.L., Trautmann, T.R., Ceyer, S.T.: *J. Am. Chem. Soc.* **116** (1994) 6001.
- 94Fan Fan, J., Trenary, M.: *Langmuir* **10** (1994) 3649.
- 94Iba Ibach, H.: *Surf. Sci.* **299/300** (1994) 116.
- 94Kub Kubota, J., Kondo, J.N., Domen, K., Hirose, C.: *J. Phys. Chem.* **98** (1994) 7653.
- 94Ome Omerod, R.M., Lambert, R.M., Hoffmann, H., Zaera, F., Wang, L.P., Bennet, D.W., Tysoe, W.T.: *J. Phys. Chem.* **98** (1994) 2134.
- 94Sla Slater, D.A., Hollins, P., Chesters, M.A.: *Surf. Sci.* **306** (1994) 155.
- 94Som Somorjai, G.A.: *Introduction to surface chemistry and catalysis*, New York: John Wiley & Sons Inc., 1994.
- 94Sou Soulen, S.A., Stinnett, J.A., Madix, R.J.: *Surf. Sci.* **303** (1994) 312.
- 94Sta Starke, U., Van Hove, M.A., Somorjai, G.A.: *Prog. Surf. Sci.* **46** (1994) 305.
- 94Tak Takaoka, T., Sekitani, T., Aruga, T., Nishijima, M.: *Surf. Sci.* **306** (1994) 179.
- 94Wu Wu, M.-C., Goodman, D.W.: *J. Am. Chem. Soc.* **116** (1994) 1364.
- 95Bao Bao, S., Hofmann, P., Schindler, K.M., Fritzsche, V., Bradshaw, A.M., Woodruff, D.P., Casado, C., Asensio, M.C.: *Surf. Sci.* **323** (1995) 19.
- 95Bol Bol, C.W.J., Friend, C.M.: *Surf. Sci.* **337** (1995) L800.
- 95Bra Bradshaw, A.M.: *Surf. Sci.* **331-333** (1995) 978.
- 95Bur Burghgraef, H., Jansen, A.P.J., Van Santen, R.A.: *Surf. Sci.* **324** (1995) 345.
- 95Cam Camplin, J., Cook, J.C., McCash, E.M.: *J. Chem. Soc. Faraday Trans.* **91** (1995) 3563.
- 95Che Chen, J.: *J. Catal.* **154** (1995) 80.
- 95Coo Cooper, E., Raval, R.: *Surf. Sci.* **333** (1995) 94.
- 95Cre1 Cremer, P.S., Stanners, C., Niemantsverdriet, J.W., Shen, Y.R., Somorjai, G.A.: *Surf. Sci.* **328** (1995) 111.
- 95Cre2 Cremer, P.S., Somorjai, G.A.: *J. Chem. Soc. Faraday Trans.* **91** (1995) 3671.
- 95Guo1 Guo, X.C., Madix, R.J.: *J. Am. Chem. Soc.* **117** (1995) 5523.
- 95Guo2 Guo, X.C., Madix, R.J.: *J. Catal.* **155** (1995) 336.
- 95Her Hermann, K., Witko, M.: *Surf. Sci.* **337** (1995) 205.
- 95Hun Hung, W.H., Bernasek, S.L.: *Surf. Sci.* **339** (1995) 272.
- 95Jac Jackman, R.B., Chua, L.H., Foord, J.S.: *Diamond Relat. Mater.* **4** (1995) 740.
- 95Kis Kiskinova, M.P., Yates, J.T.: *Surf. Sci.* **325** (1995) 1.
- 95Kli Klivenyi, G., Solymosi, F.: *Surf. Sci.* **342** (1995) 168.
- 95Nie Nielsen, B.O., Luntz, A.C., Holmblad, P.M., Chorkendorff, I.: *Catal. Lett.* **32** (1995) 15.
- 95Paw1 Pawela-Crew, J., Madix, R.J.: *Surf. Sci.* **339** (1995) 8.

- 95Paw2 Pawela-Crew, J., Madix, R.J., Vasquez, N.: *Surf. Sci.* **340** (1995) 119.
- 95Rav Raval, R.: *Surf. Sci.* **333** (1995) 1.
- 95Sch Schaff, O., Stampfl, A.P.J., Hofmann, P., Bao, S., Schindler, K.M., Bradshaw, A.M., Davis, R., Woodruff, D.P., Fritzsche, V.: *Surf. Sci.* **343** (1995) 201.
- 95Sou Soulen, S.A., Madix, R.J.: *Surf. Sci.* **323** (1995) 1.
- 95Stu Stuck, A., Wartnaby, C.E., Yeo, Y.Y., King, D.A.: *Phys. Rev. Lett.* **74** (1995) 578.
- 95Tja Tjandra, S., Zaera, F.: *J. Am. Chem. Soc.* **117** (1995) 9749.
- 95Ver Verhoef, R.W., Kelly, D., Mullins, C.B., Weinberg, W.H.: *Surf. Sci.* **325** (1995) 93.
- 95Wei Weinelt, M., Huber, W., Zebisch, P., Steinrück, H.-P., Ulbricht, P., Birkenheuer, U., Boettger, J.C., Rösch, N.: *J. Chem. Phys.* **102** (1995) 9709.
- 95Yan Yang, Q.Y., Maynard, K.J., Johnson, A.D., Ceyer, S.T.: *J. Chem. Phys.* **102** (1995) 7734.
- 95Yat Yata, M., Madix, R.J.: *Surf. Sci.* **328** (1995) 171.
- 95Yeo Yeo, Y.Y., Wartnaby, C.E., King, D.A.: *Science* **268** (1995) 1731.
- 95Yos Yoshinobu, J., Ogasawara, H., Kawai, M.: *Phys. Rev. Lett.* **75** (1995) 2176.
- 95Zae Zaera, F.: *Chem. Rev.* **95** (1995) 2651.
- 96Ber Bertolini, J.C., Cassuto, A., Jugnet, Y., Massardier, J., Tardy, B., Tourillon, G.: *Surf. Sci.* **349** (1996) 88.
- 96Bui Buisset, J., Rust, H.-P., Schweizer, F.K., Cramer, L., Bradshaw, A.M.: *Phys. Rev. B* **54** (1996) 10373.
- 96Cer Cerny, S.: *Surf. Sci. Rep.* **26** (1996) 3.
- 96Cre1 Cremer, P.S., Su, X., Shen, Y.R., Somorjai, G.A.: *J. Phys. Chem.* **100** (1996) 16302.
- 96Cre2 Cremer, P.S., Su, X., Shen, Y.R., Somorjai, G.A.: *J. Am. Chem. Soc.* **118** (1996) 2942.
- 96Cre3 Cremer, P.S., Su, X., Shen, Y.R., Somorjai, G.A.: *Catal. Lett.* **40** (1996) 143.
- 96Cre4 Cremer, P.S., Su, X., Shen, Y.R., Somorjai, G.A.: *J. Chem. Soc. Faraday Trans.* **92** (1996) 4717.
- 96Gut Gutdeutsch, U., Birkenheuer, U., Bertel, E., Cramer, J., Boettger, J., Rösch, N.: *Surf. Sci.* **345** (1996) 331.
- 96Kra Kratzer, P., Hammer, B., Norskov, J.K.: *J. Chem. Phys.* **105** (1996) 5595.
- 96Rob Roberts, A., Haq, S., Raval, R.: *J. Chem. Soc. Faraday Trans. I* **92** (1996) 4823.
- 96She Sheppard, N., De La Cruz, C.: *Adv. Catal.* **41** (1996) 1.
- 96Sho Shorthouse, L.J., Haq, S., Raval, R.: *Surf. Sci.* **368** (1996) 296.
- 96Ste Steinrück, H.-P.: *J. Phys. Condens. Matter* **8** (1996) 6465.
- 96Sti Stinnett, J.A., McMaster, M.C., Schroeder, S.M.L., Madix, R.J.: *Surf. Sci.* **365** (1996) 683.
- 96Tou Tourillon, G., Cassuto, A., Jugnet, Y., Massardier, J., Bertolini, J.C.: *J. Chem. Soc. Faraday Trans.* **92** (1996) 4835.
- 96Tys Tysoe, W.T.: *Langmuir* **12** (1996) 78.
- 96Yos1 Yoshinobu, J., Kawai, M.: *Surf. Sci.* **368** (1996) 239.
- 96Yos2 Yoshinobu, J., Ogasawara, H., Kawai, M.: *Surf. Sci.* **363** (1996) 234.
- 96Zae Zaera, F., Janssens, T.V.W., Öfner, H.: *Surf. Sci.* **368** (1996) 371.
- 97And Andersen, J.N., Beutler, A., Sorensen, S.L., Nyholm, R., Setlik, B., Heskett, D.: *Chem. Phys. Lett.* **269** (1997) 371.
- 97Bra Bradshaw, A.M.: *Curr. Opin. Solid State Mater. Sci.* **2** (1997) 530.
- 97Cam Camplin, J.P., Eve, J.K., McCash, E.M.: *Surf. Rev. Lett.* **4** (1997) 1371.
- 97Döl Döll, R., Gerken, C.A., Van Hove, M.A., Somorjai, G.A.: *Surf. Sci.* **374** (1997) 151.
- 97Dys Dyson, A.J., Smith, P.V.: *Surf. Sci.* **375** (1997) 45.
- 97Fuh Fuhrmann, D., Wöll, C.: *Surf. Sci.* **377** (1997) 544.
- 97Kal Kaltchev, M., Thompson, A.W., Tysoe, W.T.: *Surf. Sci.* **391** (1997) 145.
- 97Kli Klier, K., Hess, J.S., Herman, R.G.: *J. Chem. Phys.* **107** (1997) 4033.
- 97Nah Nahm, T.U., Gomer, R.: *Surf. Sci.* **389** (1997) 177.
- 97Par Parker, B.R., Jenkins, J.F., Stair, P.C.: *Surf. Sci.* **372** (1997) 185.
- 97Rau Raut, J.S., Sholl, D.S., Fichthorn, K.A.: *Surf. Sci.* **389** (1997) 88.
- 97She Sheppard, N., De La Cruz, C.: *Adv. Catal.* **42** (1997) 181.
- 97Som Somorjai G.A., Rupprechter, G.: *Stud. Surf. Sci. Catal.* **109** (1997) 35.
- 97Sti Stinnett, J.A., Weaver, J.F., Madix, R.J.: *Surf. Sci.* **380** (1997) 489.

- 97Tho Thomas, J.M., Thomas, W.J.: Principles and practice of heterogeneous catalysis, Weinheim: VCH GmbH, 1997.
- 97Tsa Tsai, Y.L., Xu, C., Koel, B.E.: Surf. Sci. **385** (1997) 37.
- 97Val Valden, M., Pere, J., Hirsimäki, M., Suhonen, S., Pessa, M.: Surf. Sci. **377** (1997) 605.
- 97Vu Vu, G., Tysoe, W.T.: Surf. Sci. **391** (1997) 134.
- 97Wea Weaver, J.F., Krzyzowski, M.A., Madix, R.J.: Surf. Sci. **393** (1997) 150.
- 97Wu Wu, G., Bartlett, B., Tysoe, W.T.: Surf. Sci. **383** (1997) 57.
- 97Zha Zhao, Y., Bao, S., Cao, P.: J. Phys. Condens. Matter **9** (1997) 9507.
- 98Au Au, C.T., Liao, M.S., Ng, C.F.: J. Phys. Chem. A **102** (1998) 3959.
- 98Bad Baddeley, C.J., Lee, A.F., Lambert, R.M., Giessel, T., Schaff, O., Fernandez, V., Schindler, K.M., Theobald, A., Hirschmugl, C.J., Lindsay, R., Bradshaw, A.M., Woodruff, D.P.: Surf. Sci. **400** (1998) 166.
- 98Dic Dickens, K.A., Stair, P.C.: Langmuir **14** (1998) 1444.
- 98Eng Eng, J., Chen, J.G.: Surf. Sci. **414** (1998) 374.
- 98Ich Ichihara, S., Yoshinobu, J., Ogasawara, H., Nantoh, M., Kawai, M., Domen, K.: J. Electron Spectrosc. Relat. Phenom. **88** (1998) 1003.
- 98Lar Larsen, J.H., Chorkendorff, I.: Surf. Sci. **405** (1998) 62.
- 98New Newell, H.E., McCoustra, M.R.S., Chesters, M.A., De La Cruz, C.: J. Chem. Soc. Faraday Trans. **94** (1998) 3695.
- 98Pec Peck, J.W., Mahon, D.I., Koel, B.E.: Surf. Sci. **410** (1998) 200.
- 98San Sandell, A., Beutler, A., Jaworowski, A., Wiklund, M., Heister, K., Nyholm, R., Andersen, J.N.: Surf. Sci. **415** (1998) 411.
- 98Sol Solymosi, F.: J. Mol. Catal. A-Chem. **131** (1998) 121.
- 98Som Somorjai, G.A., Rupprechter, G.: J. Chem. Educ. **75** (1998) 161.
- 98Spi1 Spiewak, B.E., Dumesic, J.A.: Thermochim. Acta **312** (1998) 95.
- 98Spi2 Spiewak, B.E., Cortright, R.D., Dumesic, J.A.: J. Catal. **176** (1998) 405.
- 98Sti1 Stinnett, J.A., Weaver, J.F., Madix, R.J.: Surf. Sci. **395** (1998) 148.
- 98Sti2 Stipe, B.C., Rezaei, M.A., Ho, W.: Science **280** (1998) 1732.
- 98Tri Triguero, L., Pettersson, L.G.M., Minaev, B., Agren, H.: J. Chem. Phys. **108** (1998) 1193.
- 98Vas Vasquez, N., Madix, R.J.: J. Catal. **178** (1998) 234.
- 98Wea Weaver, J.F., Ho, K.L., Krzyzowski, M.A., Madix, R.J.: Surf. Sci. **400** (1998) 11.
- 98Wet Wetterer, S.M., Lavrich, D.J., Cummings, T., Bernasek, S., Scoles, G.: J. Phys. Chem. B **102** (1998) 9266.
- 98Wit Witko, M., Hermann, K.: Appl. Catal. A-General **172** (1998) 85.
- 98Wu1 Wu, G., Tysoe, W.: Surf. Sci. **397** (1998) 197.
- 98Wu1 Wu, G.F., Molero, H., Tysoe, W.T.: Surf. Sci. **397** (1998) 179.
- 98Yu Yu, H., Leung, K.T.: Surf. Sci. **401** (1998) 269.
- 99Ans Anson, C.E., Sheppard, N., Bender, B.R., Norton, J.R.: J. Am. Chem. Soc. **121** (1999) 529.
- 99Bro1 Brown, W.A., Kose, R., King, D.A.: J. Mol. Catal. A-Chem. **141** (1999) 21.
- 99Bro2 Brown, W.A., Kose, R., King, D.A.: Surf. Sci. **440** (1999) 271.
- 99Chu Chuang, T.J., Chan, Y.L., Chuang, P., Klauser, R.: J. Electron Spectrosc. Relat. Phenom. **99** (1999) 149.
- 99Cor Cortright, R.D., Watwe, R.M., Spiewak, B.E., Dumesic, J.A.: Catal. Today **53** (1999) 395.
- 99Dum Dumas, P., Weldon, M.K., Chabal, Y.J., Williams, G.P.: Surf. Rev. Lett. **6** (1999) 225.
- 99Gie Giessel, T., Terborg, R., Schaff, O., Lindsay, R., Baumgärtel, P., Hoeft, J.T., Schindler, K.M., Bao, S., Theobald, A., Fernandez, V., Bradshaw, A.M., Chrysostomou, D., McCabe, T., Lloyd, D.R., Davis, R., Booth, N.A., Woodruff, D.P.: Surf. Sci. **440** (1999) 125.
- 99Kal Kaltchev, M., Stacchiola, D., Molero, H., Wu, G., Blumenfeld, A., Tysoe, W.T.: Catal. Lett. **60** (1999) 11.
- 99Kos Kose, R., Brown, W.A., King, D.A.: Chem. Phys. Lett. **311** (1999) 109.
- 99Lau Lauhon, L.J., Ho, W.: J. Chem. Phys. **111** (1999) 5633.
- 99Liv Livneh, T., Asscher, M.: J. Phys. Chem. B **103** (1999) 5665.
- 99Mid Middleton, R.L., Lambert, R.M.: Catal. Lett. **59** (1999) 15.

- 99Oht Ohtani, T., Kubota, J., Kondo, J.N., Hirose, C., Domen, K.: *J. Phys. Chem. B* **103** (1999) 4562.
- 99Som Somorjai, G.A., Rupprechter, G.: *J. Phys. Chem. B* **103** (1999) 1623.
- 99Tja Tjandra, S., Zaera, F.: *J. Phys. Chem.* **103** (1999) 2312.
- 99Wu Wu, G.F., Kaltchev, M., Tysoe, W.T.: *Surf. Rev. Lett.* **6** (1999) 13.
- 99Yag Yagyu, S., Kino, Y., Ozeki, K., Yamamoto, S.: *Surf. Sci.* **435** (1999) 779.
- 99Zae Zaera, F., Gleason, N.R., Klingenberg, B., Ali, A.H.: *J. Mol. Catal. A-Chem.* **146** (1999) 13.
- 00Aza Azad, S., Kaltchev, M., Stacchiola, D., Wu, G., Tysoe, W.T.: *J. Phys. Chem. B* **104** (2000) 3107.
- 00Azi Azizian, S., Gobal, F.: *J. Mol. Catal. A-Chem.* **153** (2000) 191.
- 00Cam Camplin, J.P., Eve, J.K., McCash, E.M.: *Phys. Chem. Chem. Phys.* **2** (2000) 4433.
- 00Car Carlsson, A.F., Madix, R.J.: *Surf. Sci.* **458** (2000) 91.
- 00Han Hansen, E.W., Neurock, M.: *J. Catal.* **196** (2000) 241.
- 00Ich Ichihara, S., Okuyama, H., Kato, H., Kawai, M., Domen, K.: *Chem. Lett.* **2** (2000) 112.
- 00Ilh Ilharco, L.M., Garcia, A.R., Hargreaves, E.C., Chesters, M.A.: *Surf. Sci.* **459** (2000) 115.
- 00Kao Kao, C.-L., Carlsson, A.F., Madix, R.J.: *Top. Catal.* **14** (2000) 63.
- 00Kis Kis, A., Smith, K.C., Kiss, J., Solymosi, F.: *Surf. Sci.* **460** (2000) 190.
- 00Lau1 Lauhon, L.J., Ho, W.: *Phys. Rev. Lett.* **84** (2000) 1527.
- 00Lau2 Lauhon, L.J., Ho, W.: *Surf. Sci.* **451** (2000) 219.
- 00Lib Libuda, J., Scoles, G.: *J. Chem. Phys.* **112** (2000) 1522.
- 00McC McCabe, P.R., Juurlink, L.B.F., Utz, A.L.: *Rev. Sci. Instrum.* **71** (2000) 42.
- 00Miu Miura, T., Kobayashi, H., Domen, K.: *J. Phys. Chem. B* **104** (2000) 6809.
- 00Neu1 Neurock, M., van Santen, R.A.: *J. Phys. Chem. B* **104** (2000) 11127.
- 00Neu2 Neurock, M., Pallassana, V., van Santen, R.A.: *J. Am. Chem. Soc.* **122** (2000) 1150.
- 00Sta Stacchiola, D., Katchev, G., Wu, G., Tysoe, W.T.: *Surf. Sci.* **470** (2000) L32.
- 00Too Toomes, R.L., Lindsay, R., Baumgärtel, P., Terborg, R., Hoeft, J.T., Koebbel, A., Schaff, O., Polcik, M., Robinson, J., Woodruff, D.P., Bradshaw, A.M., Lambert, R.M.: *J. Chem. Phys.* **112** (2000) 7591.
- 00Wat1 Watanabe, K., Matsumoto, Y.: *Surf. Sci.* **454** (2000) 262.
- 00Wat2 Watwe, R.M., Bengaard, H.S., Rostrup-Nielsen, J.R., Dumesic, J.A., Norskov, J.K.: *J. Catal.* **189** (2000) 16.
- 00Wu Wu, G., Stacchiola, D., Kaltchev, M., Tysoe, W.T.: *J. Am. Chem. Soc.* **122** (2000) 8232.
- 00Zae Zaera, F., Chrysostomou, D.: *Surf. Sci.* **457** (2000) 89.
- 01Car Carlsson, A.F., Madix, R.J.: *Surf. Sci.* **479** (2001) 98.
- 01Cey Ceyer, S.T.: *Acc. Chem. Res.* **34** (2001) 737.
- 01Gab Gabelnick, A.M., Burnett, D.J., Gland, J.L., Fischer, D.A.: *J. Phys. Chem. B* **105** (2001) 7748.
- 01Hei Heitzinger, J., Beck, D.E., Koel, B.E.: *Surf. Sci.* **491** (2001) 63.
- 01Oga Ogasawara, H., Ichihara, S., Okuyama, H., Domen, K., Kawai, M.: *J. Electron Spectrosc. Relat. Phenom.* **114** (2001) 339.
- 01Oht Ohtani, T., Kubota, J., Kondo, J.N., Hirose, C., Domen, K.: *Surf. Sci.* **415** (2001) L983.
- 01Pan Panja, C., Saliba, N.A., Koel, B.E.: *J. Phys. Chem. B* **105** (2001) 3786.
- 01Ron Ronning, M., Bergene, E., Borg, A., Ausen, S., Holmen, A.: *Surf. Sci.* **477** (2001) 191.
- 01Sta1 Stacchiola, D., Azad, S., Burkholder, L., Tysoe, W.T.: *J. Phys. Chem. B* **105** (2001) 11233.
- 01Sta2 Stacchiola, D., Wu, G., Kaltchev, M., Tysoe, W.T.: *J. Mol. Catal. A-Chem.* **167** (2001) 13.
- 01Sta3 Stacchiola, D., Wu, G., Molero, H., Tysoe, W.T.: *Catal. Lett.* **71** (2001) 1.
- 01Sta4 Stacchiola, D., Molero, H., Tysoe, W.T.: *Catal. Today* **65** (2001) 3.
- 01Wea Weaver, J.F., Ikai, M., Carlsson, A.F., Madix, R.J.: *Surf. Sci.* **470** (2001) 226.
- 01Whe Whelan, C.M., Neubauer, R., Borgmann, D., Denecke, R., Steinrück, H.P.: *J. Chem. Phys.* **115** (2001) 8133.
- 02Ber Bertolini, J.C., Jugnet, Y.: in: *The chemical physics of solid surfaces, Vol. 10: Surface alloys and alloy surfaces*, Woodruff, D.P. (ed.), Elsevier, 2002.
- 02Cho Choudhary, T.V., Goodman, D.W.: *Top. Catal.* **20** (2002) 35.
- 02Ge Ge, Q., Neurock, M.: *Chem. Phys. Lett.* **358** (2002) 377.

- 02Ho Ho, W.: *J. Chem. Phys.* **117** (2002) 11033.
- 02Kao Kao, C.L., Weaver, J.F., Madix, R.J.: *Surf. Sci.* **505** (2002) 115.
- 02Kat1 Katano, S., Kim, Y., Furukawa, M., Ogasawara, H., Komeda, T., Kato, H., Nilsson, A., Kawai, M., Domen, K.: *Jpn. J. Appl. Phys. Part 1* **41** (2002) 4911.
- 02Kat2 Katano, S., Ichihara, S., Ogasawara, H., Kato, H., Komeda, T., Kawai, M., Domen, K.: *Surf. Sci.* **502** (2002) 164.
- 02Neu Neurock, M., Mei, D.: *Top. Catal.* **20** (2002) 5.
- 02Ols Olsson, F., E. Persson, M., Lorente, N., Lauhon, L.J., Ho, W.: *J. Phys. Chem. B.* **106** (2002) 8161.
- 02Pal Pallassana, V., Neurock, M., Lusvardi, V.S., Lerou, J.J., Kragten, D.D., van Santen, R.A.: *J. Phys. Chem. B* **106** (2002) 1656.
- 02Ram1 Ramsvik, T., Borg, A., Worren, T., Kildemo, M.: *Surf. Sci.* **511** (2002) 351.
- 02Ram2 Ramsvik, T., Borg, A., Venvik, H.J., Hansteen, F., Kildemo, M., Worren, T.: *Surf. Sci.* **499** (2002) 183.
- 02Rup Rupprechter, G., Unterhalt, H., Morkel, M., Galletto, P., Hu, L., Freund, H.-J.: *Surf. Sci.* **502-503** (2002) 109.
- 02Sch Schmid, M.P., Maroni, P., Beck, R.D., Rizzo, T.R.: *J. Chem. Phys.* **117** (2002) 8603.
- 02Stac1 Stacchiola, D., Burkholder, L., Tysoe, W.T.: *Surf. Sci.* **511** (2002) 215.
- 02Stac2 Stacchiola, D., Tysoe, W.T.: *Surf. Sci.* **513** (2002) L431.
- 02Val Valcarcel, A., Ricart, J.M., Clotet, A., Markovits, A., Minot, C., Illas, F.: *J. Chem. Phys.* **116** (2002) 1165.
- 02Whe Whelan, C.M., Neubauer, R., Denecke, R., Steinrück, H.-P.: *Surf. Rev. Lett.* **9** (2002) 789.
- 02Zae1 Zaera, F.: *Mol. Phys.* **100** (2002) 3065.
- 02Zae2 Zaera, F.: *J. Phys. Chem. B* **106** (2002) 4043.
- 03Doy Doyle, A.M., Shaikhutdinov, S.K., Jackson, S.D., Freund, H.-J.: *Angew. Chem. Int. Ed. Engl.* **42** (2003) 5240.
- 03Fre Freund, H.-J., Bäumer, M., Libuda, J., Risse, T., Rupprechter, G., Shaikhutdinov, S.: *J. Catal.* **216** (2003) 223.
- 03Kha Khan, N.A., Chen, J.G.: *J. Vac. Sci. Technol. A* **21** (2003) 1302.
- 03Lee Lee, A.F., Wilson, K.: *J. Vac. Sci. Technol. A* **21** (2003) 563.
- 03Liu Liu, Z.P., Hu, P.: *J. Am. Chem. Soc.* **125** (2003) 1958.
- 03Med Medlin, J.W., Allendorf, M.D.: *J. Phys. Chem. B* **107** (2003) 217.
- 03Mei Mei, D.H., Hansen, E.W., Neurock, M.: *J. Phys. Chem. B* **107** (2003) 798.
- 03Mit Mittendorfer, F., Thomazeau, C., Raybaud, P., Toulhoat, H.: *J. Phys. Chem. B* **107** (2003) 12287.
- 03Mor Morkel, M., Rupprechter, G., Freund, H.-J.: *J. Chem. Phys.* **119** (2003) 10853.
- 03Neu Neubauer, R., Whelan, C.M., Denecke, R., Steinrück, H.-P.: *J. Chem. Phys.* **119** (2003) 1710.
- 03She Sheth, P.A., Neurock, M., Smith, C.M.: *J. Phys. Chem. B* **107** (2003) 2009.
- 03Soc Sock, M., Eichler, A., Surnev, S., Andersen, J.N., Klötzer, B., Hayek, K., Ramsey, M.G., Netzer, F.P.: *Surf. Sci.* **545** (2003) 122.
- 03Stac1 Stacchiola, D., Tysoe, W.T.: *Surf. Sci.* **540** (2003) L600.
- 03Stac2 Stacchiola, D., Burkholder, L., Tysoe, W.T.: *Surf. Sci.* **542** (2003) 129.
- 03Wan Wang, J.: *Surf. Sci.* **540** (2003) 326.
- 03Wea Weaver, J.F., Carlsson, A.F., Madix, R.J.: *Surf. Sci. Rep.* **50** (2003) 107.
- 03Zhe Zheng, T., Tysoe, W.T., Poon, H.C., Saldin, D.K.: *Surf. Sci.* **543** (2003) 19.
- 04Ans Anson, C.E., Sheppard, N., Pearman, R., Moss, J.R., Stossel, P., Koch, S., Norton, J.R.: *Phys. Chem. Chem. Phys.* **6** (2004) 1070.
- 04Doy Doyle, A.M., Shaikhutdinov, S.K., Freund, H.-J.: *J. Catal.* **223** (2004) 444.
- 04Fuh Fuhrmann, T., Kinne, M., Whelan, C.M., Zhu, J.F., Denecke, R., Steinrück, H.-P.: *Chem. Phys. Lett.* **390** (2004) 208.
- 04Kao Kao, C.L., Madix, R.J.: *Surf. Sci.* **557** (2004) 215.
- 04Rup Rupprechter, G., Morkel, M., Freund, H.-J., Hirschl, R.: *Surf. Sci.* **554** (2004) 43.
- 04Val Valcarcel, A., Clotet, A., Ricart, J.M., Delbecq, F., Sautet, P.: *Surf. Sci.* **549** (2004) 121.

- 
- 04Zhe Zheng, T., Stacchiola, D., Poon, H.C., Saldin, D.K., Tysoc, W.T.: *Surf. Sci.* **564** (2004) 71.  
05Den Denecke, R.: *Appl. Phys. A* **80** (2005) 977.  
05Fuh1 Fuhrmann, T., Kinne, M., Tränkenschuh, B., Papp, C., Zhu, J.F., Denecke, R., Steinrück, H.-P.: *New J. Phys.* **7** (2005) 107.  
05Fuh2 Fuhrmann, T., Kinne, M., Zhu, J.F., Tränkenschuh, B., Denecke, R., Steinrück, H.-P.: to be published (2005).  
05Jug Jugnet, Y., Sedrati, R., Bertolini, J.C.: *J. Catal.* **229** (2005) 252.  
05Mat Matsumoto, C., Kim, Y., Okawa, T., Sainoo, Y., Kawai, M.: *Surf. Sci.* **587** (2005) 19.  
05Mor Morkel, M., Rupprechter, G., Freund, H.-J.: *Surf. Sci.* **588** (2005) L209.  
05Sav Savio, L., Vattuone, L., Rocca, M.: *Surf. Sci.* **587** (2005) 110.  
05Tes Teschner, D., Pestryakov, A., Kleimenov, E., Havecker, M., Bluhm, H., Sauer, H., Knop-Gericke, A., Schlögl, R.: *J. Catal.* **230** (2005) 195.